“*It is the struggle itself that is most important. We must strive to be more than we are. It does not matter that we will not reach our ultimate goal. The effort itself yields its own reward."*

- Gene Roddenberry

University of Alberta

The jaw adductor muscles in *Champsosaurus* and their implications for feeding mechanics

by

Michael Spencer Brian James

A thesis submitted to the Faculty of Graduate Studies and Research
in partial fulfillment of the requirements for the degree of

Master of Science
in
Systematics and Evolution

Biological Sciences

Fall 2010
Edmonton, Alberta

Examining Committee

Philip J. Currie, Biological Sciences

Michael W. Caldwell, Biological Sciences

Richard C. Fox, Biological Sciences

John Acorn, Renewable Resources

Abstract

The jaw musculature of *Champsosaurus* has been enigmatic since the taxon was first described. The extant phylogenetic bracketing method is used to determine the morphology of the jaw adductor musculature. Rotational mathematics is used to calculate the muscle forces, torques, angular accelerations, and angular velocities generated by the jaw muscles. The mechanical strength of the skulls of neochoristoderes and crocodilians are investigated using finite element analysis. Finally, the hydrodynamic performance of the skulls of neochoristoderes and crocodilians is studied. The analysis is used to compare neochoristoderes to their extant ecological analogues, crocodilians, and determine the palaeoecological implications of the results. It was found that *Champsosaurus* rotates the lower jaw faster, the mechanical strength was lower, and shows better hydrodynamic performance than crocodilians. The results suggest that *Champsosaurus* was ideally suited to prey upon small or juvenile fish, and did not overlap its niche with sympatric crocodilians.

Acknowledgements

I would like to thank the following people for their contributions to the making of this thesis: Dr. Philip Currie for his supervision and guidance, Dr. Michael Caldwell, Dr. Richard Fox, and John Acorn for providing suggestions and feedback on my thesis, Eric Snively and Victoria Arbour for teaching me the basics of biomechanics and assistance in operating the computer programs used in this study, Dr. Don Henderson for devising the computer program used to calculate rotational inertia, Eva Koppelhus for her support over these past few years, Ken Soehn for finding UALVP 47243, the graduate students of the palaeontology lab, Rhian Russell for digitizing the specimen of *Crocodylus* and her support, and my parents Leanne and Anthony Bowen for the free meals and supporting my interest in palaeontology since childhood.

Table of Contents

Tables

Figures

CHAPTER 1: INTRODUCTION

Overview of the Choristodera

The Order Choristodera is an extinct group of diapsid reptiles, with uncertain phylogenetic affinities, that are present in Laurasia from the Middle Jurassic (Evans, 1990; Averianov et al., 2006) to the Miocene (Hecht, 1992; Evans and Klembara, 2005). The Choristodera has been classified as Diapsida *incertae sedis* (Carroll and Currie, 1991), basal diapsids (Evans, 1988; Dilkes, 1998; Gao and Fox, 1998), lepidosaurians (Erickson, 1972), closely related to sauropterygians (Caldwell, 1996; Müller, 2004), the sister group to the Archosauromorpha (Evans, 1988; Rieppel, 1998), or within the Archosauromorpha (Erickson, 1985; Gauthier et al., 1988; Evans, 1990; Rieppel, 1993; Storrs and Gower, 1993; Storrs et al., 1996; de Braga and Rieppel, 1997; Jalil, 1997).

Despite the considerable uncertainty of the phylogenetic position of the Choristodera within the Diapsida they are united by the following characters (Gao and Fox, 2005): prefrontals having median sutural contact for their entire length, parietal foramen absent choana retracted close to midpoint of marginal tooth row, pterygoid flange consisting of pterygoid and ectopterygoid having a horizontal overlap, basipterygoid/ pterygoid joint is a sutural contact, parasphenoid and pterygoid having a clear sutural contact, postorbital process of jugal much shorter than anteroventral process, interpterygoid vacuity enclosed anteriorly by pterygoids and posteriorly by parasphenoid, neomorph in braincase present as part of external wall of braincase and medial wall of temporal fossa, free odontoid

process unfused to axis, vertebral centra amphiplatyan with notochordal canal closed, sacral vertebrae three in number, and the sacral and caudal ribs remain free from the vertebrae

The earliest record of choristoderes comes from the late Triassic of Europe. *Pachystropheus rhaeticus* has been attributed to the Choristodera based on vertebral and girdle elements (Storrs and Gower, 1993; Storrs et al., 1996). However, the vertebral and girdle characters are considered to be common in many aquatic reptiles, and are not unique to choristoderes (Matsumoto et al., 2009). Until cranial or articulated post cranial remains are found, *Pachystropheus* will likely continue to be left out of phylogenetic analyses (Gao and Fox, 1998, 2005; Ksepka et al., 2005; Matsumoto et al., 2009).

Cteniogenys lived during Middle to Late Jurassic times in Europe and North America (Evans, 1990), making it the earliest undisputed occurrence of choristoderes. A possible occurrence in the Late Cretaceous of Alberta has also been described (Gao and Fox, 1998), but the isolated maxilla and dentary fragments have been criticized for not being sufficiently diagnostic for attribution to a genus (Matsumoto et al., 2009). *Cteniogenys* is often considered to be the most basal choristodere (Evans, 1990; Gao and Fox, 1998; Gao and Fox, 2005; Ksepka et al., 2005). However, other authors place it as the second most basal choristodere (Hecht, 1992; Evans and Hecht, 1993; Evans and Klembara, 2005; Matsumoto et al., 2007; Matsumoto et al., 2009).

Lazarussuchus (Hecht, 1992) is a problematic diapsid from the late Oligocene of France and the early Miocene of the Czech Republic. Phylogenetic

analyses consistently place *Lazarussuchus* either as the most basal choristodere (Hecht, 1992; Evans and Klembara, 2005), or as the sister group to the Choristodera (Gao and Fox, 1998; Evans and Manabe, 1999; Gao and Fox, 2005; Ksepka et al., 2005). Gao and Fox (1998, 2005), and Ksepka et al. (2005) argue that *Lazarussuchus* lacks key synapomorphies of the Choristodera such as the presence of a neomorph bone in the braincase and a pterygoquadrate foramen.

The relationships between the genera more advanced than *Cteniogenys* and basal to the Neochoristodera are inconsistent between studies (Evans and Hecht, 1993; Gao and Fox, 1998, 2005; Ksepka et al., 2005; Matsumoto et al., 2009). The closest genera in terms of body plans to the basal *Cteniogenys* are *Monjurosuchus* (Endo, 1940) and *Philydrosaurus* (Gao and Fox, 2005). *Monjurosuchus* is found in the Upper Jurassic/Lower Cretaceous strata of western Liaoning, China (Gao et al., 2000). *Monjurosuchus* differs notably from other choristoderes in having a smaller, lizard-like skull and a short neck (Gao et al., 2000; Matsumoto et al., 2007). The presence of webbed feet indicates that it occupied an aquatic habitat (Gao et al., 2000). *Philydrosaurus* hails from the Early Cretaceous of Liaoning, and is similar to *Monjurosuchus* in morphology and niche (Gao and Fox, 2005). Gao and Fox (2005), Gao and Li (2007), and Gao et al. (2007) have grouped *Monjurosuchus* and *Philydrosaurus* into the Monjurosuchidae. Subsequent authors have found little support for the Monjurosuchidae and have instead placed *Monjurosuchus* and *Philydrosaurus* in a polytomy with the Hyphalosauridae (Matsumoto et al., 2007; Skutschas, 2008; Matsumoto et al., 2009).

Gao and Fox (2005) described the Hyphalosauridae, which includes *Hyphalosaurus* and *Shokawa*. These two choristoderes most closely resemble other semi-aquatic long-necked reptiles such as pachypleurosaurs with their long necks, deep tails, and pachyostotic ribs and gastralia. *Hyphalosaurus* is thought to have preyed upon small animals because of the presence of small peg-like teeth, small head, and long neck (Gao and Ksepka, 2008). The method of prey capture is thought to be a sideways strike due to the flattened nature of the skull, a feature shared with neochoristoderes (Taylor, 1987; Gao and Ksepka, 2008). The similarities in the postcranial skeleton of *Hyphalosaurus* and *Shokawa* indicate that the latter shared a comparable lifestyle. However, the lack of any cranial remains precludes a more precise reconstruction of its lifestyle.

Recent phylogenetic analyses have postulated a close relationship between Hyphalosauridae and *Khurendukhosaurus* (Matsumoto et al., 2009). *Khurendukhosaurus* is either the sister group to the Hyphalosauridae, or is within the Hyphalosauridae, being between *Hyphalosaurus* and *Shokawa*. The latter relationship was found after more outgroups were added (Matsumoto et al., 2009). A caveat is that cranial remains of both *Shokawa* and *Khurendukhosaurus* have been found as of yet, which could obscure the phylogenetic signal (Matsumoto et al., 2009). *Khurendukhosaurus* has been thought to have a more terrestrial lifestyle than other members of the Choristodera because of the lack of pachyostotic ribs, coossiffied scapula and coracoid, and closed neurocentral sutures (Skutschas, 2008). Matsutmoto et al. (2009) did not concur, and note that *Khurendukhosaurus* has unfused sacral ribs, tall caudal neural spines (indicating a

deep swimming tail), weak development of the distal ends of the humeri, and a dorsoventrally compressed body profile, all of which are considered to be features of aquatic tetrapods. Without cervical or cranial material Matsumoto et al. (2009) note that the niche occupied by *Khurendukhosaurus* cannot be determined.

Classically the most recognizable of the choristoderes are the Neochoristodera (Evans, 1990). The Neochoristodera include the Champsosauridae (Cope 1876, 1884), and the Simoedosauridae (Sigogneau-Russell and Russell, 1978; Erickson, 1987). The relationship between the neochoristoderan genera is strong, consistently forming a monophyletic group (Evans, 1990; Gao and Fox, 1998; Gao and Fox, 2005; Ksepka et al., 2005; Matsumoto et al., 2007, 2009). The Champsosauridae are monogeneric, with *Champsosaurus* (Cope, 1876, 1884) being the only member. The Simoedosauridae contain several genera: *Simoedosaurus* (Sigogneau-Russell and Russell, 1978; Erickson, 1987), *Tchoiria* (Efimov, 1975; Ksepka et al., 2005), and *Ikechosaurus* (Sigogneau-Russell, 1981; Brinkman and Dong, 1993).

Champsosaurus is currently the only valid genus within the Family Champsosauridae. There are currently seven species recognized in North America; *C. albertensis* Parks, 1927, *C. laramiensis* Brown, 1905, *C. ambulator* Brown, 1905, *C. gigas* Erickson, 1972, *C. tenuis* Erickson, 1981, *C. natator* Parks, 1933, and *C. lindoei* Gao and Fox, 1998. In North America *Champsosaurus* is found in upper Cretaceous to lower Eocene strata and in Europe from the Paleocene to Eocene (Gao and Fox, 1998). Geographically, their range extends from New Mexico, USA, to the high arctic of Canada (Vandermark

et a., 2007). Typically *Champsosaurus* was living in environments thought to be fluvial systems bordering the Western Interior Seaway.

Two species of *Champsosaurus* are presently considered valid from Dinosaur Provincial Park, Alberta, Canada. *C. natator* was first described by Parks (1933), and later by Russell (1956). *C. natator* is differentiated from other species by having a larger body size than *C. lindoei*, more robust snout, laterally swollen lower temporal bar, a medially and laterally expanded subtemporal fenestra, and a posteromedial extension of the postfrontral that prevents contact between the postorbital and the frontal (Gao and Fox, 1998). Occurring sympatrically with *C. natator* is *C. lindoei*, which has a slender snout with an expanded tip, weakly developed pterygoid flange with a reduced number of teeth, a nearly straight inferior temporal arch, and a rectangular subtemporal fenestra (Gao and Fox, 1998).

Also from Alberta is *C. albertensis* (Parks, 1927) which is found in the Horseshoe Canyon Formation. *C. albertensis* was described by Parks (1927) based solely on postcranial material. *C. albertensis* can be distinguished from other species in the genus by the proportions of the snout, and shape and position of the orbits, greater robustness in comparison to size, posterior position of the craniomandibular joint, strongly twisted and screw-shaped articular surface of quadrate for craniomandibular joint, and extent of jugal anterior to lacrimal greater than total length of lacrimal (Gao and Fox, 1998).

C. laramiensis and *C ambulator* are present in the Hell Creek Formation (upper most Cretaceous) and Tullock Formation (lower Paleocene) in eastern

Montana (Brown, 1905; Erickson, 1972; Gao and Fox, 1998). Brown (1905) distinguished between *C. laramiensis* and *C. ambulator* based largely upon appendicular skeletal characters, the skull being nearly the same between the two species. A revised diagnosis is need for these two species (Gao and Fox, 1998).

C. tenuis hails from the Bullion Creek (Tongue River) Formation (upper Paleocene) of North Dakota (Erickson, 1981). Like *C. ambulator* and *C. laramiensis*, *C. tenuis* also requires a revised diagnosis (Gao and Fox, 1998). *C. gigas* has also been found in the Bullion Creek (Tongue River) Formation as well as the Sentinel Butte (upper Paleocene) of North Dakota (Erickson, 1972, 1985), and the Ravenscrag Formation (Paleocene) of southern Saskatchewan (Gao and Fox, 1998).

The type genus of the Simoedosauridae, *Simoedosaurus*, was originally described by Gervais (1887) from the Paleocene of Europe, and later specimens were described by Sigogneau-Russell and Baird (1978) from roughly the same age in Montana. Sigogneau-Russell (1985) diagnosed *Simoedosaurus* based on the following characters: muzzle represents about 2/5, of the total length of the skull, muzzle narrow throughout its length, choanae situated in the posterior half of the muzzle, lacrimal short, contact between postorbitofrontal and parietal situated approximately at the level of the anterior edge of the upper temporal fossa, premaxillary teeth large compared to those on the maxilla, maxillary teeth decrease in size anteriorly to posteriorly.

Tchoiria has been described from two localities in Mongolia. Efimov (1975) described the type species, *T. namsarai*, based on material collected by the

1971 Soviet-Mongolian expedition. Three more species of *Tchoiria* have since been described, two of which were later placed in other genera. The only other species is *T. klauseni* collected in 1998 (Ksepka et al., 2005). Phylogenetic analyses place *Tchoiria* in the basal position of the Simoedosauridae (Gao and Fox, 1998; Evans and Manabe, 1999; Ksepka et al., 2005). The morphology of *Tchoiria* closely resembles that of *Simoedosaurus* in that it is also a neochoristodere that is highly crocodiliform.

Ikechosaurus is another choristodere from Asia, this time from the Ordos Basin of China. Sigogneau-Russell (1981) described *I. sunailinae* based on a snout fragment, and the species was later redescribed after a nearly complete specimen was found from the same area (Brinkman and Dong, 1993). Efimov (1979) described *Tchoiria magna* from the Early Cretaceous of Mongolia, but it was reassigned to *Ikechosaurus* based on the presence of mediolaterally elongate, rectangular tooth bases (Efimov, 1983). Phylogenetic analyses consistently place *Ikechosaurus* as the sister taxon to *Simoedosaurus* (Brinkman and Dong, 1993; Gao and Fox, 1998; Ksepka et al., 2005; Matsumoto et al., 2007, 2009). Despite the close relationship between *Ikechosaurus* and *Simoedosaurus*, *Ikechosaurus* has a skull morphology most closely resembling *Champsosaurus*. *Ikechosaurus* has an expanded temporal region and an elongate snout, although the snout does not share the same degree of elongation as seen in *Champsosaurus*.

All neochoristoderes have a skeletal morphology that is most often thought of as being highly crocodiliform. *Champsosaurus* is often compared to extant piscivorous crocodilians such as *Gavialis gangeticus* (gharial) and

Tomistoma schlegelii (false gharial) because of cranial features such as an elongate snout and needle-like teeth. Feeding habits are thought to differ between *Champsosaurus* and the aforementioned crocodilians despite having the same food source (Erickson, 1985). The external nares on *Gavialis* and *Tomistoma* are directed dorsally and these animals are ideally suited for resting at the surface of the water, with only the external nares and eyes protruding from the surface (Erickson, 1985). The external nares of *Champsosaurus* are open anteriorly, which is unlike crocodilians. The orientation of the external nares has been hypothesized (Erickson, 1985) to allow *Champsosaurus* to use its snout as a snorkel when it rested on the bottom of a shallow body of water, or swam in deep water under the surface. *Ikechosaurus*, although being more closely related to *Simoedosaurus*, shares the elongate snout of *Champsosaurus* and thus probably shared the same strategy.

Simoedosaurus and *Tchoiria*, although sharing many cranial features with *Champsosaurus*, have shorter, broader snouts and are most often compared more with alligators and crocodiles in their ecological niche. *S. dakotensis* may not have been as aquatic (as good a swimmer) as *Champsosaurus*, and it is thought that it fed on fish and small tetrapods (Erickson, 1987). *S. lemoinei* from Europe appears to be more robust than its North American relative, and likely was more terrestrial, attacking mostly larger tetrapods for consumption (Erickson, 1987). *Tchoiria* shares the same cranial morphology with *Simoedosaurus* and most likely occupied a similar niche.

Jaw Musculature of Neochoristoderes

The cranium of the neochoristoderes is unique amongst tetrapods. The skull is dorso-ventrally flattened and the temporal chambers are enlarged compared to the remainder of the skull, most likely housing large jaw muscles (Gao and Fox, 1998). Surrounding this large temporal chamber are gracile temporal arches. The musculature within the temporal chamber of neochoristoderes has yet to be reconstructed. Previous authors recognized that there must have been a considerable mass of jaw musculature present in these animals, but as of yet no hypothesis has been generated regarding the morphology of the jaw musculature (Gao and Fox, 1998). As per Witmer (1995) the importance of reconstructing soft tissues (the jaw musculature) and their relationships to the skeleton in extinct animals is as follows: soft tissues are largely responsible for the existence, maintenance, and form of bones; inferences about the form and function of these soft-tissues is at the core of paleobiological hypotheses; and soft tissue relationships might provide testable hypotheses on independence or nonindependence of phylogenetic characters.

It has been demonstrated that bones are a product of epigenetic systems involving the interaction of nonosseous tissues (Hall, 1983, 1988, 1990). The existence and pattern of skeletal elements is partly dependent upon the action of soft tissues. For example, the formation of the dermal skull roof is initiated by the developing brain, and its morphology is determined by the combined pressure of the brain and cerebrospinal fluid (Carlson, 1981). Maintenance of skeletal morphology also is controlled by soft-tissues to such an extent that removing or

denervation of a particular soft tissue can result in the loss of its associated skeletal feature (Witmer, 1995). Thus morphological primacy falls on soft tissues rather than bones (Witmer, 1995).

Another benefit of reconstructing soft tissues is that soft tissues can help inform phylogenetic analyses (Witmer, 1995). If correlated features are counted as being separate in a cladistic analysis, the composite of which they are a part becomes more heavily weighted thereby increasing branch length. Witmer (1995) states that even though character splitting may give a boost to the consistency index of the analysis, it could invalidate the entire analysis by violating the assumption of independence. Knowledge of soft tissues can help merge correlated features into a single character.

The last and undoubtedly more applicable reason (in this study) is that the reconstruction of soft tissue characters is important for making inferences about the paleoecology of extinct organisms (Witmer, 1995). One needs only to observe extant animals to gauge the importance of soft tissues in regards to their ecology. Soft tissues are just as important for making paleobiological inferences. There is a chain of inference that is associated with paleoecology. The first link in the chain is to determine whether the soft tissue could be present, and if so what its morphology is. We can then proceed to the next link which is to determine how the soft tissue functions. Further inferences can be made regarding how this soft tissue contributes to our understanding of the behaviour or mode of life of this animal, which can then lead to inferences about how they interact with their community. However, each link in the chain is dependent upon the determination

at the previous link. Witmer (1995) cautions that incorrect assessments about soft tissue can exponentially change inferences the higher up in the hierarchy you proceed. Witmer and Rose (1991) use the jaw musculature of the bird *Diatryma* as an example of this problem. Analysis of the jaw musculature in *Diatryma* could indicate that the large bird was either a carnivore or herbivore (each with wider implications in the community as a whole). If *Diatryma* was herbivorous it might compete for resources with other large herbivores such as *Phenacodus*. Alternatively, if it was carnivorous it would be eating them. In either case the evolution of the community would be affected by the presence and extinction of *Diatryma*. Therefore, the study of soft-tissues in fossil taxa is not simply determining what the morphology and function of soft tissue, it is about fitting the fossil animal into the paleoecology of the community it was a part of.

In chapter 2 the morphology of the jaw adductor musculature of neochoristoderes is reconstructed herein using the extant phylogenetic bracketing method outlined in Witmer (1995). In chapter 3 the reconstructed jaw musculature will be used to investigate whether the differences between neochoristoderes and extant crocodilian correspond to differences in the function of the jaw adductor musculature. Rotational mathematics will be used to calculate the bite force, angular acceleration, and angular velocities of the lower jaws of both neochoristoderes and crocodilians. In chapter 4 digital models of *Champsosaurus natator*, *Champsosaurus lindoei*, *Simoedosaurus dakotensis*, *Crocodylus cataphractus*, *Alligator mississippiensis*, *Gavialis gangeticus*, and *Tomistoma schlegelii* will be created and their mechanical strength compared using finite

element analysis software. Fluid dynamic analyses will be used to determine how the skulls of neochoristoderes and crocodilians compare in hydrodynamics during lateral striking. The analyses in this study have not been conducted on neochoristoderes before and will be used to make inferences regarding their palaeoecology and how they compare to their extant ecological analogues, crocodilians.

CHAPTER 2: JAW ADDUCTOR MUSCLES OF THE NEOCHORISTODERA

Introduction

One of the greatest mysteries associated with *Champsosaurus* is the structure of the jaw musculature contained in their temporal chambers. The temporal chamber has expanded posteriorly and laterally and the temporal arches and the quadrate are gracile. The expanded temporal region has been hypothesized to house a large mass of muscle, but previous studies have only speculated on the morphology of the jaw adductor muscles and no concrete hypotheses have been made (Russell, 1956; Brinkman and Dong, 1993; Gao and Fox, 1998). This study will reconstruct the jaw musculature of *Champsosaurus* using the technique of extant phylogenetic bracketing (EPB) (Witmer, 1995), combined with observations of osteological features associated with the presence of muscle attachments. The reconstruction generated herein will be used in Chapter 3 to calculate the force generated by the muscles, the torque, and the angular acceleration and velocity of the mandibles.

The Extant Phylogenetic Bracketing (EPB) Method

The EPB method is used to reconstruct soft tissues or any other feature not typically preserved in a fossil specimen. The EPB was developed to provide a methodology to hypothesize about soft tissues in extinct organisms using phylogenetic relationships as constraints. The process is generally conducted by

determining the relationships between the soft tissues in question and their osteological correlates in the extant relatives of the fossil taxon, formulating hypotheses based on the idea that similarities among the extant relatives are due to inheritance from a common ancestor, and testing these hypotheses by surveying the fossil taxa for the osteological correlates.

The EPB method relies on the first two extant outgroups of the fossil organism in question to determine the ancestral condition of the soft tissue. To reconstruct a soft tissue in a fossil taxon, the osteological correlates between the fossil and its two closest extant relatives must pass the test of similarity (Patterson, 1982) or a 1:1 correspondence (Stevens, 1984). For example, both of the extant relatives must share the presence of a bone, and a similar morphology. Also, the osteological correlates in the bracket taxa must past the test of congruence (Patterson, 1982), in that the osteological features in question must be homologous. However, not only do the fossil taxon and its EPB need to have homologous osteological features, the causal relationships between the soft and hard tissues must be homologous (homologous soft tissues must produce homologous osteological correlates). Correlates are typically in the form of tuberosities, crests, grooves, fossae, foramina, fenestrae, septa, trochanters, or any features that are unambiguously a result of the presence of a soft tissue. Caution must be observed because more than one soft tissue may be responsible for an osteological feature. In the context of this study, the correlates being sought are the shared points of origin and insertion of the jaw adductor muscles.

The EPB method assumes that if the bracket taxa share a soft tissue character and its osteological correlate, then a strong hypothesis can be made that the fossil taxon also has the soft tissue character. But, what about cases where the bracket taxa do not share the same soft tissues? For example, Witmer (1995) uses the case of feathers in the entantiornithine bird *Ichthyornis*. The bracket taxa for *Ichthyornis* are birds and crocodilians, which leads to an equivocal conclusion because crocodilians lack feathers. However, Witmer (1995) stipulates that when the criteria of the EPB method are not met, compelling morphological evidence can justify a hypothesis. Because *Ichthyornis* shares with birds many of the characters associated with the presence of feathers, it can be said with confidence that feathers were present in *Ichthyornis*.

The EPB approach will be used to determine the morphology of the jaw musculature in the Choristodera. The position of the Choristodera within the Diapsida has a profound effect on what the two bracket taxa would be. If the Choristodera is near the base of the Diapsida as Evans (1988), Carroll and Currie (1991), Dilkes (1998), and Gao and Fox (1998) suggest, then it would fall between the Testudines (turtles) and Ledpidosauria (or Crocodylia) (Figure 2.1a), assuming that the Testudines are anapsids. If the Testudines is closely related to the Archosauromorpha, as suggested by Rieppel (2000), the Choristodera would then be bracketed by the Amphibia and the Lepidosauria (Figure 2.1b). If the Choristodera are the sister group to or within the Archosauromorpha (Currie, 1981; Erickson, 1985; Gauthier et al., 1988; Evans, 1990; Rieppel, 1993; Storrs and Gower, 1993; Storrs et al., 1996; de Braga and Rieppel, 1997; Jalil, 1997;

Rieppel, 1998) the extant phylogenetic bracket would be the Lepidosauria and the Crocodylia (Figure 2.1c). For the purposes of this study, the third alternative (brackets are the Lepidosauria and Crocodylia) was chosen because the majority of phylogenetic analyses suggest that the Choristodera is either the sister group or within the Archosauromorpha and the cranial morphology of lepidosaurs is more similar to choristoderes than that of turtles.

To reconstruct the jaw musculature of the neochoristoderes (*Champsosaurus* and *Simoedosaurus*), the musculature of *Sphenodon* will be used as a model. Traditionally, *Sphenodon* has been considered to be the most basal lepidosaur, however, recent research suggests that it is instead highly derived and that the lower temporal bar is secondarily acquired (Wu, 2003; Jones et al., 2009). However, even though the lower temporal bar in *Sphenodon* secondarily derived, it is preferable to the condition seen in other lepidosaurs in which the lower temporal bar remains absent. In addition, the jaw musculature of neochoristoderes will be reconstructed on the basis of crocodilian jaw muscles. The purpose of using both brackets independently is to determine which muscles have a 1:1 correspondence with both brackets, and only these can be reconstructed with confidence. Not all muscles will share the same origins and insertions in both brackets. The secondary purpose of applying the EPB is to determine which bracket taxon results in the greatest 1:1 correspondence overall, to determine which bracket neochoristoderes most closely resemble.

Jaw musculature in Sphenodon

The jaw musculature of *Sphenodon* was used as one of the models to reconstruct the jaw musculature in neochoristoderes. The jaw musculature of *Sphenodon* has been described in numerous studies (Byerly, 1925; Lakjer, 1926; Edgeworth, 1935; Ostrom, 1962; Barghusen, 1973; Haas, 1973; Gorniak et al., 1982; Wu, 2003; Holliday and Witmer, 2007; Jones et al., 2009). However, each study differs in the terminology and morphology of the jaw musculature. Haas (1973), Gorniak et al. (1982), Wu (2003), Holliday and Witmer (2007), and Jones et al. (2009) agree upon the following muscle groups in the jaw adductor chamber of *Sphenodon*: the musculus adductor mandibulae internus (mAMI), the M. adductor mandibulae externus (mAME), and the M. adductor mandibulae posterior (mAMP). These groups are defined based on which branches of the trigeminal nerve border each group. The mAMI contains four muscles that are bordered by the ophthalmic, and maxillary branches of the trigeminal nerve (Lakjer, 1926; Ostrom, 1962; Haas, 1973; Holliday and Witmer, 2007; Jones et al., 2009): the M. pseudotemporalis profundus (mPSTP) and superficialis (mPSTS), and the M. pterygoideus dorsalis (mPTD) and ventralis (mPTV). The last two are termed the M. pterygoideus atypicus and typicus respectively by Wu (2003) and Jones et al. (2009).

The mAME is defined as those muscles that are bordered by the maxillary and mandibular branches of the trigeminal nerve (Lakjer, 1926; Ostrom, 1962; Haas, 1973; Holliday and Witmer, 2007; Jones et al., 2009). The nomenclature of the muscles of the mAME is consistent in recent studies (Wu, 2003; Holliday and

Witmer, 2007; Jones et al., 2009) and included in the mAME are the M. adductor mandibulae superficialis (mAMES), medialis (mAMEM), and profundus (mAMEP). The last group, the mAMP, contains only one muscle and it is bordered solely by the mandibular branch of the trigeminal nerve (Lakjer, 1926; Ostrom, 1962; Haas, 1973; Holliday and Witmer, 2007; Jones et al., 2009).

The studies of Haas (1973), Gorniak at al. (1982), Wu (2003), Holliday and Witmer (2007), and Jones et al. (2009) do not agree upon the morphology of the jaw adductor muscles. Haas (1973) and Wu (2003) divide the mAMES into three distinct parts: the M. retractor aguli oris (mRAO), the M. levator aguli oris (mRAO), and the M adductor mandibulae externus superficialis sensu stricto (mAMESss). Other authors have divided the mAMES into Part 1a (mRAO + mLAO), and Part 1b (mAMESss) (Lakjer, 1926; Rieppel and Gronowski, 1981).

The mRAO according to Haas (1973) and Wu (2003) originates from the medial surface of the ventral half of the descending process of the squamosal, and at the suture between the squamosal and the quadratojugal. The fibres are oriented anteroventrally and the insertion of the mRAO is found on the dorsal-most margin of the lateral rictal plate (Haas, 1973; Wu 2003). The mLAO is described as a strap-shaped muscle that originates via a weak tendon on the medial surface of the postorbital near the suture with the post-frontal (Wu, 2003). The fibres of the mLAO are oriented posteroventrally and insert on the medial surface of the lateral rictal plate (Wu, 2003). Other researchers describe the mLAO as originating from the fascia of the lateral temporal fenestra, or the medial surface of the lower temporal bar (Poglayen-Neuwall, 1953; Rieppel and Gronowski, 1981).

The mAMES *sensu stricto* originates on the lateral temporal fascia, medial surface of the upper temporal bar, the posteromedial surface of the descending process of the jugal, and the medial surface of the descending process of the squamosal (Edgeworth, 1935; Anderson, 1936; Poglayen-Neuwall, 1953; Haas, 1973; Gorniak et al., 1982; Wu, 2003; Jones et al., 2009). The insertion is on the lateral surface of the dentary, coronoid, and surangular (Anderson, 1936; Rieppel and Gronowski, 1981; Gorniak et al., 1982) and possibly on the lateral surface of the basal aponeurosis (Haas, 1973; Wu, 2003; Jones et al., 2009). Wu (2003) divided the muscle into a larger anterolateral portion and a smaller posteromedial portion. Holliday and Witmer (2007) and the figures of Jones et al. (2009) do not acknowledge any divisions within the mAMES, and suggest that the origin is from the anterolateral surface of the squamosal and postorbital, and the insertion is on the lateral surface of the surangular.

The mAMEM originates from the posteromedial boundary of the upper temporal fenestra (Jones et al., 2009) and inserts upon the lateral surface of the basal aponeurosis (Anderson, 1936; Haas, 1973; Gorniak et al., 1982; Wu, 2003; Jones et al., 2009). Holliday and Witmer (2007) describe the origin of the mAMEM from the ventrolateral surface of the quadrate, lateral to the origin of the mAMP. Wu (2003) and Holliday and Witmer (2007) could not distinguish any subdivisions of the mAMEM, but Gorniak et al. (1982) described three: 1) a ventrolateral head that arises on the posteroventral and posterolateral surface of the parietal and from the anterior surface of the dorsal process of the squamosal, and inserts onto the anterior and central portion of the basal aponeurosis, 2) an

anteromedial head which originates on the dorsolateral surface of the parietal and inserts upon the anterodorsal extension of the basal aponeurosis, and 3) the posterior head, originates from the posterolateral surface of the parietal and the anterodorsal surface of the squamosal, and inserts onto the anterior and central portions of the basal aponeurosis dorsal to the insertions of the ventrolateral head. Haas (1973) divided the mAMEM into five subdivisions: the first two are the anteromedial and posterior heads (equal to the anteromedial and posterior heads described by Gorniak et al. [1982]), and the remaining three heads originate from the upper temporal arch (equated to the mAMES or mAMES *sensu stricto* described by other authors [Poglayen-Neuwall, 1953; Jones et al., 2009]). However, Jones et al. (2009) figures only one origin site for the mAMEM.

The mAMEP consists of two heads that arise deep to the mAMEM and insert on the medial surface of the basal aponeurosis (Haas, 1973; Gorniak et al., 1982; Wu, 2003; Jones et al., 2009). The description of the two heads of the mAMEP differs between authors. Haas (1973) described a posteroventral head that arises from the posterodorsal surface of the prootic, and a dorsal head that originates from the anterior surface of the squamosal process of the parietal and the posteromedial surface of the squamosal. Gorniak et al. (1982) described the medial and lateral heads that both originate from the anterolateral and posterolateral surfaces of the prootic. Wu (2003) does not show the prootic contributing to the origin of the mAMEP. The main portion of the muscle originates from the posterior wall of the upper temporal fenestra, while the posteroventral head originates from the anterolateral surface of the medial process

of the squamosal and the dorsolateral surface of the quadrate. Jones et al. (2009) found that the muscle originates from the posteroventral edge of the posterior temporal bar, which includes both the parietal and squamosal, and possibly from the anterodorsal surface of the quadrate.

The mPSTS originates from the anterolateral surface of the parietal and the posterior surface of the postfrontal (Anderson, 1936; Haas, 1973; Jones et al., 2009). Anderson (1936), Gorniak et al. (1982), and Holliday and Witmer (2007) include the prootic and the posterolateral surface of the lateral process of the postorbital in the surface of origin. Later studies (Wu, 2003; Jones et al., 2009) do not confirm the contribution of the prootic or the postorbital. Wu (2003) describes the origin of the mPSTS as extending onto the posterodorsal tip of the epipterygoid. The mPSTS inserts onto the medial surface of the basal aponeurosis (Anderson, 1936; Haas, 1973; Gorniak, 1982; Wu, 2003; Jones et al., 2009). Wu (2003) also show the insertion extending onto the posteromedial surface of the coronoid process.

The mPSTP has been divided into external and internal layers (Haas, 1973; Gorniak et al., 1982). The external layer originates from the anterolateral edge of the parietal and epipterygoid and from the posterodorsal expansion of the epipterygoid (Haas, 1973; Gorniak et al., 1982). The internal layer originates from the membranous wall of the braincase (Haas, 1973), but Gorniak et al. (1982) describe fibres also originating from the anterior surface of the epipterygoid. Wu (2003) does not divide the muscle into these layers and states that the mPSTP originates from the dorsal part of the epipterygoid and the anterodorsal wall of the

braincase. Holliday and Witmer (2007) describe the mPSTP as only originating from the medial surface of the prootic. The insertion is onto the medial surface of the coronoid, or just ventral to the coronoid (Anderson, 1936; Haas, 1973; Gorniak et al., 1982; Wu, 2003; Holliday and Witmer, 2007; Jones et al., 2009). Wu (2003) also includes the anteromedial surface of the surangular in the insertion of the mPSTP.

Gorniak et al. (1982) divide the mPTV into three separate parts: dorsal, middle, and ventrolateral. The dorsal part of the mPTV is the deepest of the three divisions and originates from the medial surface of the pterygoid and inserts onto the dorsomedial surface of the dentary (Gorniak et al., 1982). The middle part arises from the medial surface of the pterygoid process of the ectopterygoid, the medial margin and posteroventral half of the pterygoid, and the anteromedial process of the quadrate (Barghusen, 1973; Haas, 1973; Gorniak et al., 1982; Wu, 1982). However, Jones et al. (2009) do not consider the fibres arising from the quadrate to be part of the mPTV, because they are outside of the mandibular branch of the trigeminal nerve, and therefore are part of the mAMP. The insertion of the middle part is onto the posteromedial surface of the dentary (Gorniak et al., 1982). Finally, the ventrolateral part originates from the lateral and ventral surfaces of the ectopterygoid-pterygoid process and inserts onto the medial, ventral, ventrolateral surfaces of the posterior third of the dentary. Holliday and Witmer (2007) describe only one origin for the mPTV, from the ventrolateral surface of the pterygoid. Jones et al. (2009) report an insertion for the mPTV on

the dorsal surface of the lower jaw in a depression behind the articular surface, but just anterior to the insertion of the depressor mandibulae.

Haas (1973), Gorniak et al. (1982), Wu (2003), and Jones et al. (2009) describe the mPTD originating from the dorsal surface of the palate on or close to the palatine-pterygoid joint below the orbits. Haas (1973) and Wu (2003) also included the base of the interorbital septum in the origin of the mPTD. Holliday and Witmer (2007) described the mPTD originating from the dorsolateral surface of the pterygoid. The muscle extends posteriorly and loops around the pterygoid flange, inserting onto the coronoid (Jones et al., 2009). Wu (2003) described two tendinous insertions; one onto the posteroventral margin of the coronoid just above and anterior to the adductor fossa, and a smaller insertion onto the lower margin of the adductor fossa. Jones et al. (2009) surmised that the differences in the insertions of the mPTD may be the result of individual variation.

The morphology of the mAMP is the least controversial of the muscles of the jaw adductor chamber. The mAMP originates from the ventrolateral surface of the quadrate and extends nearly vertically to insert into the mandibular fossa (Haas, 1973; Wu, 2003; Holliday and Witmer, 2007; Jones et al., 2009).

The function of the M. depressor mandibulae (mDM) is opposite to that of the jaw adductor muscles; when it contracts it opens the jaws. In *Sphenodon* the mDM originates from the posterodorsal edge of the parietal and squamosal and from a small midline sheet of connective tissue (Byerly, 1925; Gorniak et al., 1982; Al-Hassawi, 2007; Jones et al., 2009). Gorniak et al. (1982) and Jones et al. (2009) describe three parts to the mDM: a thin dorsal portion, a thick middle part,

and a ventral portion that tapers towards the insertion on the lower jaw. Ridges and pits have been reported on the areas of origin (Al-Hassawi, 2007). However, this observation has not been fully supported in other studies (Jones et al., 2009). Gorniak et al. (1982) and Jones et al. (2009) further subdivide the mDM into medial and lateral portions based on textural and colour differences. The mDM is figured in Wu (2003) and Jones et al. (2009) as inserting onto the ventral surface of the articular, posterior to the insertion of the mPTV.

Crocodilian Jaw Musculature

Numerous myological studies have been conducted on the jaw musculature of crocodilians *Alligator mississippiensis* (Iordansky, 1973; Schumacher, 1973; Busbey, 1989), *Crocodylus* (Holliday and Witmer, 2007), caiman (van Drongelen and Dullemeijer, 1982; Cleuren and De Vree, 1992; Holliday and Witmer, 2007), and longirostrine crocodilians (Iordansky, 1973; Langston, 1973; Endo et al., 2002). There are inconsistencies regarding the terminology and morphology of the muscles of the adductor chamber in crocodilians in recent studies (Busbey, 1989; Cleuren and De Vree; 1992; Iordansky, 2000; Endo et al.,2002). Holliday and Witmer (2007) standardized the nomenclature of crocodilian jaw musculature with the terminology used in lepidosaurian myological studies. The description of the jaw musculature in crocodilians described by Holliday and Witmer (2007) has also been used to reconstruct the jaw musculature of *Iharkutosuchus* (Osi and Weishampel, 2009).

The mAMES attaches to the ventrolateral surface of the quadrate and the quadratojugal (Holliday and Witmer, 2007), lateral to the origin of the mAMP. The muscle extends vertically and slightly anteriorly, and some fibres insert onto the lateral lamina of the mandibular adductor tendon; the remainder insert on the dorsolateral surface of the surangular (Holliday and Witmer, 2007).

The mAMEM originates from the anteromedial surface of the quadrate, posteroventral to the trigeminal foramen, dorsolateral to the origin of the mAMP, and ventromedial to the origin of the mAMEP (Busbey, 1989; Holliday and Witmer, 2007). The muscle merges with the mAMES and mAMEP to attach onto the coronoid eminence (Holliday and Witmer, 2007). Some fibres also attach to the dorsal surface of the surangular (Holliday and Witmer, 2007).

Holliday and Witmer (2007) found that the mAMEP in crocodilians originates from the ventrolateral surface of the parietal and inserts onto the dorsomedial surface of the coronoid eminence of the surangular. The muscle is small, semicircular in cross-section, and pinnate in alligatorids and many crocodylids (Holliday and Witmer, 2007). In longirostrine crocodilians it becomes larger and more circular in cross section (Iordansky, 1973; Langston, 1973; Endo et al., 2002; Holliday and Witmer, 2007).

The mPSTS originates from the posterior surface of the postorbital process of the laterosphenoid, anterior to the mAMEP and anterodorsal to the maxillomandibular foramen (Holliday and Witmer, 2007). Holliday and Witmer (2007) described that the mPSTS inserts onto to the dorsal surface of the lower surface of the mandibular fossa, anterior to the insertion of the mAMP, with some

fibres merging with the mAMEP near the medial surface of coronoid eminence. The mPSTP in crocodilians originates from the lateral bridge of the laterosphenoid ventral to the mPSTS, and some fibres were found to attach to the ventrolateral surface of the maxillary nerve as well (Holliday and Witmer, 2007). The mPSTP merges with the dorsal fibres of the mPTD and inserts near the posterodorsal surface of the angular (Holliday and Witmer, 2007).

The mPTV originates from the posterior rim of the pterygoid flange and the posterolateral surface of the ascending process of the pterygoid (Holliday and Witmer, 2007). The mPTV extends posteriorly and wraps around the mPTD and the retroarticular process to attach onto the posterolateral surface of the angular (Holliday and Witmer, 2007). The mPTD is a large muscle that originates from the dorsal surface of the palate of the suborbital area with cranial attachments in the cavioconchal fossa of the maxillary and palatine suture, the posterolateral surface of the postconchal nasal cartilage, the dorsomedial surface of the palatine, the ventrolateral surface of the lacrimal, the dorsomedial surface of the maxilla/ectopterygoid contact, the margins of the suborbital fenestra, the cartilaginous interorbital septum, the lateral surface of the cultiform process, and the ascending process of the pterygoid (Holliday and Witmer, 2007). The muscle extends posteriorly and inserts onto the ventromedial surfaces of the angular and articular ventral to the glenoid of the lower jaw (Holliday and Witmer, 2007). The medial part of the muscle inserts via a tendon onto the ventromedial edge of the medial mandibular fossa, just posterior to the pterygoid flange (Holliday and

Witmer, 2007). The lateral part inserts as a tendon onto the dorsomedial edge of the articular (Holliday and Witmer, 2007).

The mAMP originates from most of the ventral surface of the quadrate, medial to the origin of the mAMES, ventral to that of the mAMEM, and lateral to that of the mPTV (Holliday and Witmer, 2007). The mAMP extends vertically to insert onto the medial surface of the margin of the mandibular fossa, filling most of the fossa (Holliday and Witmer, 2007). The mAMP is one of the largest muscles of the adductor chamber, being dwarfed only by the pterygoideus muscles (Schumacher, 1973; Busbey, 1989). The position of the mDM is consistent in all studies (Busbey, 1989; Iordanksy; Endo et al., 2002), originating from the posterior surface of the squamosal and quadrate and inserting upon the dorsal surface of the retroarticular process, the portion of the mandible that extends posteriorly from the articular surface in crocodilians.

Materials and Methods

Specimens

TMP 1981.47.1 – Partial mandible of *Champsosaurus*.

TMP 1986.12.11 – Partial cranium and mandible of *Champsosaurus albertensis*.

TMP 1987.36.41 – Partial cranium of *Champsosaurus lindoei*.

TMP 1994.163.1 – Partial cranium of *Champsosaurus lindoei*.

UALVP 931 – Nearly complete skeleton of *Champsosaurus lindoei*.

UALVP 33928 – Partial cranium of *Champsosaurus lindoei* missing the anterior half of the snout.

UALVP 47243 – Partial cranium of *Champsosaurus natator*, missing the left temporal arch, and braincase.

UAMZ HER-R405 – complete skeleton of *Sphenodon punctatus*

UAMZ HER-R800 – complete skull of *Alligator mississippiensis.*

UAMZ HER-R802 – complete skull of *Gavialis gangeticus.*

UAMZ HER-R803 – complete skull of *Crocodylus cataphractus.*

UAMZ HER-R805 – complete skull of *Tomistoma schlegelii.*

The osteology of the cranium and mandible of *Champsosaurus* is illustrated in Figure 2.2, and a similar morphology has been described in *Simoedosaurus* (Erickson, 1987). All specimens were examined for osteological features associated with muscle attachment. These osteological markers were used to constrain the locations of the hypothesized muscle attachment sites of the EPB method. Rugosities, fossae, and crests strongly suggest the presence of muscles, and could support or contradict the EPB method.

The attachment sites in neochoristoderes were reconstructed so that they shared a 1:1 correspondence with *Sphenodon* as described by Wu (2003) and Jones et al. (2009). A second reconstruction using the jaw musculature of *Sphenodon* as described by Holliday and Witmer (2007) was made because of the differences between them and the descriptions of Wu (2003) and Jones et al. (2009). However, because rhynchocephalians and crocodilians do not share a 1:1 correspondence between their muscle origins and insertions (Holliday and Witmer, 2007) it cannot be assumed that a 1:1 correspondence will exist between

Sphenodon and neochoristoderes. Therefore, a separate jaw muscle reconstruction of neochoristoderes was also conducted with a 1:1 correspondence with crocodilians (Holliday and Witmer, 2007).

Results

Examinations of UALVP 931, UALVP 33928, UALVP 47243, TMP 1981.47.1 TMP 1986.12.11, and TMP 1987.36.41 reveal that there are few osteological features indicating the presence of muscle attachments. In UALVP 33928, UALVP 47243, and TMP 1986.12.11, the portion of the parietal on the dorsal wall of the braincase forms a small crest that indicates the presence of muscle attachment. Rugosities are present on the dorsal surfaces of the surangular and coronoid in TMP 1981.47.1. The only other clear indications of the presence of muscle attachments in UALVP 33928, UALVP 33929, UALVP 47243, TMP 1986.12.11, TMP 1987.36.41, and TMP 1994.163.1 are shallow fossae on the lateral wall of the braincase, the dorsal surface of the quadrate, and the dorsal surface of the pterygoid. The mandibular fossa and a shallow fossa on the dorsal surface of the surangular were observed in TMP 1986.12.11 and TMP 1981.47.1.

In UAMZ HER-R405 (*Sphenodon punctatus*) there are few direct indicators of the presence of the jaw muscles. In crocodilians, muscle scars are present only on the dorsal surface of the coronoid. The dorsal surface of the pterygoid, ventral surface of the quadrate, and lateral wall of the braincase have shallow fossae encompassing their surfaces. On the mandible there are large

fossae on the ventromedial and ventrolateral surfaces of the articular, and a large mandibular fossa.

When the muscles of *Sphenodon* was compared to that of crocodilians was compared, the only two muscles that shared the same origin in both were the mAMP and the mAMEP. For insertions, the only common muscles were the mAMP, mAMES, mAMEM, and mAMEP. The differences of the origins and insertions of the three reconstructions are summarized in Tables 1.1 and 1.2.

Reconstruction 1: Sphenodon (Wu, 2003; Jones et al., 2009) (Figure 2.3)

The reconstruction of the jaw musculature of neochoristoderes resulting from a 1:1 correspondence with the description of the jaw musculature of *Sphenodon* found in Wu (2003) and Jones et al. (2009) is depicted in Figure 2.3. The muscles of the mAME attach to the dorsolateral and dorsoposterior margins of the adductor chamber. The mAMES was the largest muscle in the adductor chamber of all neochoristoderes, being approximately half of the total muscle attachment area in the adductor chamber in *Champsosaurus*, and forty percent of the total attachment area in *Simoedosaurus* (due to the increased size of the mAMEM and mAMEP). The mAMES originated from the ventral surfaces of the upper temporal bar, from the postorbital and squamosal. Wu (2003) and Jones et al. (2009) report the presence of fascia covering the lateral temporal fenestra from which part of the mAMES originated, and is incorporated in this reconstruction. The insertion was on the lateral surface of the mandible, on the surangular and dentary.

The mAMEM originated from the dorsoposterior margin of the parietal and squamosal. The mAMEP originated from the dorsoanterior, and possibly the ventroanterior margin of the parietal, and extended onto to the squamosal. Both muscles formed thin sheets that extend to and inserted upon the dorsal surface of the coronoid and surangular. Myological studies have demonstrated that the mAMEM and mAMEP insert directly on the lateral and medial surfaces, respectively, of the basal aponeurosis (Haas, 1973; Gorniak et al., 1982; Wu, 2003; Jones et al., 2009). The basal aponeurosis in neochoristoderes inserted upon the shelf of the dorsal surface of the surangular. In *Champsosaurus* the mAMEM and AMEP were each approximately seven to ten percent of the total muscle attachment area. In *Simoedosaurus* these muscles were larger, being twelve and nine percent respectively. The mAMP was the second largest muscle in the adductor chamber. The mAMP originated from the dorsal surface of the quadrate, and inserted into the mandibular fossa.

Immediately anterior to the medial border of the mAMEM was the attachment site for the mPSTS. The location of the mPSTS was further supported by the presence of a rugose surface texture present on the dorsolateral surface of the braincase in UALVP 33928 and UALVP 47243. The size of the mPSTS was dependent upon the area of the dorsolateral surface of the parietal. The mPSTS in UALVP 33928, TMP 1984.3.9, and *Simoedosaurus* formed between five and six percent of the origin attachment area and eleven percent in UALVP 47243. The mPSTS extended laterally to the insert upon the medial surface of the coronoid. The mPSTP was one of the smallest muscles in the adductor chamber at one to

three percent of the attachment area. The mPSTP originated from the anterolateral surface of the prootic and some fibres originated from the epipterygoid (a thin, rod-like bone anterior to the braincase [Gao and Fox, 1998]). The mPSTP extended ventrolaterally to insert immediately ventral to the mPSTS on the medial surface of the coronoid.

The pterygoideus muscles were the deepest muscles of the adductor muscles in neochoristoderes. The larger of the two was the mPTV, which comprised three to six percent of the attachment area in the adductor chamber. The mPTV formed a sheet of muscle originating anterior to the base of the braincase, specifically from the dorsolateral surface of the pterygoid, and extending onto the dorsoposterior surface of the ectopterygoid. The mPTV inserted onto the posteromedial, ventral, and ventrolateral surfaces of the angular. The mPTD originated from the dorsal surfaces of the pterygoid and palatine. The mPTD wrapped over the mPTV and inserted ventral to the insertion of the mPSTP on the medial surface of the coronoid.

The mDM originated from the posterior surface of the posttemporal bar and inserted on the ventral surface of the articular. The origins of the medial and lateral divisions of the mDM form thin strips of muscle that taper as they approach their insertions.

Reconstruction 2: Sphenodon (Holliday and Witmer, 2007) (Figure 2.4)

The second neochoristodere reconstruction (Figure 2.4), developed from the description of the jaw musculature of *Sphenodon* in Holliday and Witmer

(2007), differs from the first reconstruction, which is based on Wu (2003) and Jones et al. (2009). Holliday and Witmer (2007) do not describe the morphology of the mDM in their description of the jaw musculature of *Sphenodon*. The mAMP occupied the same position on the dorsal surface of the quadrate and inserts into mandibular fossa.

The mAMEM originated lateral to the mAMP on the dorsal surface of the squamosal, rather than on the posterodorsal surface of the posttemporal bar (formed by the postorbital and squamosal) as in the previous reconstruction. The mAMEP was the sole muscle occupying the dorsal surface of the posttemporal bar, including the squamosal and parietal contributions. The mAMES occupied the same position as in the previous reconstruction, but Holliday and Witmer (2007) do not describe the presence of any fascia covering the lateral temporal fenestra, and therefore the mAMES is not reconstructed covering the fenestra.

The mPSTS originated from the dorsolateral surface of the parietal, and the origin extended onto the prootic. The mPSTP originated from the lateral surface of the prootic and the epipterygoid. The mPTD originated from the dorsal surfaces of the pterygoid and ectopterygoid and inserted onto the ventromedial surface of the angular. The mPTV was located more ventrally compared to the previous reconstruction, originating from the ventrolateral edge of the pterygoid, posterior to the ectopterygoid, and extending onto the anteroventral edge of the quadrate.

Reconstruction 3: Crocodilian (Holliday and Witmer, 2007) (Figure 2.5)

The final reconstruction is based on the jaw musculature of crocodilians as described by Holliday and Witmer (2007) and is illustrated in Figure 2.5. The origin and insertion of the mAMP remains consistent with those of the previous reconstructions, arising from the dorsal surface of the quadrate and inserting into the mandibular fossa. The mAMEP originated from the dorsal surface of the parietal, extending from the dorsal part of the wall of the braincase and the posttemporal bar. The mAMEM originated as a thin strip medial to the origin of the mAMP. The mAMES originated lateral to the mAMP, from the dorsal surface of the squamosal, and formed a thin strip tucked under the upper temporal bar. The insertions of the mAME are the same as those in the second reconstruction.

The origins of the pseudotemporalis muscles cannot be accurately reconstructed. However, the insertion of the mPSTP can be reconstructed and was further posterior compared to the prior reconstructions, and attached to the dorsomedial surface of the angular. The mPTD and mPTV originated from the palate. The mPTV arose from the dorsal surface of the pterygoid, between the base of the braincase and the ectopterygoid, and inserted upon the ventrolateral surface of the angular and may have extended dorsally onto the posterolateral surface of the surangular. The mPTD originated anteriorly to the mPTV upon the dorsal surfaces of the pterygoid and the ectopterygoid. The mPTD inserted onto the ventromedial surface of the angular.

The position of the mDM also differs from the position seen in the first reconstruction. The mDM originated from the ventral surface of the quadrate and

overlaps onto the ventral surface of the squamosal. The mDM inserted onto the ventral surface of the articular.

Discussion

The three reconstructions resulting from the use of the EPB method differ considerably from one another and there are few similarities found. The only consistencies (and results of the EPB method) between the three reconstructions are the locations of the mAMP and AMEP. The mAMP originated from the dorsal surface of the quadrate and inserted into the mandibular fossa. Therefore, the position of the mAMP is reconstructed with confidence, because it shares a 1:1 correspondence with *Sphenodon* and crocodilians. The orientation of the mAMP differs from those of *Sphenodon* and crocodilians. In the extant taxa, the mAMP is nearly vertical, whereas in neochoristoderes it is nearly horizontal and must curve towards its insertion, due to the skull in neochoristoderes being dorsoventrally flattened.

The position of the mAMEP remains similar throughout the reconstructions as well. In all cases the mAMEP originates from the dorsal surface of the posttemporal bar and inserts onto the dorsomedial surfaces of the coronoid and surangular. However, the relationships of the mAMEP to the remaining muscles are contentious. The mAMEP in the Wu (2003) and Jones et al. (2009) *Sphenodon* reconstruction shares the posttemporal bar with the mAMEM, which is not indicated by the descriptions in Holliday and Witmer (2007). The insertion of the mAMEP is consistently on the dorsomedial surface of

the coronoid and surangular in all three reconstructions, although Holliday and Witmer (2007) do not describe the presence of the basal aponeurosis. The resulting muscle line of action for the mAMEP in all cases is anteroventral and must wrap over the mAMP.

The origin of the mAMEM differs dramatically in the three reconstructions. The mAMEM in the first reconstruction originates from the anteroventral surface of the posttemporal bar, whereas in the second reconstruction the mAMEM is not on the posttemporal bar and occupies a position lateral to the posttemporal fenestra and the origin of the mAMP. The difference between the two reconstructions also impacts the size, and thus the force produced, of the mAMEM and mAMEP relative to the remaining jaw musculature. The size of the mAMEM and mAMEP is smallest in the Wu (2003) and Jones et al. (2009) *Sphenodon* reconstruction. The mAMEM differs in the crocodilian reconstruction, and originates from the dorsomedial surface of the quadrate. The insertion of the mAMEM is consistently upon the dorsal surface of the coronoid and surangular, but only the reconstruction based on the descriptions of Wu (2003) and Jones et al. (2009) accounts for the presence of the basal aponeurosis. The mAMEM extends anteroventrally, and in the first reconstruction must wrap over the mAMEP and mAMP.

The position of the mAMES is different in each reconstruction. The fascia over the lateral temporal fenestra is only present in the first reconstruction (based on Wu (2003) and Jones et al. (2009)), and is absent in the reconstruction based on Holliday and Witmer (2007). The fascia over the lateral temporal fenestra has

been described in many previous studies (Edgeworth, 1935; Anderson, 1936; Poglayen-Neuwall, 1953; Haas, 1973; Gorniak et al., 1982; Wu, 2003). The reconstruction based on the jaw musculature of crocodilians is unique because the mAMES originates from the dorsal surface of the squamosal and leaves the upper temporal bar and the lateral temporal fenestra barren of any musculature. Previous studies have attributed the presence of temporal fenestrae to frequent loading creating net tensions on the surfaces of the bones, which results in bone being replaced by membranes (Oxnard et al.,1995; Witzel and Preuschoft, 2005). Therefore, the formation of the lateral temporal fenestra could be the result of loading caused by the frequent contraction of jaw musculature, and the reconstruction using the crocodilian musculature does not account for the presence of the expanded lateral temporal fenestra in neochoristoderes.

The pterygoideus muscles consistently originate from the surface of the pterygoid, but their origins differ between the reconstructions. The mPTD consistently remains on the dorsal surface of the pterygoid. In the first reconstruction the mPTD must wrap over the mPTV and the ectopterygoid, whereas in the remaining two reconstructions the mPTD extends directly to the insertion. The mPTV originates from either the dorsal surface of the pterygoid (Reconstructions 1 and 3), or from the ventral edge of the pterygoid (Reconstruction 2).

The pseudotemporalis muscles in the *Sphenodon* reconstructions originate from the dorsolateral wall of the braincase and from the epipterygoid. However, the crocodilian reconstruction does not contain either of the pseudotemporalis

muscles. The origin in crocodilians is from the lateral surfaces of the laterosphenoid, a bone that is not ossified in *Champsosaurus* (Russell, 1956; Fox, 1968; Gao and Fox, 1998). Therefore, when using the crocodilian model, a 1:1 correspondence between the osteological features of choristoderes and crocodilians could not be established, and the pseudotemporalis muscles cannot be reconstructed.

The mDM also does not share a 1:1 correspondence between the bracket taxa, leading to an equivocal conclusion regarding its morphology in neochoristoderes. The origin in *Sphenodon* is from the posterior surface of the posttemporal bar (parietal and squamosal) (Gorniak et al. 1982; Jones et al., 2009), whereas in crocodilians the mDM originates from the posterior surface of the quadrate and squamosal. The retroarticular process, onto which the mDM in crocodilians inserts, is not present in either *Sphenodon* or choristoderes. Therefore, the only possible insertion is on the ventral surface of the articular. Because choristoderes share with *Sphenodon* the lack of certain osteological features, it suggests a greater affinity of choristoderes with rhynchocephalians in the case of the mDM. Thus, it is likely that the origin of the mDM in neochoristoderes is best represented by the Wu (2003) and Jones et al. (2009) *Sphenodon* reconstruction. The size of the attachment sites of the mDM in neochoristoderes suggests that they were weak muscles, even less than the mDM of crocodilians. This may suggest that neochoristoderes may have taken longer to open their jaws and thus must have had to wait longer between strikes.

The morphology of the mDM affects the morphology of the neck muscles that attach to the posterior of the skull. The large surface area of the quadrate and squamosal suggest the presence of extensive neck musculature, which may have flexed the skull laterally with great speed. The neck muscles of *Sphenodon* have been described in previous studies (Bylery, 1925; Von Wettstein, 1931; Gasc, 1981; Al-Hassawi, 2007; Tsuihiji, 2005 and 2007; Jones et al., 2009) and the application of the EPB method could resolve their morphology and biomechanics.

None of the reconstructions utilize the surface of the neomorph bone that is present in the posterolateral wall of the braincase (Fox, 1968; Gao and Fox, 1998). The presence of the neomorph on the lateral wall of the braincase is unique to all of the members of the Choristodera (Evans, 1990; Gao and Fox, 1998). Therefore, the EPB method cannot be used to hypothesize the contribution of this bone to the surrounding musculature. The mPSTS, mPSTP, and mAMP originate from bones adjacent to the neomorph (Figure 2.2). The most likely muscle partly originating from the neomorph is the mPSTP, which would expand posteriorly and form a sheet of muscle.

Of the three reconstructions of the jaw musculature of neochoristoderes the most plausible is the reconstruction based on the *Sphenodon* work of Wu (2003) and Jones et al. (2009). The musculature of the crocodilian reconstruction poses uncertainties regarding the origins and insertions of two muscles. According to the criteria of extant phylogenetic bracketing, a 1:1 correspondence of the osteological feature in question is required to confidently reconstruct any soft tissue (Witmer, 1995). Therefore, under this strict criterion the pseudotemporalis

muscles cannot be reconstructed because the laterosphenoid (from which the muscles originate in crocodilians) does not ossify in *Champsosaurus* (Russell, 1956; Fox, 1968; Gao and Fox, 1998).

From a functional perspective, the third reconstruction (crocodilian model) does not account for the presence of the enlarged lateral temporal fenestra in neochoristoderes. Fenestrae have been thought to form as a result of frequent tension being applied to the bone surface (Oxnard et al.,1995; Witzel and Preuschoft, 2005). For example, when a muscle contracts it pulls on the surface of the bone, resulting in tension (stretching). Therefore, functionally speaking, if the lateral temporal fenestra does not have any musculature attaching to it why would it be so large in neochoristoderes? However, it is possible that the presence and morphology of the lateral temporal fenestra is partially the result of the evolutionary history of the Neochoristodera and its size correlating with the increase in size of the temporal region.

Excluding the reconstruction based on the crocodilian bracket leaves only the *Sphenodon* reconstructions based on Holliday and Witmer (2007) or that of Wu (2003) and Jones et al. (2009). The origins of the mAMEP, mPSTS, and the mPTD differ dramatically between the two reconstructions. Jones et al. (2009) state that other than individual variation, discrepancies between different studies (Haas, 1973; Gorniak et al., 1983; Wu, 2003; Holliday and Witmer, 2007) could be the result of specimen quality, descriptive accuracy, homology criteria, and illustration quality. Jones et al. (2009) criticized the illustrative quality of the temporal chamber in Holliday and Witmer (2007) because some of the muscles do

not correspond to those of any previous description and the mAMEP as figured and described originates superficial to the traditionally more superficial mAMEM. Additionally, Holliday and Witmer (2007) do not describe the presence of the basal aponeurosis, a feature consistently reported as connecting the mAMEM and mAMEP to the mandible (Haas, 1973; Gorniak et al., 1983; Wu, 2003; Jones et al., 2009). Therefore based on the illustrative and descriptive quality of the jaw musculature of *Sphenodon* as described by Holliday and Witmer (2007), the reconstruction based on the comprehensive descriptions of Wu (2003) and Jones et al. (2009) is preferred for use in the analysis of jaw muscle function.

The morphology of the musculature in the preferred reconstruction indicates that the primary muscles responsible for the adduction of the jaw in choristoderes are the mAMES and the mAMP due to the greatly expanded lateral temporal fenestra and quadrate. Of the remaining musculature, the mPSTP and the mPTD are the least important for jaw adduction. This differs from the condition seen in crocodilians in which the pterygoideus muscles are the largest muscles in the skull.

Conclusion

This chapter examined the most likely jaw adductor morphology present in the crania of neochoristoderes using the EPB method. The preferred hypothesis of the jaw muscle morphology was based on *Sphenodon* as described by Wu (2003) and Jones et al. (2009) (Figure 2.2). The reconstruction resulting from the musculature of *Sphenodon* as described by Holliday and Witmer (2007) (Figure

2.3) was deemed to be unsatisfactory due to the lack of descriptive quality in regards to rhynchocephalians. The morphology seen in crocodilians, as described by Holliday and Witmer (2007), was used as one of the models (Figure 2.4), but was not preferred because it did not share a complete 1:1 correspondence between osteological features. The laterosphenoid (to which the pseudotemporalis muscles attach) does not ossify in neochoristoderes and could not be reconstructed (Russell, 1956; Fox, 1968; Gao and Fox, 1998). Additionally, no musculature originates from the upper temporal bar and lateral temporal fenestra. Considering that fenestra can form as a result of frequent tension (from a muscle) acting upon bone (Oxnard et al.,1995; Witzel and Preuschoft, 2005), the presence of the large lateral temporal fenestra is puzzling from a functional perspective. Although, the evolutionary history of the Neochoristodera (expanding temporal region) could be a contributing factor determining the presence and size of the lateral temporal fenestra.

In the preferred reconstruction the most significant muscles of the temporal chamber are the mAMES and the mAMP as a result of the enlargement of the quadrate, the squamosal, and the temporal openings. The least important muscles are the mPSTP, and mPTD. Not only does the enlarged adductor chamber result in a size increase of the mAMES and mAMP, it possibly results in enlarged neck musculature for rotating the head laterally when striking at prey. The hypothesis presented in this chapter can be used to speculate as to which muscles of the temporal chamber were most important in biting. However, further research into the biomechanics of the jaw musculature, utilizing rotational

mathematics (Halliday et al., 2001; Snively and Russell, 2007) can give additional insight into the function of the jaws in neochoristoderes and is the subject of the next chapter.

Chapter 2: Tables

Muscle	Reconstruction 1 (*Sphenodon*; Wu [2003[, and Jones et al. [2009])	Reconstruction 2 (*Sphenodon*; Holliday and Witmer [2007])	Reconstruction 3 (crocodilian; Holliday and Witmer [2007])
M. adductor mandibulae posterior (mAMP) (Green)	Dorsal surface of the quadrate	Dorsal surface of the quadrate	Dorsal surface of the quadrate
M. adductor mandibulae externus superficialis (mAMES) (Light Blue)	Ventral surface of the upper temporal bar, margin and fascia of the lateral temporal fenestra	Ventral surface of the upper temporal bar	Dorsal surface of the quadrate and squamosal lateral to the M. adductor mandibulae posterior
M. adductor mandibulae externus medialis (mAMEM) (Purple)	Dorsal surface of the parietal (posttemporal bar)	Dorsal surface of the quadrate and squamosal lateral to the M. adductor mandibulae posterior	Dorsal surface of the quadrate medial to the M. adductor mandibulae posterior
M. adductor mandibulae externus profundus (mAMEP) (Dark Blue)	Dorsoanterior surface of the parietal (posttemporal bar) anterior to the M. adductor mandibulae externus medialis	Dorsal surface of the parietal (posttemporal bar)	Dorsal surface of the parietal (posttemporal bar)
M. pseudotemporalis superficialis (mPSTS) (Pink)	Dorsolateral surface of the parietal (braincase)	Dorsolateral surface of the parietal, and lateral surface of the prootic (braincase)	—
M. pseudotemporalis profundus (mPSTP) (Yellow)	Lateral surface of the prootic	Lateral surface of the prootic	—
M. pterygoideus dorsalis (mPTD) (Orange)	Dorsal surface of the pterygoid and palatine	Dorsal surface of the pterygoid and ectopterygoid	Dorsal surface of the ectopterygoid
M. pterygoideus ventralis (mPTV) (Red)	Dorsal surface of the pterygoid and ectopterygoid	Ventrolateral surface of the pterygoid	Dorsal surface of the pterygoid
M. depressor mandibulae (mDM) (Not shown)	Posteroventral surface of the posttemporal bar (parietal and squamosal)	—	Posteroventral surface of the quadrate and squamosal

Table 1.1: Origins of the jaw musculature in neochoristoderes reconstructed using extant phylogenetic bracketing.

Muscle	Reconstruction 1 (*Sphenodon*; Wu [2003[, and Jones et al. [2009])	Reconstruction 2 (*Sphenodon*; Holliday and Witmer [2007])	Reconstruction 3 (crocodilian; Holliday and Witmer [2007])
M. adductor mandibulae posterior (mAMP) (Green)	Manibular fossa (dorsal surface of angular and splenial)	Manibular fossa (dorsal surface of angular and splenial)	Manibular fossa (dorsal surface of angular and splenial)
M. adductor mandibulae externus superficialis (mAMES) (Light Blue)	Lateral surface of the surangular	Lateral surface of the surangular	Lateral surface of the surangular
M. adductor mandibulae externus medialis (mAMEM) (Purple)	Lateral surface of the basal aponeurosis (dorsal surface of the surangular)	Dorsolateral surface of the surangular	Dorsolateral surface of the surangular
M. adductor mandibulae externus profundus (mAMEP) (Dark Blue)	Medial surface of the basal aponeurosis (dorsal surface of the angular)	Dorsomedial surface of the surangular	Dorsomedial surface of the surangular
M. pseudotemporalis superficialis (mPSTS) (Pink)	Dorsomedial surface of the surangular and coronoid	Dorsomedial surface of the surangular and coronoid	—
M. pseudotemporalis profundus (mPSTP) (Yellow)	Medial surface of the coronoid	Medial surface of coronoid	Dorsomedial surface of the angular
M. pterygoideus dorsalis (mPTD) (Orange)	Medial surface of the coronoid and splenial	Ventromedial surface of the angular	Ventromedial surface of the angular
M. pterygoideus ventralis (mPTV) (Red)	Ventrolateral surface of the angular	Ventrolateral surface of the angular	Ventrolateral surface of the angular
M. depressor mandibulae (mDM) (Not shown)	Ventral surface of the articular	—	Ventral surface of the articular

Table 1.2: Insertions of the jaw musculature in neochoristoderes reconstructed using extant phylogenetic bracket.

Chapter 2: Figures

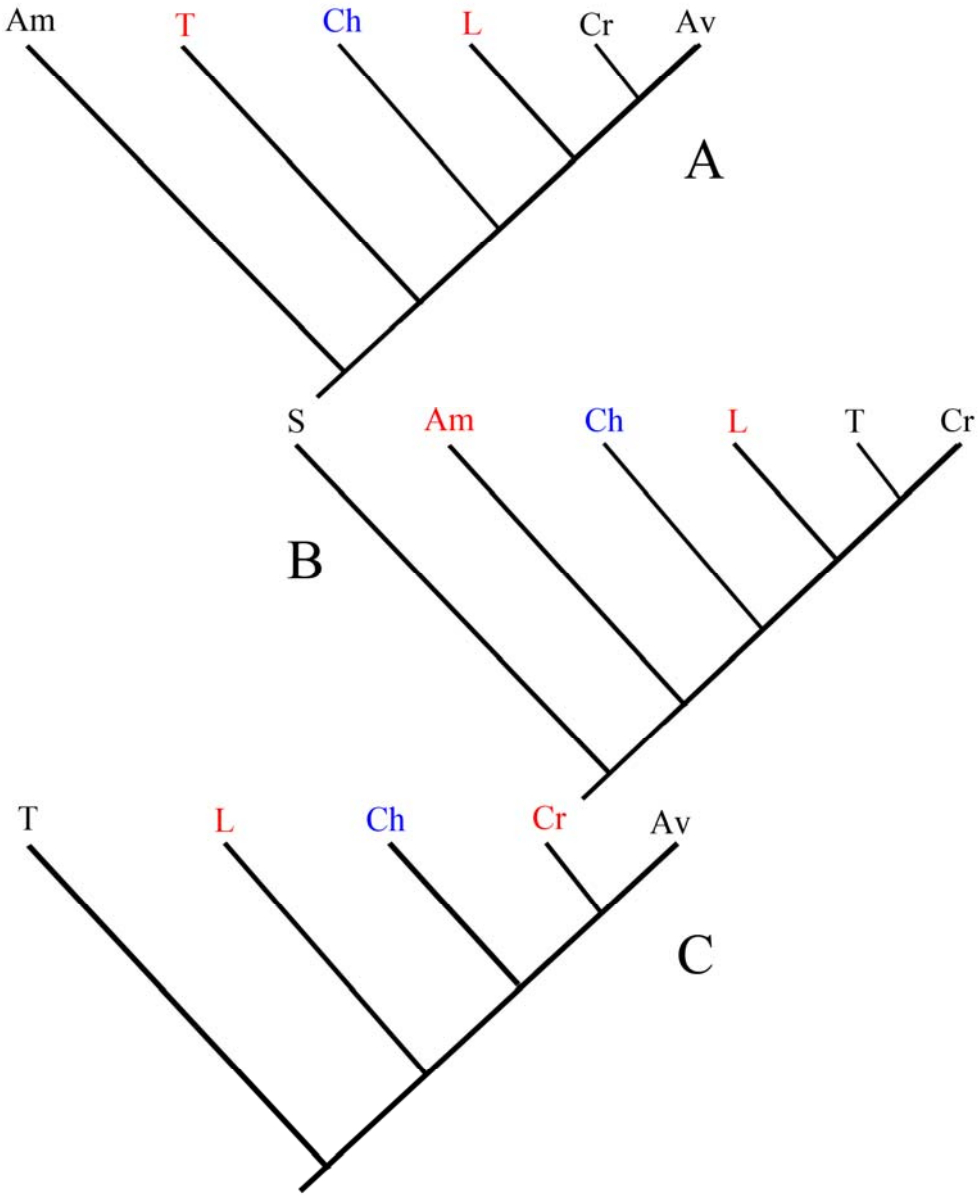

Figure 2.1: Three possible phylogenetic relationships between the Choristodera (Ch [blue]) and their extant phylogenetic brackets (red). A; the Choristodera are basal diapsids. B; the Choristodera are basal diapsids and the Testudines (T) are the sister group to or within the Archosauromorpha. C; the Choristodera are the sister group to or within the Archosauromorpha. Other groups included are the Amphibia (Am), Lepidosauria (L), the Crocodylia (Cr), Aves (Av), and Sarcopterygii(S).

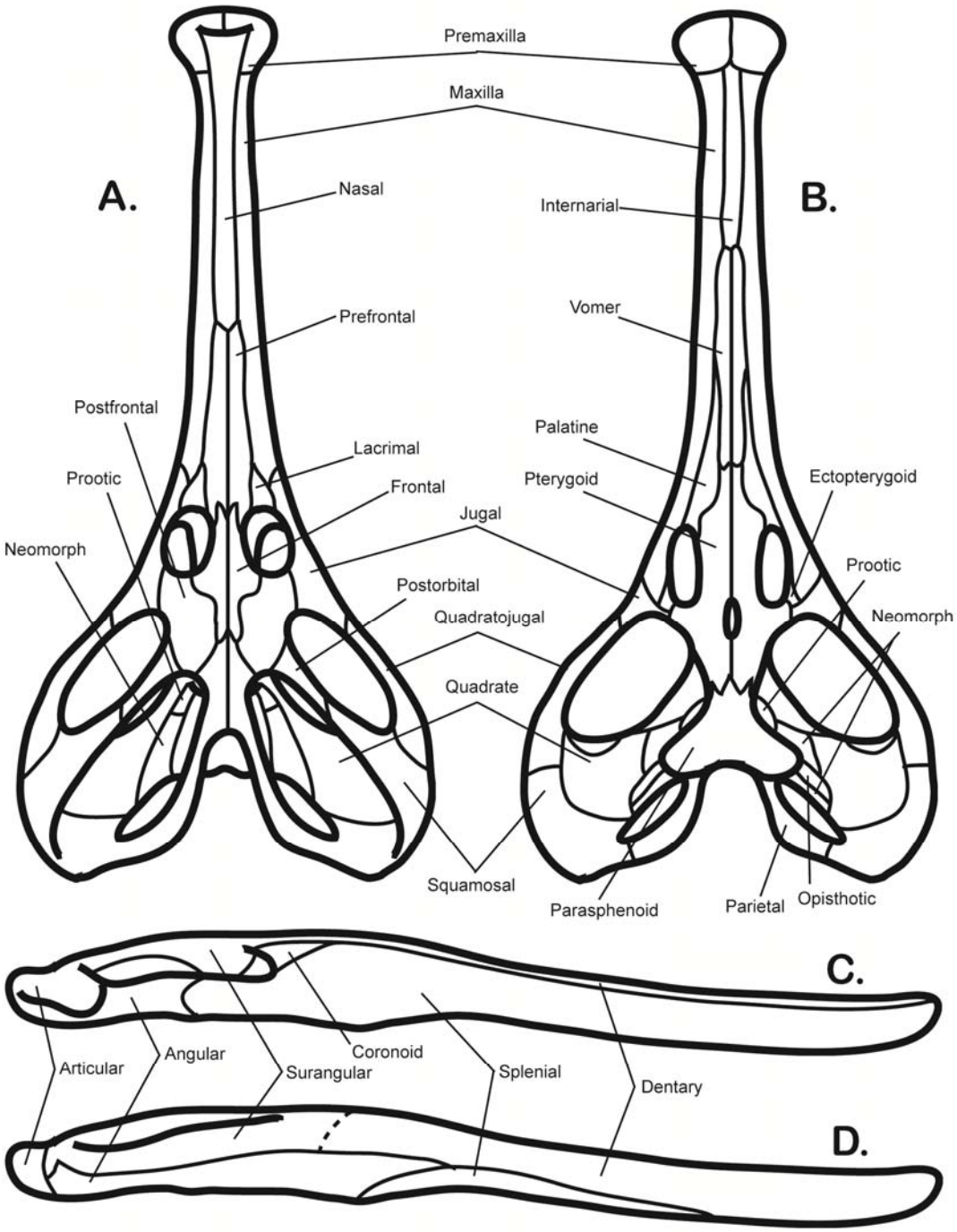

Figure 2.2: Cranial osteology of *Champsosaurus* redrawn from Russell (1956) and Gao and Fox (1998). A. Dorsal view of the cranium. B. Ventral view of the cranium. C. Medial view of the mandible. D. Lateral view of the mandible.

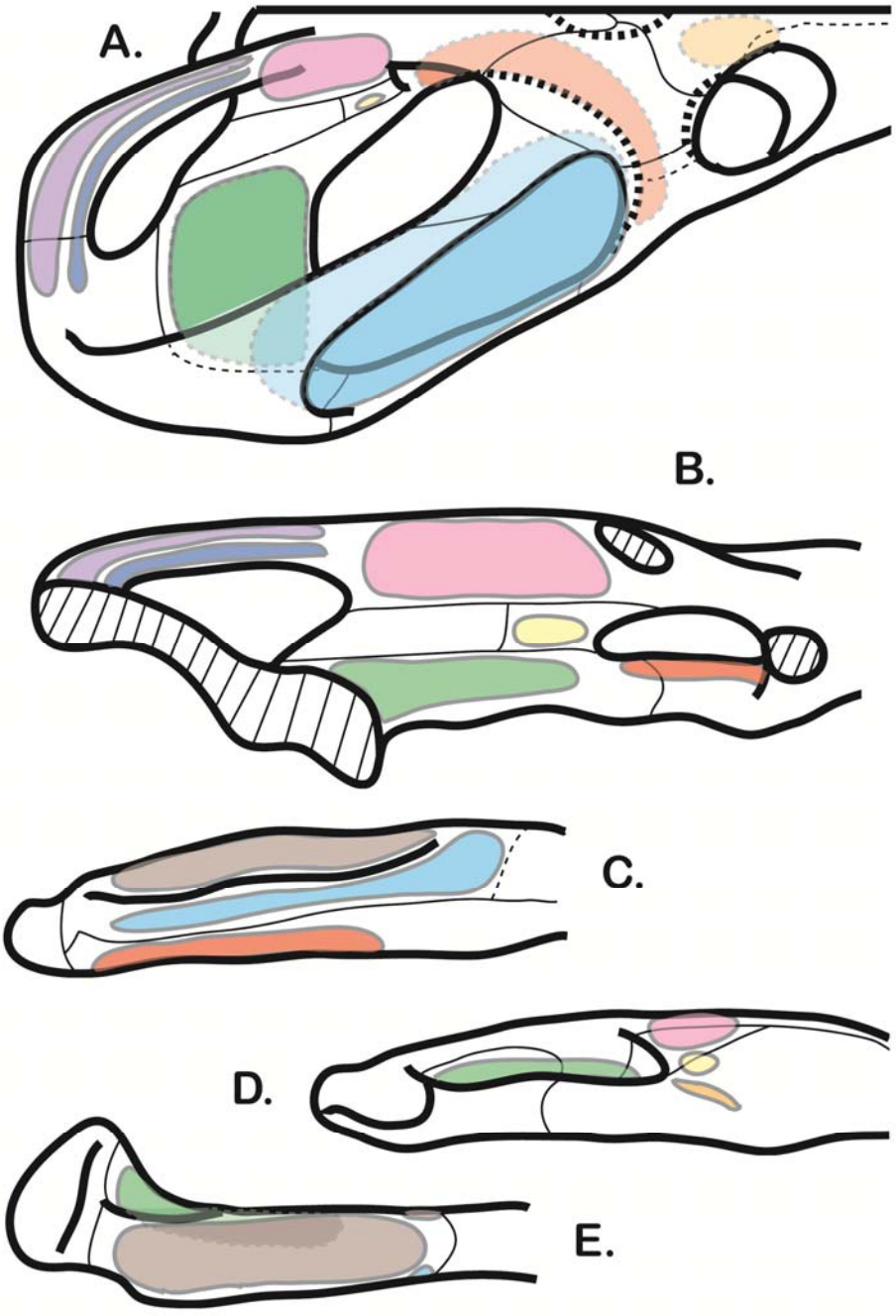

Figure 2.3: Reconstruction of the jaw adductor muscle origins and insertions in *Champsosaurus* based on the descriptions of *Sphenodon* jaw musculature by Wu (2003) and Jones et al. (2009). Green, mAMP; Light Blue, mAMES; Purple, mAMEM; Dark Blue, mAMEP; Pink, mPSTS; Yellow, mPSTP; Orange, mPTD; Red, mPTV; Grey, basal aponeurosis. A. Dorsal view of the temporal chamber. B. Lateral view of the braincase. C. Posterolateral view of the mandible. D. posteromedial view of the mandible. E. Posterodorsal view of the mandible.

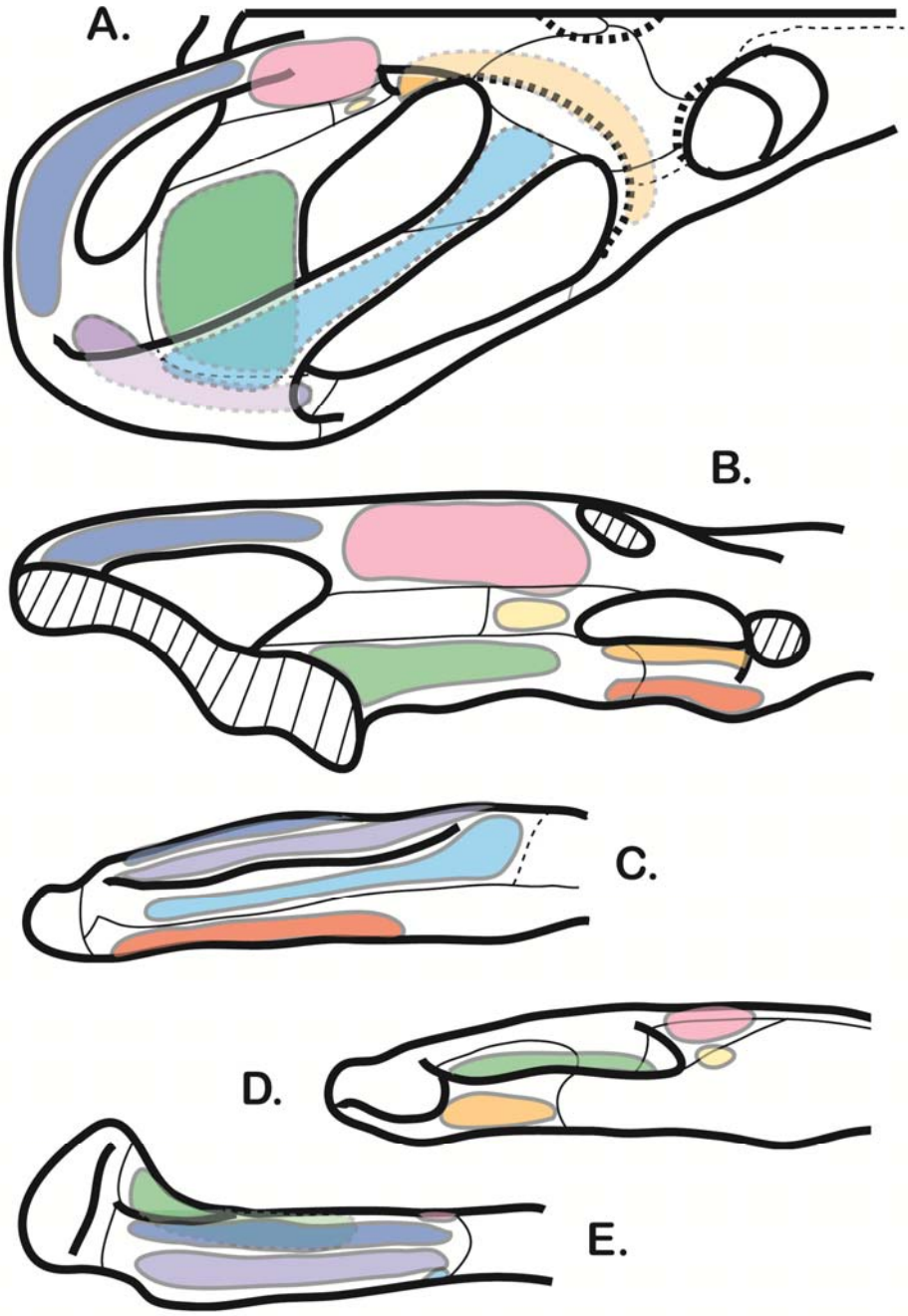

Figure 2.4: Reconstruction of the jaw adductor muscle origins and insertions in *Champsosaurus* based on the description of *Sphenodon* jaw musculature by Holliday and Witmer (2007). Green, mAMP; Light Blue, mAMES; Purple, mAMEM; Dark Blue, mAMEP; Pink, mPSTS; Yellow, mPSTP; Orange, mPTD; Red, mPTV. A. Dorsal view of the temporal chamber. B. Lateral view of the braincase. C. Posterolateral view of the mandible. D. posteromedial view of the mandible. E. Posterodorsal view of the mandible.

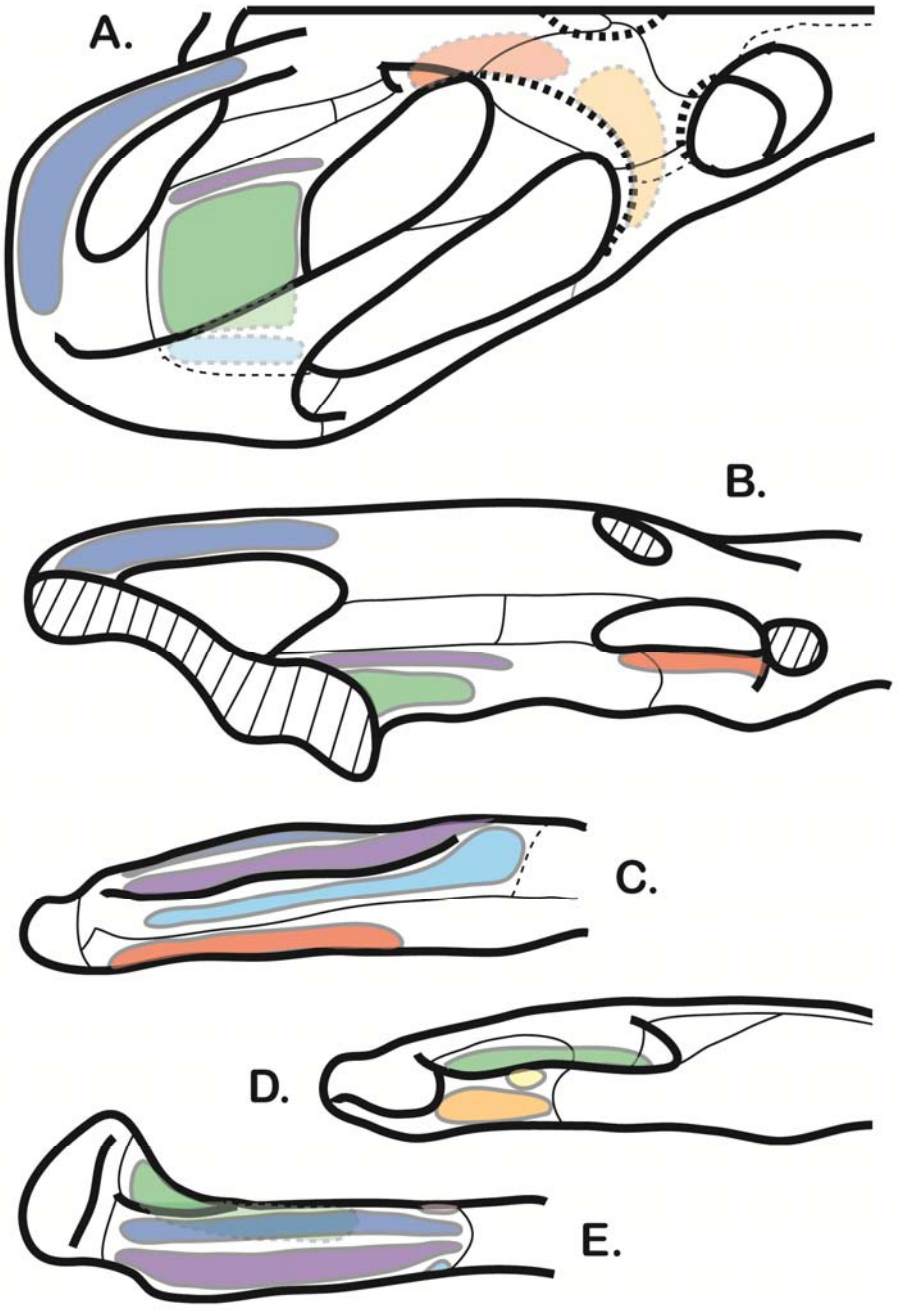

Figure 2.5: Reconstruction of the jaw adductor muscle origins and insertions in *Champsosaurus* based on the description of crocodilian jaw musculature by Holliday and Witmer (2007). Green, mAMP; Light Blue, mAMES; Purple, mAMEM; Dark Blue, mAMEP; Pink, mPSTS; Yellow, mPSTP; Orange, mPTD; Red, mPTV. A. Dorsal view of the temporal chamber. B. Lateral view of the braincase. C. Posterolateral view of the mandible. D. posteromedial view of the mandible. E. Posterodorsal view of the mandible.

CHAPTER 3: BIOMECHANICS OF THE JAW ADDUCTOR MUSCLES OF *CHAMPSOSAURUS*

Introduction

The hypothesized morphology of the musculature of the adductor chamber of neochoristoderes enables further research into the biomechanics of the feeding apparatus as a whole. The purpose of the jaw musculature is to rotate the mandibles for the purpose of capturing and subduing prey. Therefore, to determine the ability of the hypothesized musculature in neochoristoderes to perform that function, it is necessary to determine their ability to do work. Work is defined as the energy transferred to or from an object by means of a force (an influence that causes acceleration in a free body) acting upon the object (Halliday et al., 2001). In the case of jaw biomechanics, force (generated by the jaw musculature) acts upon the lower jaw. The work performed is thus the resulting rotation of the jaw, or biting.

The preferred jaw muscle morphology of neochoristoderes, specifically *Champsosaurus natator* (UALVP 47243, TMP 1984.3.9), *Champsosaurus lindoei* (UALVP 33928), and *Simoedosaurus dakotensis* (Erickson, 1987) as described in the previous chapter will be investigated for its capacity to rotate the lower jaw and thus do work. As a basis of comparison, a similar procedure will be conducted on four extant crocodilians that represent four distinct snout morphologies: *Alligator mississippiensis*, *Crocodylus cataphractus*, *Gavialis gangeticus*, and *Tomistoma schlegelii*. Previous studies regarding the feeding

mechanics of extinct vertebrates have generally sought answers regarding the bite force of the taxon in question (Erickson et al., 1996; Erickson, 2001; Rayfield et al, 2004; McHenry, 2009). This study will aim to provide bite force estimates of neochoristoderes; however, the ability to capture prey is not limited to the strength of the bite of the animal. Rotational mathematics will be used to calculate the acceleration and velocity of jaw adduction in both neochoristoderes and crocodilians.

This study will also examine the functional differences between slender-snouted and broad-snouted neochoristoderes and crocodilians. Within the Crocodylia, convergent evolution has resulted in similar skull morphologies in distantly related groups (Densmore and Owen, 1989; Cleuren and De Vree, 2000; Pierce et al., 2008). Neochoristoderes have also converged on skull morphologies seen in crocodilians, and thus can be considered to share the same categories used to distinguish the skull morphologies of crocodilians. The various skull morphologies of the crocodilian skull have been classified in several studies. Lydekker (1888) and Von Zittel (1890) classified crocodilians as either being longirostrine (slender snouts), and brevirostrine (wide snouts). The classification of Lydekker (1888) and Von Zittel (1890) was later supplanted because it does not include the total range of skull morphologies present in crocodilians, nor did it account for phylogeny. Busbey (1995) divided the morphologies into long, normal, and short on the basis of the ratio of skull length to rostrum length. Brochu (2001) modified the work of Busbey (1995) and categorized crocodilians into slender snouted, generalized, and blunt snouted. Lastly, McHenry et al.

(2006) divided crocodilians into longirostrine, tall and narrow mesorostrine, flat and broad mesorostrine, and brevirostrine. Amongst neochoristoderes, *Champsosaurus* closely resembles *Gavialis* and *Tomistoma* and thus falls into the longirostrine category, *Ikechosaurus* and *Tchoiria* fall into the broad and flat mesorostrine group, and *Simoedosaurus* could be considered brevirostrine or possibly flat and broad mesorostrine.

Once the effect of the muscles upon the rotation of the lower jaw is calculated it is the aim of this study to provide hypotheses to explain how the jaw musculature of neochoristoderes evolved and functioned. The biomechanical differences between longirostrine and brevirostrine morphologies will be investigated in both neochoristoderes and crocodilians. This study will also examine the possible palaeoecology of neochoristoderes in the context of extant crocodilian analogues, and investigate the ecological relationship between neochoristoderes and sympatric crocodilians.

Materials and Methods

Specimens

Specimens of neochoristoderes and crocodilians were digitally modelled and scaled to have the same length between the quadrate condyle and the anterior margin of the orbit (Table 3.1). The specimens are:

TMP 1984.3.9 – Idealized skull cast of *Champsosaurus natator*.

UALVP 33928 – Incomplete cranium of *Champsosaurus lindoei* missing the anterior half of the snout.

UALVP 47243 – Incomplete cranium of *Champsosaurus natator*, missing the left temporal arch, and braincase.

UAMZ HER-R800 – complete skull of *Alligator mississippiensis.*

UAMZ HER-R803 – complete skull of *Crocodylus cataphractus.*

UAMZ HER-R802 – complete skull of *Gavialis gangeticus.*

UAMZ HER-R805 – complete skull of *Tomistoma schlegelii.*

Measurements and formulae

The ability of a muscle to generate force, and thus do work, is dependent upon the contractile properties of that muscle. The physiology and contractile properties of vertebrate skeletal muscle remain similar across taxa (Snively and Russell, 2007). The contractile properties of vertebrate skeletal muscles include the cross sectional area, the length of the muscle, the internal geometry of the individual muscle fibres, and the composition of those fibres (Snively and Russell, 2007).

Regardless of the composition of the fibres of the muscles in the adductor chamber, the ability of any muscle to perform work is dependent upon the number of muscle fibres in parallel (Snively and Russell, 2007). Therefore, the force the muscle is capable of performing is directly influenced by its cross sectional area. The force the muscle generates per unit of area (typically N [Newtons]$\cdot cm^{-2}$) is referred to as the specific tension (ST). It is multiplied by the cross sectional area of the muscle (CS) to calculate the contractile force of the muscle (F_m) under

investigation (Kawakami et al., 1995; Fukunaga et al., 2001; Snively and Russell, 2007).

Equation 1: $F_m = CS \times ST$

The cross sectional area of a muscle can be divided into two kinds, physiological cross sectional area (PCSA), and anatomical cross sectional area (ACSA). The PCSA is defined as the area of the muscle in a cross section through the widest point, perpendicular to the pennation angle. The ACSA differs in that it does not take into account the pennation angle, and instead measures the area of the cross section of the muscle at its greatest width. Generally, in fusiform muscles, the PCSA and ACSA are close (Snively and Russell, 2007). However, in muscles where the pennation angle (the angle of the fibres relative to the direction of the muscle pull) is high the PCSA, and therefore force, will greatly exceed estimates derived from the use of the ACSA (Cheng and Scott, 2000; Snively and Russell, 2007). The formula to calculate the PCSA is:

Equation 2: $PCSA = m \cdot \cos \sigma / l \cdot \rho$

In Equation 2 m is the mass of the muscle in question, which can be determined by dissecting and measuring the isolated muscle, or estimating it by using physical or digital reconstructions. The pennation angle (the angle of the muscle fibres relative to the direction of the muscle) is represented by σ. The fascicle length, l, can be determined through dissection and MRI (Akima et al., 2000; Juul-Kristensen et al., 2000). Muscle density is represented by ρ, and is approximately 1.06 $g \cdot cm^{-3}$ (Snively and Russell, 2007). In fossil specimens the variables needed to calculate PCSA cannot be directly measured. The mass and

fascile length of a muscle can be determined by reconstruction through the use of sculpturing or computer modelling, whereas the pennation angle must be determined through dissection. ACSA can be used as a proxy for the cross sectional area of the muscle, because ACSA and PCSA are approximately equal, assuming that the fibres of the muscle are oriented parallel to the direction of the muscle.

Rayfield et al. (2001), Wroe et al. (2005), and McHenry (2009) used a method termed "dry skull measurement", in which an estimate of the ACSA can be measured by using the fenestrae and other osteological landmarks to outline the area that the muscles occupied. The assumption is that the cross sectional area of a muscle, or group of muscles, is limited by the area of the subtemporal fenestrae. In McHenry (2009) the ACSA of the average direction of two groups of muscles (the pterygoideus and temporalis muscles) in crocodilians and *Kronosaurus* were measured to determine the force generated. This methodology is also used for the crocodilian models in this study. The pterygoideus muscles generally extend posteroventrally in lateral view and lateroventrally in anterior view. The muscles in the temporalis group extend vertically in lateral view and lateroventrally in anterior view.

The dry skull method was used to determine the ACSA values of the neochoristodere specimens. However, the morphology of the temporal chamber and thus the orientation of the jaw adductor muscles differ from those of crocodilians, and separating the jaw musculature of the choristoderes as per crocodilians was not possible. The jaw musculature of the choristoderes can be

separated into a group consisting of the mandibulae (M). adductor mandibulae externus and M. adductor posterior muscles, and a group containing the muscles of the M. adductor internus muscles. The first group is united in that the muscles extend ventroanteriorly from the lateral and posterior borders of the adductor chamber in lateral view. The second group generally extends ventrolaterally from the braincase and the dorsal surface of the pterygoid. For both groups, the ACSA was measured along its average orientation.

The second variable needed to calculate the force a muscle exerts is the specific tension (ST) of a muscle. The ST of a muscle is described as the stress, or force per unit area that the muscle exerts (Snively and Russell, 2007). This value varies depending on the type of muscle, the animal being studied, and the way in which the muscle contracts. ST is similar in muscles undergoing concentric contraction, which is defined as when a muscle is able to shorten. ST has been measured at 24 $N \cdot cm^{-2}$ in cat neck muscles (Keshner et al., 1997), and 20-22 $N \cdot cm^{-2}$ in human leg muscles (Bamman et al., 2000). In muscles that are contracting but not shortening, also known as isometric contraction, ST has been measured at 30 $N \cdot cm^{-2}$ (Johnston, 1985). In the context of jaw muscle function, concentric contraction occurs during the bite when the jaw is closing around a prey item (striking), whereas isometric contraction occurs when handling prey (grasping). In this study, both phases of a bite were modelled and so the total force of the adductor chamber muscles was calculated with ST of 24 $N \cdot cm^{-2}$ and 30 $N \cdot cm^{-2}$ to simulate two kinds of biting behaviour. Modeling the muscles during grasping behaviour assumes that the muscles are undergoing isometric

contraction, and therefore the lower jaw is unable to rotate. Modeling striking behaviour assumes that the muscles are still able to contract and that the jaw is able to rotate.

Force was calculated independently for each muscle group and added together to obtain the total force generated by the jaw adductor muscles. However, this method does not differentiate individual muscles. It is assumed that the size of the attachment area of a muscle correlates with its contribution to the force produced by the jaw adductor muscles. Therefore, to determine the force of each muscle, the ratio of the attachment area to the total area for all of the muscles was calculated and the same ratio was applied to the total force of the jaw adductor muscles.

The variables needed in the following equations are illustrated in Figure 3.3. The moment, or torque (τ_m), of a muscle, or group of muscles, can be calculated once the force is known. Torque can be defined as the turning or twisting action of a force (Halliday et al., 2001), or the ability of a force to rotate an object about an axis (Snively and Russell, 2007). The torque can be calculated using the following equation:

$$\text{Equation 3: } \tau_m = RF\sin\phi$$

R is the distance from the rotational axis to the point where the force is applied. F is the magnitude of the force being applied. Finally, sin ϕ is the sine of the angle between the direction of R and the vector of F. R was determined in two different ways. The first method was done by measuring the centroid (the geometric center) of both the origin and insertion of a muscle and calculating the angle of the

muscle vector from the anteroposterior direction of the mandible. However, this method does not account for muscles wrapping over each other. In neochoristoderes, the mAMP, mAMEM, mAMEP, and mPTD (when modeled using the centroid method) would each either pass through another muscle or bone. Therefore, for these muscles, landmarks were chosen that allowed for the highest angle of insertions for each muscle, in order to compensate for muscles wrapping over one another. In the mAMP, the middle of the anterior edge of the origin was connected to the middle of the posterior edge of the insertion. For each of the mAMEM and mAMEP a point of the anteromedial edge of the origin was connected to the anteromedial edges of their respective insertions. Lastly, the mPTD must wrap over the mPTV and the ectopterygoid, therefore the point was chosen on the posterior surface of the ectopterygoid and connected to the centroid of the insertion.

When applying a force to a rotating object there are two components to that force. The radial component does not rotate the object because this is the component that acts along the direction of R and along a line that extends through the axis of rotation. The second component is the tangential component (F_t) which acts perpendicular to R and rotates the object. The magnitude of Ft can be calculated using the formula:

Equation 4: $F_t = F \sin\phi$

Thus, the formula to calculate the torque can be simplified to:

Equation 5: $\tau_m = RF_t$

In the case of jaw adductor function, F_t will always be in the direction of the dorsal surface of the mandible. Therefore the value of F_t, and thus τ_m, will change depending on the angle of the lower jaw relative to the cranium, because the vector of the force of the muscle will change due to the insertion being in a different position relative to the origin. Presumably this would result in different muscles being more important at different points during jaw adduction. The torque generated by the musculature was calculated at gapes of 0°, 25°, and 50°.

The torque can then be used calculate the bite force exerted at any point on the jaw using the formula:

$$\text{Equation 6: } F_r = \tau_m / r$$

Where F_r is the force at a given point, and r is the distance between the axis of rotation and the point. This formula assumes that the lower jaw operates using the same mathematics as a class 3 lever, a lever in which the force is applied between the fulcrum and the load (Halliday et al., 2001).

The torque that the muscles are able to produce can also be used to calculate the angular acceleration generated by each muscle. Angular acceleration is defined as the change in the angular velocity of a rotating object over time. The angular acceleration of an object is typically calculated by dividing the change in velocity by the change in time. However, angular acceleration (α) can also be calculated using torque and rotational inertia (I) with the formula:

$$\text{Equation 7: } \alpha_m = \tau_m / I$$

Rotational inertia is the measure of how the mass of a rotating object is distributed about its axis of rotation (Halliday et al., 2001). The formula to

determine rotational inertia varies depending on the shape of the object. The formula for a particle rotating freely about a central axis is additive and the rotational inertia for multiple particles is:

Equation 8: $I = \Sigma\, m_i r_i^2$

Where *m* is the mass of the particle and *r* is the distance from the axis of rotation. However, the lower jaw is not a free particle, rather it is continuous. The lower jaw can be divided into multiple segments and the rotational inertia for each individual segment summed (Snively and Russell, 2007). A program similar to that found in Henderson (2003) for determining the buoyancy of crocodilians was used to calculate rotational inertia. The program divided the lowers jaws of each specimen into discrete segments, and calculated the rotational inertia for each (Figure 3.4). The models used in this study for the finite element analysis do not have any soft tissues. However, when calculating the rotational inertia the soft tissues filling the space between the rami were reconstructed. The densities of bone and soft tissue differ and therefore different values were used for each. For bone a density of 2.3×10^3 kg/m^3 was used, and the soft tissues were given a density of 1.0×10^3 kg/m^3 (McHenry et al., 2006; Snively and Russell, 2007).

Equation 6 gives the angular acceleration of the jaw musculature in radians per second, which can be useful for comparative purposes, but is not necessarily useful for determining how fast the jaw closes in each specimen. The angular acceleration can be converted to tangential acceleration (α_t) at any point in the jaw (*r*) using:

Equation 9: $\alpha_t = \alpha_m \times r$

Once α_t and the angular excursion (θ) are known, the time in which it takes to close the jaw and the angular velocity can be calculated. The time (t) that it takes to close the jaw can be calculated using:

$$\text{Equation 10: } t = \sqrt{\theta / \alpha_m}$$

Which can be used to calculate the angular velocity (ω):

$$\text{Equation 11: } \omega = \alpha_m t$$

And lastly, the tangential velocity (v_r) at a any distance (r) from the axis of rotation:

$$\text{Equation 12: } v_r = \omega r$$

In summary, the cross sectional area of the muscles is used to calculate the force of the individual muscles, which then is used to determine the torque of each muscle. The total torque generated by the jaw adductor muscles is then used to determine the bite force (at any point along the jaw) and the angular acceleration of the jaw. The angular acceleration of the jaw is then used to calculate the tangential acceleration at a given point along the jaw and the angular velocity, which in turn is used to calculate the tangential velocity.

Results

The ACSA of the jaw adductor muscles of the neochoristodere specimens (Table 3.2, 3.3; Figure 3.1) was measured along the orientation of the m. adductor mandibulae externus and posterior, and the m. adductor mandibulae internus groups. In all cases the m. adductor mandibulae externus and posterior group was approximately one and a half to two times larger than the m. adductor mandibulae

internus. Therefore, the force produced by the adductor is predominately due to the muscles of the m. adductor externus and posterior. The ACSA of the two major muscle groups in the crocodilian specimens (Table 3.4, 3.5; Figure 3.2) are nearly equal to those of the neochoristoderes.

To determine the force each individual muscle generates, the ratio of its attachment area to the total attachment area was applied to the force calculated from the total ACSA of the muscles (Tables 3.6 – 3.9). The dominant muscle is the mAMES, followed by the AMP in all choristoderes. In UALVP 47243 the next major muscle is the mPSTS followed by the mAMEM and mAMEP. However, in UALVP 33928, TMP 1984.3.9, and *Simoedosaurus* the mAMEM and AMEP are the third and fourth strongest muscles respectively, followed by the mPSTS. In all choristoderes the mPSTP, mPTV, and mPTD contribute the least of total force of the jaw adductor muscles.

In the crocodilian specimens (Tables 3.10 – 3.13), with the exception of *Gavialis gangeticus*, the pterygoideus group of McHenry (2009) is the dominant muscle group of the adductor chamber. In *Crocodylus cataphractus* and *Alligator mississippiensis* the pterygoideus group is 1.27 and 1.58 times larger than the muscles of the temporalis group. *Tomistoma schlegelii* is nearly equal between the two groups, but the pterygoideus group has the larger ACSA. In *Gavialis gangeticus* the temporalis group has the larger ACSA, being 1.26 times larger than the pterygoideus group.

The mAMP, mPTV and mPTD are the largest muscles in the adductor chamber in the crocodilian specimens. In *Alligator mississippiensis*, and

Tomistoma schlegelii the largest muscle is the mPTD, in *Crocodylus cataphractus* it is the mPTV, and lastly the mAMP is the dominant muscle in *Gavialis gangeticus*. Apart from the aforementioned muscles, the contribution of the m. adductor mandibulae externus varies amongst the crocodilians. In *Alligator mississippiensis* the mAMES contributes the greatest force of the remaining muscles. The mAMES and the mAMEP are the same area and thus produce the same force in *Crocodylus cataphractus*, and are followed by the mAMEM. In *Gavialis gangeticus* the mAMEP is the fourth largest muscle, followed by the mAMES, the pterygoideus muscles, and lastly the mAMEM. In *Tomistoma schlegelii* the remaining musculature follows the same pattern as seen in *Gavialis gangeticus*, with the exception that the mPSTP is the smallest muscle in the adductor chamber.

Tangential Force

Despite the size of an individual muscle, work is only done in the direction perpendicular to the orientation of the mandible, and therefore the size of a muscle does not necessarily correspond to its contribution to jaw adduction. The tangential component of each muscle force, aside from the size of the muscle, depends on the gape of the jaw. In all of the neochoristoderan specimens (Tables 3.14 – 3.17) the mAMP has the second greatest tangential force during all gape angles, with the exception of TMP 1984.3.9, where at 50° the mAMP is surpassed by the mPTV. The tangential force of the mAMP generally decreases the further the mandible is depressed, but in UALVP 33928 the pattern is reversed.

The mAMES has the greatest tangential force in all choristoderes at all gapes. The optimum force is achieved when the mouth is closed and as the mouth opens the tangential force decreases. Between the jaw being closed and a gape of 50° in UALVP 33928 and UALVP 47243 the tangential force decreased by 23.47% and 11.85% respectively, whereas in *Simoedosaurus* the decrease is 44.62% and in TMP 1984.3.9 it is 58.86%. The mAMEM and mAMEP in UALVP 33928 and UALVP 47243 are nearly equal; however, the mAMEM provides the greater tangential force of the two. In TMP 1984.3.9 and *Simoedosaurus* the mAMEM produces nearly double the tangential force of the mAMEP. The tangential forces of the mAMEM and mAMEP decrease as the jaw is opened.

The pseudotemporalis muscles follow the same pattern as seen in the m. adductor mandibulae externus, the tangential force produced by the muscles decreases the further the jaw is opened. In all neochoristoderes the mPSTS exceeds the tangential force generated by the mPSTP. The pattern seen in the mPTD varies. In UALVP 47243 the tangential force provided by mPTD decreases by 12.49% as the jaw is opened to 50°. This trend is reversed in *Simoedosaurus* and the tangential force provided by the mPTD increases by 27.76%. In UALVP 33928 and TMP 1984.3.9 the highest tangential force of the mPTD occurs when the jaw is depressed by 25°.

The overall trend in the total tangential force of the crocodilian specimens (Tables 3.18 – 21) is opposite to that seen in neochoristoderes, in that the total force increases the further the mandible is depressed. In *Alligator mississippiensis*

the tangential force provided by one adductor chamber increases by 72.24% between a closed jaw and a gape of 50°. Similar increases are seen in the remaining crocodilians, although of less magnitudes. *Crocodylus cataphractus* has an increase of 57.84%, *Gavialis gangeticus* a 43.98% increase, and finally *Tomistoma schlegelii* has an increase of 46.03%.

The pattern in the mAMP remains consistent between all of the crocodilian specimens and as the gape is increased, the tangential force provided by the mAMP decreases. The drop in tangential force is lowest in *Alligator mississippiensis* and *Tomistoma schlegelii* which experience decreases in tangential force of 4.81% and 4.58% respectively. *Crocodylus cataphractus* and *Gavialis gangeticus* have decreases of 10.23% and 9.12% respectively.

There is no consistent pattern present in either the mAMES or mAMEM of crocodilians. The tangential force of the mAMES increases slightly in *Alligator mississippiensis* and *Tomistoma schlegelii*. In *Crocodylus cataphractus* this trend is reversed, and in *Gavialis gangeticus* the highest tangential force is produced at a gape of 25°. The mAMEM in *Alligator mississippiensis* and *Tomistoma schlegelii* increases the further the jaw is opened, whereas in *Crocodylus cataphractus* and *Gavialis gangeticus* the highest tangential force occurs at a gape of 25°. The trend in the mAMEP remains consistent between all crocodilians sampled. The tangential force peaks when the mandible is depressed by 25°.

The trend generally seen in the mPSTS is that the tangential force exerted increases between the jaw being closed and a gape of 25°. When the gape increases beyond 25° the tangential force decreases. However, in *Alligator*

mississippiensis, the more the jaw opens results in progressive decreases in tangential force. In all specimens the change in tangential force is minor when compared to that of the larger mAMP or pterygoideus muscles. The mPSTP in all crocodilian increases in tangential force the further the mandible is depressed. The magnitude of the increase is smallest in *Alligator mississippiensis* and *Crocodylus cataphractus*, which experience increases of approximately 2.4 N between the jaw being closed and a gape of 50°. The tangential force of the mPSTP is greater in the longirostrine crocodilians, and the increases experienced between the jaws being closed and depressed by 50° are 6.9 N in *Tomistoma schlegelii* and 12.0 N in *Gavialis gangeticus*.

In all of the crocodilian specimens, both pterygoideus muscles experience a dramatic increase in tangential force the further the jaw is depressed. The mPTD is found to be the stronger of the two pterygoideus muscles in *Alligator mississippiensis* and *Gavialis gangeticus*. The mPTD of *Alligator mississippiensis* is the second strongest muscle in the adductor chamber when the jaw is closed and increases its tangential force by 332.44% as the jaw opens to 50°, surpassing the force provided by the mAMP, which then becomes the strongest muscle in the adductor chamber. The mPTD in *Gavialis gangeticus* initially produces less tangential force than the mAMEP, but goes through a 461.22% increase as the jaw is opened and becomes the second largest contributor to tangential force, behind the mAMP. In *Crocodylus cataphractus* the mPTD and mPTV produce nearly equal tangential forces when the jaw is closed, however the force produced by the mPTD does not increase as quickly as the mPTV when the jaw is opened. The

mPTD in *Tomistoma schlegelii* initially is one of the lowest contributors to tangential force, however by the time the jaw opens to 25° the mPTD is the third largest contributor to the total tangential force. The mPTV in all crocodilians experiences the same dramatic increase in tangential force as the jaw approaches a gape of 50°. The tangential force increases by 688.04%, 443.376%, 458.69%, and 442.21% in *Alligator mississippiensis*, *Crocodylus cataphractus*, *Gavialis gangeticus*, and *Tomistoma schlegelii* respectively.

Torque and Bite Force

When the torque of the muscles was calculated, the pattern observed in the total tangential force was generally adhered to. For the neochoristoderes (Tables 3.22 – 3.25), the torque decreased the further the mandible was depressed. The magnitude of the decrease is not consistent amongst neochoristoderes. The lowest decrease occurs in UALVP 47243 at 17.51%, followed by UALVP 33928 at 18.57%. The remaining neochoristoderes experience more dramatic decreases in torque as the jaws open. *Simoedosaurus* has a decrease of 48.92% and TMP 1984.3.9 a decrease of 62.68%. The crocodilian specimens (Tables 3.26 – 3.29) generally have the opposite trend. *Alligator mississippiensis*, *Gavialis gangeticus*, and *Tomistoma schlegelii* experience increases of 22.20%, 30.12%, and 13.97% respectively. *Crocodylus cataphractus* is unique in that the greatest torque is produced when the jaw is opened by 25°. The aforementioned patterns that exist in how the tangential force changes between the different gapes are identical in the torque generated by each muscle in both neochoristoderes and crocodilians.

For the neochoristoderes the mAMES produces most of the torque generated by the adductor chamber. The mAMP and the mPSTS are the next largest contributors to the total torque in all of the neochoristoderan specimens. In *Simoedosaurus* the mAMEM is also a prominent contributor initially. At 50° the mPTD and mPTV generally contribute torques equal to or greater than those of the mAMP and mPSTS, although in UALVP 47243 neither the mPTD nor mPTV surpass the torque of the mAMP or mPSTS.

In all of the crocodilian specimens the mAMP generates the greatest torque in the adductor chamber in all measured gapes. The mAMES is also a prominent contributor to the torque produced within the adductor chamber in all crocodilians, especially in *Tomistoma schlegelii* where it is consistently produces the second greatest torque. The mAMEP plays a significant role as well, especially in *Gavialis gangeticus* where it is the second greatest producer of torque at all gapes. The mPSTS is also one of the more significant producers of torque. The pterygoideus muscle, similar to the patterns observed in their tangential forces, produce greater torques the further the jaw is opened. Despite the dramatic increase calculated in the tangential force of the combined pterygoideus muscles does not correspond to a similar increase in torque. The pterygoideus muscle complex in all crocodilians is unable to exceed the torque generated by the aforementioned muscles even when the jaw is depressed by 50°. In *Alligator mississippiensis* the pterygoideus muscles fall behind the mAMP. In *Crocodylus cataphractus* the mAMP, mAMES, and mAMEP surpass the pterygoideus muscles, whereas the mAMEM slightly exceeds the torque of the

mPTD. The torque of the combined pterygoideus muscles is only exceeded by the mAMP and mAMEP in *Gavialis gangeticus*. Finally, in *Tomistoma schlegelii* the mAMP and the mAMES exceed the pterygoideus muscles, and the mPTV is nearly equal in torque to the mAMEP and mPSTS.

The total torque at each gape that is generated by the adductor chambers of each of the specimens is used to calculate the bite force at several points along the jaw: the terminus of the lower jaw, the middle of the jaws between the anterior margin of the orbit and the tip of the snout, and directly under the anterior margin of the orbit. Table 3.30 summarizes the bite force calculations in all specimens. In all specimens the bite force decreases towards the tip of the snout. The relationship between the bite forces and the gape of the jaw is identical to that between the torque and gape of the jaw: all neochoristoderes see a decrease in bite force as the jaw opens, whereas the bite force in all crocodilians increases. Greater bite forces are present in neochoristoderes compared to crocodilians. The more generalized skull shape of *Simoedosaurus* is calculated to have the greatest forces of both the neochoristodere and crocodilian specimens. The longirostrine specimens have lower bite forces, and *Champsosaurus lindoei*, UALVP 33928 has the lowest bite forces of the neochoristoderes. The crocodilians follow the same pattern in that blunt snouted *Alligator mississippiensis* has the greatest bite forces of the crocodilians, followed by the more general *Crocodylus cataphractus*, and lastly the longirostrine species *Gavialis gangeticus* and *Tomistoma schlegelii*.

Rotational Inertia, Angular and Tangential Acceleration, and Angular and Tangential Velocity

The rotational inertia is a measure of how the mass of an object is distributed about its axis of rotation (Halliday et al., 2001). Rotational inertia can alternatively be thought of as the measure of how easily an object can be rotated about its axis. As the rotational inertia increases, so too does the difficulty associated with rotating the object. The mandibles of neochoristoderes (Tables 3.31 – 3.34) all have lower rotational inertias when compared to crocodilians (Tables 3.35 – 3.38). Of the neochoristoderes, TMP 1984.3.9 has the lowest rotational inertia, measuring 1.66×10^{-2}, whereas *Simoedosaurus* has the greatest with a calculated rotational inertia of 1.99×10^{-2}. The lowest rotational inertia of the crocodilians is calculated for *Tomistoma schlegelii* at 2.43×10^{-2}. In the crocodilians, the highest rotational inertia is found in *Alligator mississippiensis*, in which the rotational inertia is 2.04×10^{-1}.

The angular acceleration of each gape was calculated for all specimens (Tables 3.31 – 3.38). The total angular acceleration and the angular acceleration for each muscle follow the identical pattern as seen in their respective torques. For neochoristoderes, the total angular acceleration decreases as the gape of the jaw increases, whereas crocodilians experience an increase. The angular accelerations in neochoristoderes are greater than those calculated in crocodilians, both in terms of the individual muscles and the total angular acceleration. *Simoedosaurus* has the greatest angular accelerations of any of the other neochoristoderes and crocodilians. The lowest angular accelerations of the neochoristoderes are those of

UALVP 39928, *Champsosaurus lindoei*. The crocodilian that most closely approaches the angular accelerations seen in the neochoristoderes is *Tomistoma schlegelii*. The lowest calculated angular accelerations are in *Alligator mississippiensis*.

The tangential acceleration in each specimen was calculated at several points along the snout; the tip of the premaxilla/dentary, the middle of the length between the anterior margin of the orbit and the tip of the snout, and lastly the tooth position directly under the anterior margin of the orbit (Table 3.39) At each point *Simoedosaurus* has the greatest tangential acceleration, and the neochoristoderes all have greater accelerations than those of the crocodilians. In all specimens the tangential acceleration increases towards the terminus of the snout.

The angular acceleration and the angular excursion can be used to determine the time in which it takes the jaws to close from gapes of 25° and 50° and are summarized in Table 3.40. From 25° the neochoristoderes have the lowest times for closing the jaws, and all fall under 0.10 seconds. The crocodilians are slower, with the greatest time calculated in *Alligator mississippiensis* at 0.252 seconds, and *Tomistoma schlegelii* is the fastest crocodilian with a closing time of 0.096 seconds. Between 50° and 25°, despite the changes in torque, the time it takes to close the jaw does not differ significantly from the time it takes to close the jaw between 25° to 0° in any specimen. To determine the time it takes for the jaw to close from a gape of 50° the time from 50° to 25° was added to the time

between 25° to 0°. As expected, the time it takes to close the jaw would be approximately double.

The angular velocities for the specimens follow the pattern observed in the angular acceleration (Table 3.40). In neochoristoderes the greatest velocity is between a gape of 25° and the jaw being closed. In the crocodilians, with the exception of *Crocodylus cataphractus* (because the greatest torque is calculated at 25°), the greatest angular velocity is between 50° and 25°. Generally, the difference between the velocities of the two ranges is negligible, although in TMP 1984.3.9 there is a sizable difference of 87.42 rad/s. The greatest angular velocity is found in *Simoedosaurus* closely followed by UALVP 47243. Of the crocodilians the highest velocity is found in *Gavialis gangeticus*, and the lowest is *Alligator mississippiensis.*

The tangential velocities (Table 3.41) at the aforementioned three points along the snout are calculated in a similar manner to those of the tangential acceleration, the difference being that the angular velocity was multiplied by the distances to the aforementioned points. The longirostrine neochoristoderes have the greatest tangential velocities at the terminus of the snout when compared to Simoedosaurus. However, the differences between the specimens of *Champsosaurus* and *Simoedosaurus* in the tangential velocities become less pronounced further posteriorly on the jaw. However, at the most posterior point *Simoedosaurus* has the greater tangential velocity. Crocodilians however, do not follow the pattern seen in neochoristoderes. Longirostrine crocodilians have greater tangential velocities at all points of the snout. As with the calculated

angular velocities, neochoristoderes have larger tangential velocities compared to crocodilian specimens.

Discussion

The mAMES is the dominant muscle of the adductor chamber in neochoristoderes. The mAMES in all neochoristoderes examined comprises approximately half of the total muscle attachment area, and once the force, tangential force, and torque are calculated the mAMES consistently dominates the other musculature in the adductor chamber. The decrease in tangential force (and thus torque) as the gape of the jaw increases indicates that the primary role of the mAMES is to adduct the jaw during gapes of 25° or less. Like the mAMES, the mAMEM and mAMEP serve a similar function. The two muscles are at their peak torque when the jaw is closed, suggesting that they function best when closing the jaw from low gapes, or in holding prey items.

The mAMP generally produces the maximum amount of torque when the jaw is closed, and decreases the more the jaw is opened. UALVP 33928 however has the reverse trend. Crocodilians share the same trend generally seen in neochoristoderes. This suggests that the mAMP functions best at small gapes, or in subduing small prey. But due to the size the mAMP, it remains a large contributor to jaw adduction at larger gapes in both neochoristoderes and crocodilians.

The pseudotemporalis muscles have different trends between neochoristoderes and crocodilians. For each of the pseudotemporalis muscles in

neochoristoderes, the torque exerted decreases as the gape is increased. This suggests that (as with the previously discussed muscles) their primary function is to operate in small prey acquisition. The patterns in crocodilians are contrary to those of neochoristoderes. Most crocodilians achieve the peak torque of the mPSTS at a gape of 25°. The exception is *Alligator mississippiensis* which shows the same trend as in neochoristoderes. The mPSTP has a consistent pattern in all crocodilians; the torque increases as the jaw is opened, although the change in torque is less than 1 N·m in all cases. The function of the mPSTP is likely to provide stabilization during biting, rather than adducting the jaw.

The only muscle that consistently increases in performance as the jaw opens is the mPTV. The crocodilians all show the same pattern as neochoristoderes in that the tangential force of the mPTV is smallest when the jaw is closed, whereas the tangential forces of the remaining muscles in the jaw become more prominent. As the jaw opens, the mPTV contributes greater torque, due to the force vector of the muscles becoming increasingly parallel to the tangential force vector. This suggests that in both crocodilians and neochoristoderes the function of the mPTV is to adduct the jaw at large gapes, or to keep the jaw closed around large prey. Its prime function was not to keep the jaw closed around small prey.

The mPTD does not have a consistent function in the neochoristoderes. The muscle must wrap over the mPTV, and consequently inserts near vertically upon the mandible when the jaw is closed. In *Simoedosaurus* the mPTD increases in torque as the jaw opens. UALVP 47243 sees a decrease in torque generated by

the mPTD as the jaw opens. Finally, UALVP 33928, and TMP 1984.3.9 have the greatest torque when the gape is 25°. Regardless of the function of the pterygoideus muscles, they are small contributors to the adduction of the jaws in neochoristoderes, contra Gao and Fox (1998), suggesting that they may be used primarily for stabilization. The mPTD of crocodilians consistently increases in torque the further the mandible is depressed. The mPTD in crocodilians therefore serves the same function as the mPTV. In neochoristoderes the mPTD does not, as calculated from the specimens used in this study provide a substantial benefit to prey acquisition.

The dry skull method used in this study previously had been used to examine the force produced in the skulls of *Crocodylus* and *Kronosaurus* (McHenry, 2009). The resulting forces in McHenry (2009) were reported to be comparable to measurements made using force plates in extant crocodilians. The results of this study were also compared to the results of direct experimentation on extant crocodilians, specifically *Alligator mississippiensis* (Erickson et al., 2003). Erickson et al. (2003) investigated the ontogeny of bite force in *Alligator mississippiensis* and were able to construct log plots detailing the expected bite force for any given skull length or body mass. The bite force measurements were collected using pressure plates placed at the eleventh maxillary tooth position, which is the most prominent tooth at the back of the jaws (Erickson et al., 2003). The *Alligator mississippiensis* skull used in this study has a length between the occipital condyle and the anterior tip of the dentary of 31.98 cm. According to the log plot of Erickson et al. (2003) the aforementioned length should yield a bite

force at the eleventh maxillary tooth position of 3079.04 N. The initial muscle forces calculated from the ASCA roughly equals that calculated from the formula of Erickson et al. (2003). However, the bite force calculated herein using the dry skull method greatly underestimates the bite force that is exerted by the jaw adductor musculature. Therefore the dry skull method used here is unable to give absolute values for the muscle and bite forces, and further calculations such as angular acceleration. However, because the same methodology was applied to all animals in this study, the dry skull method does allow for valid comparisons to be made between neochoristoderes and crocodilians.

Despite the underestimation of the bite forces resulting from the dry skull method, differences in the bite forces resulting from differences in the shape of the snout are evident. The longirostrine specimens, *Champsosaurus natator*, *Champsosaurus lindoei*, *Gavialis gangeticus*, *Tomistoma schlegelii*, and *Crocodylus cataphractus* have lower bite forces than their mesorostrine or brevirostrine relatives. The factors that directly influence bite at any point along the snout are the gross force produced by the adductor chamber and their resulting tangential forces, and the length of the snout. This suggests that brevirostrine snouts are as McHenry et al. (2006) ascertained, adapted for preying upon larger, terrestrial animals, as greater bite forces would be required to subdue them. *Simoedosaurus*, having a significantly greater bite force than its longirostrine relatives, therefore shares a niche similar to that of *Alligator* and mesorostrine, or more brevirostrine members of *Crocodylus*, and likely preyed upon large fish, and terrestrial vertebrates. Conversely, the lower bite forces of the longirostrine

specimens reinforce that the preferred prey do not require the same magnitude of force to capture and handle prey.

The fundamental difference between how the jaw functions in neochoristoderes and crocodilians is how the tangential force and torque change between different gapes. In neochoristoderes there is a negative correlation between the torque produced by the jaw adductor musculature and increasing the gape of the jaw. Crocodilians have the opposite trend, and there is a strong positive correlation between torque and gape. This indicates a difference in feeding habits between the two groups. The increasing torque seen in crocodilians suggests that they are better adapted for handling larger prey than neochoristoderes. The pattern seen in neochoristoderes indicates that they may have preferred prey that could be accommodated by small gapes. There is no apparent distinction between longirostrine specimens, and their brevirostrine or mesorostrine neochoristodere relatives. Considering that torque is a function of the tangential force and the distance from the axis of rotation to the point of insertion it is therefore no surprise that longirostrine animals are capable of exerting similar torques to those of other snout shapes.

Calculating the theoretical accelerations and velocities of the lower jaws for each specimen further supports the assertion that neochoristoderes preferred smaller prey than crocodilians. The accelerations and velocities calculated for the neochoristoderes greatly exceed those calculated for the crocodilians. This supports the hypothesis that the greatly expanded temporal region was adapted for delivering a quick snap for catching small prey (Russell, 1956). However, the

great speed is not solely facilitated by the large musculature present in the adductor chamber, even considering that neochoristoderes have greater musculature. The key difference in jaw closing speed between crocodilians and neochoristoderes is the morphology and rotational inertia of the lower jaw.

Rotational inertia is a proxy for how easily an object can be rotated; the higher the value, the greater the difficulty in rotating the object. The rotational inertia for the neochoristoderes is considerably lower than what is calculated in crocodilian mandibles. This difference is primarily due to the lower mass of the neochoristodere mandibles compared to those of similarly sized crocodilians, even those with slender snouts. Therefore the mandibles of neochoristoderes are adapted to minimize rotational inertia to aid in maximizing the angular acceleration and therefore velocity of biting, ideal for catching small, agile prey.

Because rotational inertia is dependent upon the mass of the object being rotated, and how that mass is distributed (Halliday et al., 2001), it is imperative to obtain an accurate measurement. Initial mass calculations for determining the rotational inertia only measured the mandibles, and did not include any soft tissues, and thus resulted in values considerably lower than those detailed in Tables 3.31 – 3.38. With the addition of soft tissues in the broad snouted specimens the mass is distributed more evenly throughout the length of the lower jaw, whereas in the slender snouted specimens the mass is distributed more posteriorly. Having a lower mass farther away from the axis of rotation, as seen in the longirostrine specimens, has the effect of lowering rotational inertia (Halliday

et al., 2001). This supports the interpretation that elongate, slender snouts are adapted for piscivory.

There are drawbacks to the method used in this study. First and foremost is the aforementioned underestimation of bite forces due to the use of the dry skull method. Another problem may be that the formulae and data collected overestimate the acceleration and velocity the jaw closes. However, because of the lack of investigation of these values in extant crocodilians, further studies directly measuring the acceleration and velocity of the bite of crocodilians is required for comparison to the theoretical values obtained in this study.

Conclusion

The original purpose of this study was to test the abilities of the jaw adductor musculature in neochoristoderes and compare them to their extant ecological analogues. The capacity to do work was judged by measuring the ability of muscles to generate force, and how that force affected bite force, angular and tangential accelerations, and angular and tangential velocities of both neochoristoderes and crocodilians. Neochoristoderes generated greater muscle forces, bite forces, angular and tangential accelerations, and angular and tangential velocities than crocodilians. Longirostrine specimens had greater accelerations and velocities than relatives with shorter jaws. These findings support the hypothesis that *Champsosaurus* may have preferentially fed on small fish, reptiles, amphibians, and invertebrates with a quick snap as described by

Russell (1956) because the jaw adductor muscles and the morphology of the snout are adapted to maximize the speed at which they are able to close their jaws.

The data shows that the two groups being studied emphasize different jaw muscles during feeding. Neochoristoderes rely heavily upon the mAMES and mAMP to adduct the mandibles, whereas crocodilians place a greater emphasis on the mAMP and the pterygoideus muscles. The patterns present in the tangential forces, torques, angular accelerations, and angular velocities show that these values decrease in neochoristoderes as the jaw is opened, whereas in crocodilians these values increase. The interpretation is that neochoristoderes have decreasing abilities to handle larger prey and thus likely focused their carnivorous intentions upon smaller animals. Crocodilians on the other hand are better able to accommodate larger prey items.

The jaw musculature of neochoristoderes is not adapted for delivering large powerful bites. Rather, the temporal region has been enlarged so that the lower jaws may be closed around prey at great speeds. It is therefore likely that *Champsosaurus* dominated the niche of piscivorous reptilians preying upon small fish, amphibians, and reptiles.

Chapter 3: Tables

Specimen	Length between occipital condyle and snout terminus	Width between quadrate condyles
Champsosaurus natator UALVP 33928	44.55	15.70
Champsosaurus natator UALVP 47243	41.47	18.06
Champsosaurus natator TMP 1984.3.9	47.17	19.48
Simoedosaurus dakotensis	33.55	18.98
Alligator mississippiensis	31.98	16.37
Crocodylus cataphractus	43.45	19.87
Gavialis gangeticus	50.69	16.47
Tomistoma schlegelii	49.93	17.32

Table 3.1: Skull length between the occipital condyle and snout terminus (cm) and width between the quadrate condyles.

	UALVP 33928		UALVP 47243		TMP 1984.3.9		*Simoedosaurus dakotensis*	
Muscle Group	ASCA	F	ASCA	F	ASCA	F	ASCA	F
mAMP+mAME	51.86	1244.52	55.48	1331.62	78.16	1875.72	58.59	1406.11
mAMI	38.30	919.08	42.52	1020.36	42.74	1025.71	52.45	1258.85
Total	90.16	2163.60	98.00	2351.98	120.90	2901.43	111.04	2664.96

Table 3.2: Actual cross sectional area (ASCA [cm^2]) and total jaw adductor muscle forces (F [N]) in neochoristoderes. Specific tension (ST) = 24 $N \cdot cm^2$.

	UALVP 33928		UALVP 47243		TMP 1984.3.9		*Simoedosaurus dakotensis*	
Muscle Group	ASCA	F	ASCA	F	ASCA	F	ASCA	F
mAMP+mAME	51.86	1555.65	55.48	1664.52	78.16	2344.65	58.59	1757.64
mAMI	38.30	1148.85	42.52	1275.45	42.74	1282.14	52.45	1573.56
Total	90.16	2704.50	98.00	2919.97	120.90	3626.79	111.04	3331.20

Table 3.3: Actual cross sectional area (ASCA [cm^2]) and total jaw adductor muscle forces (F [N]) in neochoristoderes. Specific tension (ST) = 30 $N \cdot cm^2$.

	Alligator mississippiensi		*Crocodylus cataphractus*		*Gavialis gangeticus*		*Tomistoma schlegelii*	
Muscle Group	ASCA	F	ASCA	F	ASCA	F	ASCA	F
Temporalis	32.93	790.32	48.34	1160.11	52.25	1254.05	43.26	1038.24
Pterygoid	50.28	1206.62	62.85	1508.35	39.89	957.29	47.38	1137.05
Total	83.21	1996.94	111.19	2668.46	92.14	2211.34	90.64	2175.29

Table 3.4: Actual cross sectional area (ASCA [cm^2]) and total jaw adductor muscle forces (F [N]) in crocodilians. Specific tension (ST) = 24 $N \cdot cm^2$.

	Alligator mississippiensi		*Crocodylus cataphractus*		*Gavialis gangeticus*		*Tomistoma schlegelii*	
Muscle Group	ASCA	F	ASCA	F	ASCA	F	ASCA	F
Temporalis	32.93	987.90	48.34	1160.11	52.25	1875.72	43.26	1297.80
Pterygoid	50.28	1508.28	62.85	1508.35	39.89	1025.71	47.38	1301.31
Total	83.21	2496.18	111.19	2668.46	92.14	2764.17	90.64	2599.11

Table 3.5: Actual cross sectional area (ASCA [cm^2]) and total jaw adductor muscle forces (F [N]) in crocodilians. Specific tension (ST) = 24 $N \cdot cm^2$.

Muscle	Ratio of total attachment area	F_m (ST = 24)	F_m (ST = 30)
mAMP	0.227	491.137	613.922
mAMES	0.485	1048.481	1310.601
mAMEM	0.068	146.692	183.365
mAMEP	0.060	129.383	161.729
mPSTS	0.059	127.652	159.566
mPSTP	0.028	59.715	74.644
mPTD	0.016	33.536	41.920
mPTV	0.055	117.916	147.395

Table 3.6: Ratio of total attachment area and force (N) of the jaw muscles of UALVP 33928.

Muscle	Ratio of total attachment area	F_m (ST = 24)	F_m (ST = 30)
mAMP	0.191	450.168	561.534
mAMES	0.497	1169.873	1462.341
mAMEM	0.064	149.586	186.982
mAMEP	0.060	141.354	176.692
mPSTS	0.110	258.953	323.691
mPSTP	0.029	67.737	84.671
mPTD	0.014	33.633	42.042
mPTV	0.034	80.438	100.547

Table 3.7: Ratio of total attachment area and force (N) of the jaw muscles of UALVP 47243.

Muscle	Ratio of total attachment area	F_m (ST = 24)	F_m (ST = 30)
mAMP	0.185	536.475	670.593
mAMES	0.516	1497.719	1872.149
mAMEM	0.104	302.039	377.549
mAMEP	0.074	214.996	268.745
mPSTS	0.055	158.128	197.660
mPSTP	0.016	46.713	58.391
mPTD	0.015	44.102	55.127
mPTV	0.035	101.550	126.938

Table 3.8: Ratio of total attachment area and force (N) of the jaw muscles of TMP 1984.3.9.

Muscle	Ratio of total attachment area	F_m (ST = 24)	F_m (ST = 30)
mAMP	0.242	644.920	806.150
mAMES	0.418	1113.953	1392.442
mAMEM	0.115	305.671	382.089
mAMEP	0.089	237.181	296.477
mPSTS	0.056	149.238	186.547
mPSTP	0.017	45.304	56.630
mPTD	0.020	53.299	66.624
mPTV	0.044	117.258	146.573

Table 3.9: Ratio of total attachment area and force (N) of the jaw muscles of *Simoedosarus dakotensis*.

Muscle	Ratio of total attachment area	F_m (ST = 24)	F_m (ST = 30)
mAMP	0.276	551.157	688.946
mAMES	0.071	141.783	177.229
mAMEM	0.018	35.945	44.931
mAMEP	0.028	55.914	69.893
mPSTS	0.020	39.939	49.924
mPSTP	0.008	15.976	19.969
mPTD	0.336	670.973	838.716
mPTV	0.243	485.257	606.572

Table 3.10: Ratio of total attachment area and force (N) of the jaw muscles of *Alligator mississippiensis*.

Muscle	Ratio of total attachment area	F_m (ST = 24)	F_m (ST = 30)
mAMP	0.237	632.426	790.532
mAMES	0.055	146.766	183.457
mAMEM	0.032	85.391	106.739
mAMEP	0.055	146.766	183.457
mPSTS	0.017	45.364	56.705
mPSTP	0.008	21.348	26.685
mPTD	0.198	528.356	660.445
mPTV	0.397	1059.380	1324.225

Table 3.11: Ratio of total attachment area and force (N) of the jaw muscles of *Crocodylus cataphractus*.

Muscle	Ratio of total attachment area	F_m (ST = 24)	F_m (ST = 30)
mAMP	0.235	519.664	649.580
mAMES	0.055	121.623	152.029
mAMEM	0.013	28.747	35.934
mAMEP	0.142	314.010	392.512
mPSTS	0.030	66.340	82.925
mPSTP	0.027	59.706	74.633
mPTD	0.314	694.360	867.949
mPTV	0.184	406.886	508.607

Table 3.12: Ratio of total attachment area and force (N) of the jaw muscles of *Gavialis gangeticus*.

Muscle	Ratio of total attachment area	F_m (ST = 24)	F_m (ST = 30)
mAMP	0.318	691.742	826.517
mAMES	0.076	165.322	197.532
mAMEM	0.029	63.083	75.374
mAMEP	0.059	128.342	153.347
mPSTS	0.037	80.486	96.167
mPSTP	0.026	56.557	67.577
mPTD	0.174	378.500	452.245
mPTV	0.303	659.112	787.530

Table 3.13: Ration of total attachment area and force (N) of the jaw muscles of *Tomistoma schlegelii*.

	Gape = 0°		Gape = 25°		Gape = 50°	
Muscle	ϕ	F_T	ϕ	F_T	ϕ	F_T
mAMP	22.777	190.142	23.709	197.482	25.176	208.930
mAMES	51.988	826.079	47.751	776.117	37.138	633.006
mAMEM	26.100	64.536	19.768	49.613	12.082	30.704
mAMEP	21.735	47.912	15.547	34.678	8.752	19.687
mPSTS	38.126	78.812	31.555	66.803	23.980	51.880
mPSTP	30.814	30.589	30.185	30.025	25.787	25.978
mPTD	40.909	21.961	60.440	29.171	57.261	28.208
mPTV	35.035	67.693	56.240	98.032	63.532	105.557
Total		1327.724		1281.920		1103.950

Table 3.14: Tangential force (F_T [N]) of the jaw muscles of UAVLP 33928.

	Gape = 0°		Gape = 25°		Gape = 50°	
Muscle	ϕ	F_T	ϕ	F_T	ϕ	F_T
mAMP	49.419	341.897	35.032	258.412	32.419	241.338
mAMES	44.148	814.833	41.068	768.555	37.878	718.281
mAMEM	17.820	45.777	15.610	40.252	9.179	23.862
mAMEP	16.320	39.721	11.920	29.196	5.734	14.123
mPSTS	34.270	145.814	32.640	139.668	22.541	99.268
mPSTP	33.496	37.383	29.079	32.921	27.745	31.534
mPTD	78.960	33.011	71.250	31.848	59.200	28.890
mPTV	34.020	45.003	53.610	64.752	64.671	72.705
Total		1503.439		1365.604		1230.000

Table 3.15: Tangential force (F_T [N]) of the jaw muscles of UALVP 47243.

	Gape = 0°		Gape = 25°		Gape = 50°	
Muscle	ϕ	F_T	ϕ	F_T	ϕ	F_T
mAMP	56.133	445.453	40.182	346.143	7.181	67.062
mAMES	49.948	1146.445	30.025	749.425	18.357	471.687
mAMEM	32.682	163.094	20.039	103.497	1.921	10.125
mAMEP	26.330	95.359	12.585	46.845	2.390	8.966
mPSTS	35.739	92.362	24.230	64.896	12.320	33.740
mPSTP	29.740	23.173	22.150	17.612	13.774	11.122
mPTD	66.213	40.355	73.526	42.291	60.746	38.477
mPTV	38.592	63.344	49.280	76.966	51.796	79.799
Total		2069.585		1447.675		720.978

Table 3.16: Tangential force (F_T [N]) of the jaw muscles of TMP 1984.3.9

	Gape = 0°		Gape = 25°		Gape = 50°	
Muscle	ϕ	F_T	ϕ	F_T	ϕ	F_T
mAMP	34.743	367.535	14.399	160.374	10.418	116.620
mAMES	37.014	670.611	21.820	414.047	19.507	371.974
mAMEM	27.219	139.812	14.340	75.707	9.540	50.661
mAMEP	22.257	89.835	10.590	43.589	7.175	29.624
mPSTS	40.330	96.585	26.800	67.288	22.336	56.716
mPSTP	32.487	24.333	21.540	16.634	21.363	16.503
mPTD	42.243	35.832	54.970	43.644	59.190	45.777
mPTV	35.007	67.268	47.350	86.244	57.169	98.529
Total		1491.812		907.528		786.403

Table 3.17: Tangential force (F_T [N]) of the jaw muscles of *Simoedosaurus datokensis.*

	Gape = 0°		Gape = 25°		Gape = 50°	
Muscle	ϕ	F_T	ϕ	F_T	ϕ	F_T
mAMP	59.824	476.467	57.290	463.752	55.379	453.562
mAMES	40.233	91.577	40.786	92.618	41.109	93.221
mAMEM	29.715	17.817	39.931	23.072	45.241	25.524
mAMEP	44.653	39.297	51.048	43.483	48.741	42.033
mPSTS	57.178	33.563	54.861	32.660	53.274	32.011
mPSTP	56.456	13.315	64.602	14.432	67.169	14.724
mPTD	13.417	155.690	39.201	424.084	50.479	517.583
mPTV	5.664	47.892	32.218	258.711	42.770	329.517
Total		875.619		1352.812		1508.176

Table 3.18: Tangential force (F_T [N]) of the jaw muscles of *Alligator mississippiensis*.

	Gape = 0°		Gape = 25°		Gape = 50°	
Muscle	ϕ	F_T	ϕ	F_T	ϕ	F_T
mAMP	62.164	559.247	57.043	530.655	52.546	502.046
mAMES	38.722	91.808	38.488	91.340	32.629	79.136
mAMEM	27.473	39.393	37.433	51.903	35.558	49.657
mAMEP	45.770	105.164	50.309	112.936	43.005	100.103
mPSTS	56.606	37.875	59.452	39.068	54.676	37.012
mPSTP	52.245	16.878	60.290	18.541	60.918	18.656
mPTD	15.400	140.308	33.840	294.229	46.241	381.608
mPTV	7.511	138.479	23.114	415.872	35.420	613.980
Total		1129.152		1554.544		1782.199

Table 3.19: Tangential force (F_T [N]) of the jaw muscles of *Crocodylus cataphractus*.

	Gape = 0°		Gape = 25°		Gape = 50°	
Muscle	ϕ	F_T	ϕ	F_T	ϕ	F_T
mAMP	74.255	500.166	71.535	492.910	61.014	454.570
mAMES	41.054	79.879	51.149	94.718	47.203	89.243
mAMEM	32.947	15.635	45.075	20.354	39.955	18.461
mAMEP	45.395	223.564	53.700	253.069	48.652	235.731
mPSTS	57.295	55.823	64.523	59.889	59.880	57.383
mPSTP	47.736	44.186	58.720	51.027	60.976	52.208
mPTD	7.226	87.339	23.374	275.474	35.460	402.822
mPTV	6.224	44.113	20.200	140.497	29.821	202.341
Total		1050.703		1387.939		1512.758

Table 3.20: Tangential force (F_T [N]) of the jaw muscles of *Gavialis gangeticus.*

	Gape = 0°		Gape = 25°		Gape = 50°	
Muscle	ϕ	F_T	ϕ	F_T	ϕ	F_T
mAMP	58.371	588.992	56.493	576.787	54.342	562.048
mAMES	30.425	83.721	35.355	95.662	36.098	97.402
mAMEM	20.370	21.958	30.103	31.640	33.991	35.267
mAMEP	41.714	85.400	45.521	91.573	43.384	88.156
mPSTS	52.986	64.267	56.707	67.276	55.596	66.407
mPSTP	47.181	41.485	55.143	46.410	58.742	48.347
mPTD	5.791	38.191	21.029	135.821	34.856	216.319
mPTV	6.928	79.503	20.090	226.402	32.230	351.517
Total		1003.517		1271.571		1465.464

Table 3.21: Tangential force (F_T [N]) of the jaw muscles of *Tomistoma schlegelii.*

Muscle	R	τ (Gape = 0°)	τ (Gape = 25°)	τ (Gape = 50°)
mAMP	0.046	8.743	9.080	9.607
mAMES	0.070	57.677	54.188	44.197
mAMEM	0.054	3.517	2.703	1.673
mAMEP	0.049	2.366	1.712	0.972
mPSTS	0.077	6.069	5.144	3.995
mPSTP	0.085	2.604	2.556	2.212
mPTD	0.083	1.832	2.434	2.354
mPTV	0.048	3.228	4.674	5.033
Total		86.036	82.493	70.042

Table 3.22: Torque (τ [N·m]) of jaw muscles of UAVLP 33928.

Muscle	R	τ (Gape = 0°)	τ (Gape = 25°)	τ (Gape = 50°)
mAMP	0.052	17.946	13.564	12.668
mAMES	0.086	69.986	66.011	61.693
mAMEM	0.066	3.003	2.641	1.566
mAMEP	0.058	2.322	1.707	0.826
mPSTS	0.086	12.524	11.996	8.526
mPSTP	0.087	3.256	2.867	2.746
mPTD	0.094	3.111	3.002	2.723
mPTV	0.049	2.201	3.167	3.556
Total		114.350	104.955	94.303

Table 3.23: Torque (τ [N·m]) of jaw muscles of UAVLP 47243.

Muscle	R	τ (Gape = 0°)	τ (Gape = 25°)	τ (Gape = 50°)
mAMP	0.038	16.721	12.993	2.517
mAMES	0.086	99.112	64.789	40.778
mAMEM	0.059	9.678	6.141	0.601
mAMEP	0.051	4.906	2.410	0.461
mPSTS	0.075	6.900	4.848	2.521
mPSTP	0.078	1.818	1.381	0.872
mPTD	0.081	3.262	3.419	3.111
mPTV	0.041	2.580	3.134	3.250
Total		144.977	99.117	54.111

Table 3.24: Torque (τ [N·m]) of jaw muscles of TMP 1984.3.9.

Muscle	R	τ (Gape = 0°)	τ (Gape = 25°)	τ (Gape = 50°)
mAMP	0.087	31.880	13.911	10.116
mAMES	0.164	110.130	67.996	61.087
mAMEM	0.116	16.149	8.745	5.852
mAMEP	0.105	9.390	4.556	3.097
mPSTS	0.143	13.828	9.633	8.120
mPSTP	0.152	3.691	2.523	2.504
mPTD	0.155	5.559	6.771	7.102
mPTV	0.087	5.873	7.530	8.602
Total		196.500	121.665	106.478

Table 3.25: Torque (τ [N·m]) of jaw muscles of *Simoedosaurus dakotensis*.

Muscle	R	τ (Gape = 0°)	τ (Gape = 25°)	τ (Gape = 50°)
mAMP	0.055	26.072	25.377	24.819
mAMES	0.055	5.011	5.068	5.101
mAMEM	0.527	9.388	12.157	13.448
mAMEP	0.501	19.684	21.781	21.054
mPSTS	0.088	2.967	2.887	2.830
mPSTP	0.040	0.532	0.577	0.589
mPTD	0.014	2.209	6.016	7.342
mPTV	0.016	0.763	4.119	5.247
Total		66.626	77.981	80.430

Table 3.26: Torque (τ [N·m]) of jaw muscles of *Alligator mississippiensis*.

Muscle	R	τ (Gape = 0°)	τ (Gape = 25°)	τ (Gape = 50°)
mAMP	0.061	34.110	32.366	30.621
mAMES	0.084	7.752	7.712	6.682
mAMEM	0.080	3.153	4.154	3.974
mAMEP	0.074	7.800	8.377	7.425
mPSTS	0.099	3.751	3.869	3.665
mPSTP	0.048	0.811	0.891	0.896
mPTD	0.010	1.434	3.007	3.900
mPTV	0.012	1.599	4.803	7.092
Total		60.409	65.178	64.254

Table 3.27: Torque (τ [N·m]) of jaw muscles of *Crocodylus cataphractus*.

Muscle	R	τ (Gape = 0°)	τ (Gape = 25°)	τ (Gape = 50°)
mAMP	0.046	23.051	22.717	20.950
mAMES	0.068	5.409	6.414	6.043
mAMEM	0.064	0.996	1.296	1.176
mAMEP	0.061	13.700	15.508	14.445
mPSTS	0.081	4.517	4.846	4.644
mPSTP	0.047	2.098	2.422	2.478
mPTD	0.032	2.825	8.910	13.029
mPTV	0.039	1.726	5.498	7.919
Total		54.322	67.612	70.684

Table 3.28: Torque (τ [N·m]) of jaw muscles of *Gavialis gangeticus*.

Muscle	R	τ (Gape = 0°)	τ (Gape = 25°)	τ (Gape = 50°)
mAMP	0.060	35.054	34.328	33.451
mAMES	0.076	6.351	7.257	7.389
mAMEM	0.073	1.604	2.311	2.576
mAMEP	0.065	5.558	5.959	5.737
mPSTS	0.089	5.722	5.990	5.912
mPSTP	0.051	2.119	2.371	2.469
mPTD	0.015	0.562	2.000	3.186
mPTV	0.016	1.282	3.651	5.668
Total		58.253	63.867	66.389

Table 3.29: Torque (τ [N·m]) of jaw muscles of *Tomistoma schlegelii*.

		Orbit		Mid Snout		Terminus of Snout	
Gape	τ (N·m)	*r*	F_B	*r*	F_B	*r*	F_B
UALVP 33928							
0°	86.036		202.964		297.236		555.037
25°	82.493	0.424	194.608	0.289	284.998	0.155	532.185
50°	70.042		165.234		241.981		451.858
UALVP 47243							
0°	114.350		280.600		406.216		739.716
25°	104.955	0.408	257.546	0.282	372.841	0.155	678.941
50°	94.303		231.409		335.003		610.039
TMP 1984.3.9							
0°	144.977		443.354		690.366		1271.727
25°	99.117	0.327	303.109	0.210	471.984	0.114	869.445
50°	54.111		165.476		257.671		474.656
Simoedosaurus dakotensis							
0°	196.500		594.098		794.366		1198.311
25°	121.665	0.331	367.843	0.247	491.841	0.164	741.948
50°	106.478		321.925		430.445		649.332
Alligator mississippiensis							
0°	66.626		200.181		276.370		446.187
25°	77.981	0.333	234.299	0.241	323.473	0.149	522.233
50°	80.430		241.657		333.631		538.633
Crocodylus cataphractus							
0°	60.409		135.140		201.700		398.409
25°	65.178	0.447	145.808	0.300	217.623	0.152	429.862
50°	64.254		143.741		214.538		423.768
Gavialis gangeticus							
0°	54.322		107.108		165.812		379.842
25°	67.612	0.507	133.313	0.328	206.379	0.143	472.773
50°	70.684		139.369		215.756		494.253
Tomistoma schlegelii							
0°	58.253		116.950		185.577		449.480
25°	63.867	0.498	128.221	0.314	203.462	0.130	492.800
50°	66.389		133.284		211.496		512.258

Table 3.30: Bite force (N) at three points (*r* [m]) on the snout in all specimens.

Muscle	*I*	α_m (Gape = 0°)	α_m (Gape = 25°)	α_m (Gape = 50°)
mAMP	0.018	486.517	505.299	534.591
mAMES		3209.617	3015.496	2459.460
mAMEM		195.690	150.441	93.104
mAMEP		131.659	95.293	54.097
mPSTS		337.746	286.281	222.331
mPSTP		144.929	142.253	123.080
mPTD		101.972	135.448	130.980
mPTV		179.610	260.110	280.075
Total		4787.741	4590.622	3897.718

Table 3.31: Angular accelerations (α_m [rad/s^2]) in UALVP 33928 at three gapes.

Muscle	*I*	α_m (Gape = 0°)	α_m (Gape = 25°)	α_m (Gape = 50°)
mAMP	0.017	1037.951	784.502	732.669
mAMES		4047.774	3817.880	3568.141
mAMEM		173.710	152.742	90.548
mAMEP		134.301	98.716	47.751
mPSTS		724.350	693.818	493.125
mPSTP		188.297	165.824	158.838
mPTD		179.946	173.609	157.481
mPTV		127.306	183.171	205.668
Total		6613.634	6070.263	5454.220

Table 3.32: Angular accelerations (α_m [rad/s^2]) in UALVP 47243 at three gapes.

Muscle	*I*	α_m (Gape = 0°)	α_m (Gape = 25°)	α_m (Gape = 50°)
mAM	0.017	1007.902	783.199	151.737
mAMES		5974.211	3905.312	2457.995
mAMEM		583.335	370.175	36.213
mAMEP		295.734	145.278	27.805
mPSTS		415.930	292.244	151.940
mPSTP		109.561	83.271	52.585
mPTD		196.647	206.081	187.494
mPTV		155.489	188.926	195.882
Total		8738.808	5974.485	3261.652

Table 3.33: Angular accelerations (α_m [rad/s^2]) in TMP 1984.3.9 at three gapes.

Muscle	*I*	α_m (Gape = 0°)	α_m (Gape = 25°)	α_m (Gape = 50°)
mAMP	0.020	1600.623	698.433	507.881
mAMES		5529.370	3413.933	3067.022
mAMEM		810.810	439.048	293.797
mAMEP		471.461	228.759	155.469
mPSTS		694.253	483.665	407.674
mPSTP		185.335	126.689	125.697
mPTD		279.118	339.974	356.589
mPTV		294.866	378.046	431.896
Total		9865.836	6108.548	5346.025

Table 3.34: Angular accelerations (α_m [rad/s^2]) in *Simoedosaurus dakotensis* at three gapes.

Muscle	*I*	α_m (Gape = 0°)	α_m (Gape = 25°)	α_m (Gape = 50°)
mAMP	0.204	127.805	124.395	121.661
mAMES		24.564	24.843	25.005
mAMEM		46.020	59.591	65.924
mAMEP		96.490	106.768	103.207
mPSTS		14.544	14.153	13.872
mPSTP		2.610	2.829	2.886
mPTD		10.826	29.489	35.991
mPTV		3.738	20.193	25.720
Total		326.598	382.262	394.266

Table 3.35: Angular accelerations (α_m [rad/s^2]) in *Alligator mississippiensis* at three gapes.

Muscle	*I*	α_m (Gape = 0°)	α_m (Gape = 25°)	α_m (Gape = 50°)
mAMP	0.070	486.590	461.713	436.821
mAMES		110.582	110.018	95.318
mAMEM		44.974	59.257	56.692
mAMEP		111.271	119.494	105.916
mPSTS		53.507	55.192	52.288
mPSTP		11.564	12.703	12.782
mPTD		20.453	42.891	55.629
mPTV		22.817	68.522	101.163
Total		861.757	929.789	916.609

Table 3.36: Angular accelerations (α_m [rad/s^2]) in *Crocodylus cataphractus* at three gapes.

Muscle	*I*	α_m (Gape = 0°)	α_m (Gape = 25°)	α_m (Gape = 50°)
mAMP	0.045	514.991	507.520	468.043
mAMES		120.845	143.295	135.012
mAMEM		22.242	28.956	26.263
mAMEP		306.074	346.468	322.730
mPSTS		100.923	108.274	103.743
mPSTP		46.862	54.118	55.370
mPTD		63.114	199.067	291.092
mPTV		38.569	122.841	176.914
Total		1213.619	1510.539	1579.168

Table 3.37: Angular accelerations (α_m [rad/s^2]) in *Gavialis gangeticus* at three gapes.

Muscle	*I*	α_m (Gape = 0°)	α_m (Gape = 25°)	α_m (Gape = 50°)
mAMP	0.024	1442.569	1412.678	1376.578
mAMES		261.371	298.651	304.084
mAMEM		66.007	95.110	106.015
mAMEP		228.711	245.242	236.092
mPSTS		235.472	246.497	243.312
mPSTP		87.200	97.552	101.625
mPTD		23.144	82.309	131.091
mPTV		52.754	150.227	233.245
Total		2397.227	2628.265	2732.042

Table 3.38: Angular accelerations (α_m [rad/s^2]) in *Tomistoma schlegelii* at three gapes.

		Orbit		Mid Snout		Terminus of Snout	
Gape	α_m	*r*	α_t	*r*	α_t	*r*	α_t
UALVP 33928							
0°	4787.741		2029.504		1385.824		742.143
25°	4590.622	0.424	1945.946	0.289	1328.767	0.155	711.588
50°	3897.718		1652.227		1128.204		604.181
UALVP 47243							
0°	6613.634		2695.182		1861.738		1022.375
25°	6070.263	0.408	2473.747	0.282	1708.779	0.155	938.378
50°	5454.220		2222.698		1535.363		843.146
TMP 1984.3.9							
0°	8738.808		2857.590		1835.150		996.224
25°	5974.485	0.327	1953.656	0.210	1254.642	0.114	681.091
50°	3261.652		1066.560		684.947		371.828
Simoedosaurus dakotensis							
0°	9865.836		3263.165		2440.487		1617.810
25°	6108.548	0.331	2020.427	0.247	1511.056	0.164	1001.686
50°	5346.025		1768.219		1322.433		876.647
Alligator mississippiensis							
0°	326.598		108.701		78.735		48.769
25°	382.262	0.333	127.227	0.241	92.154	0.149	57.080
50°	394.266		131.223		95.048		58.873
Crocodylus cataphractus							
0°	861.757		385.217		258.096		130.665
25°	929.789	0.447	415.628	0.300	278.472	0.152	140.980
50°	916.609		409.736		274.524		138.982
Gavialis gangeticus							
25° - 0°	1213.619		615.508		397.593		173.561
50° - 25°	1510.539	0.507	766.096	0.328	494.866	0.143	216.024
50°	1579.168		800.902		517.350		225.838
Tomistoma schlegelii							
0°	2397.227		1194.059		752.490		310.681
25°	2628.265	0.498	1309.139	0.314	825.012	0.130	340.623
50°	2732.042		1360.830		857.588		354.073

Table 3.39: Tangential acceleration (α_t [m/s^2]) in all specimens at three points on the jaws (*r* [m]).

Gape	α_m	*t*	ω
UALVP 33928			
25° - 0°	3897.718	0.080	312.159
50° - 25°	4590.622	0.074	338.771
UALVP 47243			
25° - 0°	5454.220	0.068	369.263
50° - 25°	6070.263	0.064	389.559
TMP 1984.3.9			
25° - 0°	3261.652	0.088	285.554
50° - 25°	5974.485	0.065	386.474
Simoedosaurus dakotensis			
25° - 0°	5346.025	0.068	365.583
50° - 25°	6108.548	0.064	390.786
Alligator mississippiensis			
25° - 0°	382.262	0.256	97.758
50° - 25°	394.266	0.252	99.281
Crocodylus cataphractus			
25° - 0°	929.789	0.164	152.462
50° - 25°	916.609	0.165	151.378
Gavialis gangeticus			
25° - 0°	1510.539	0.129	194.328
50° - 25°	1579.168	0.126	198.694
Tomistoma schlegelii			
25° - 0°	2628.265	0.098	256.333
50° - 25°	2732.042	0.096	261.345

Table 3.40: Jaw closing time (s) and angular velocity (ω [rad/s]) of the lower jaws in all specimens.

		Orbit		Mid Snout		Terminus of Snout	
Gape	ω	*r*	v_r	*r*	v_r	*r*	v_r
UALVP 33928							
25° - 0°	338.771	0.424	143.604	0.289	98.058	0.155	52.512
50° - 25°	312.159		132.323		90.355		48.387
UALVP 47243							
25° - 0°	389.559	0.408	158.753	0.282	109.661	0.155	60.220
50° - 25°	369.263		150.482		103.948		57.083
TMP 1984.3.9							
25° - 0°	386.474	0.327	126.377	0.210	81.160	0.114	44.058
50° - 25°	285.554		93.376		59.966		32.553
Simoedosaurus dakotensis							
25° - 0°	390.786	0.331	129.254	0.247	96.668	0.164	64.081
50° - 25°	365.583		120.918		90.433		59.949
Alligator mississippiensis							
25° - 0°	97.758	0.333	32.536	0.241	23.567	0.149	14.597
50° - 25°	99.281		33.043		23.934		14.825
Crocodylus cataphractus							
25° - 0°	152.462	0.447	68.153	0.300	45.662	0.152	23.117
50° - 25°	151.378		67.668		45.338		22.953
Gavialis gangeticus							
25° - 0°	194.328	0.507	98.557	0.328	63.664	0.143	27.791
50° - 25°	198.694		100.771		65.094		28.415
Tomistoma schlegelii							
25° - 0°	256.333	0.498	127.679	0.314	80.463	0.130	33.221
50° - 25°	261.345		130.176		82.036		33.870

Table 3.41: Tangential velocity (v_r [m/s]) in all specimens at three points on the jaws.

Chapter 3: Figures

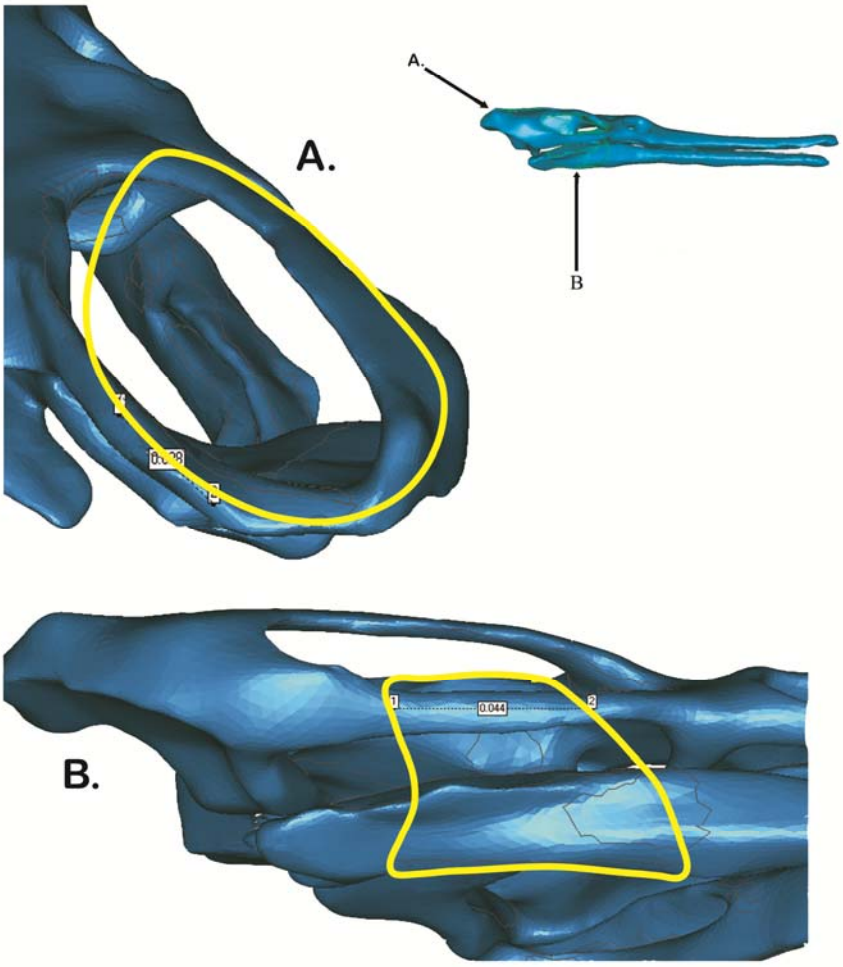

Figure 3.1: ASCA measurements in neochoristoderes. A, ASCA of the M. adductor mandibulae posterior + M. adductor mandibulae externus. B, ASCA of the M.adductor mandiblae internus. Inset indicates the views of A and B.

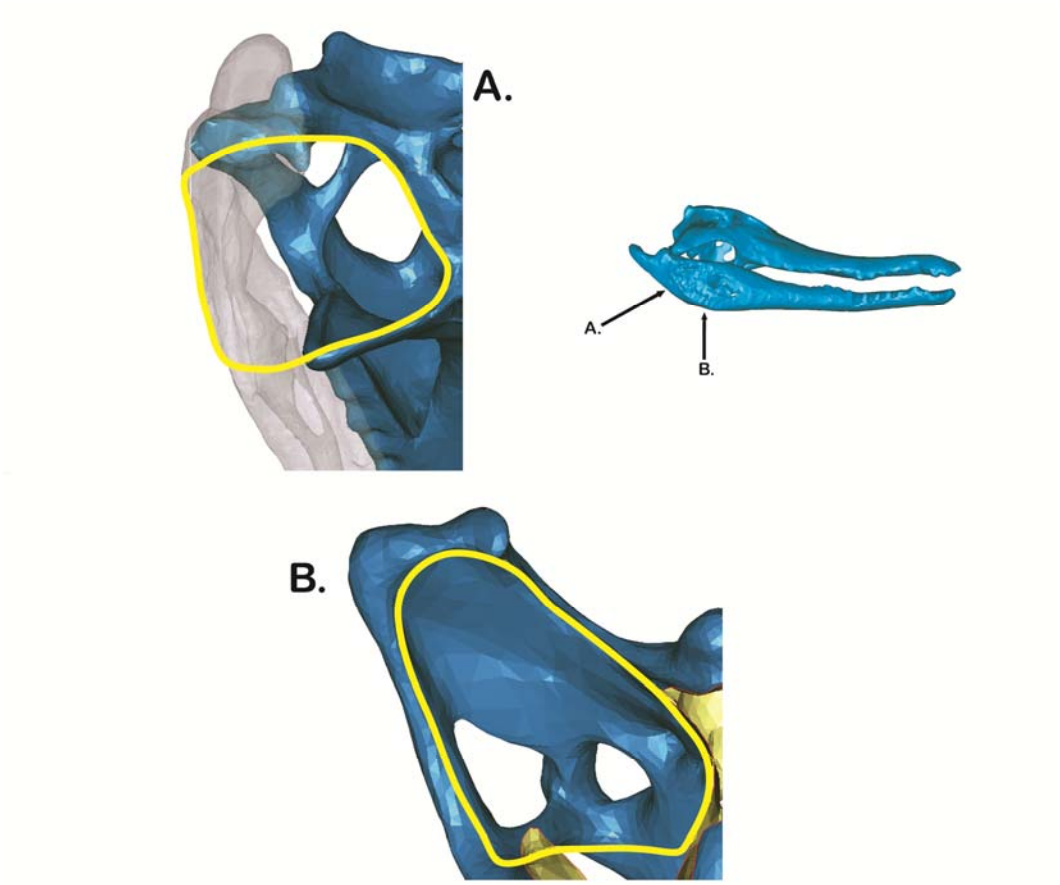

Figure 3.2: ASCA measurements of crocodilians. A, ASCA of the pterygoideus muscles. B, ASCA of the temporalis group. Inset shows the views of A and B.

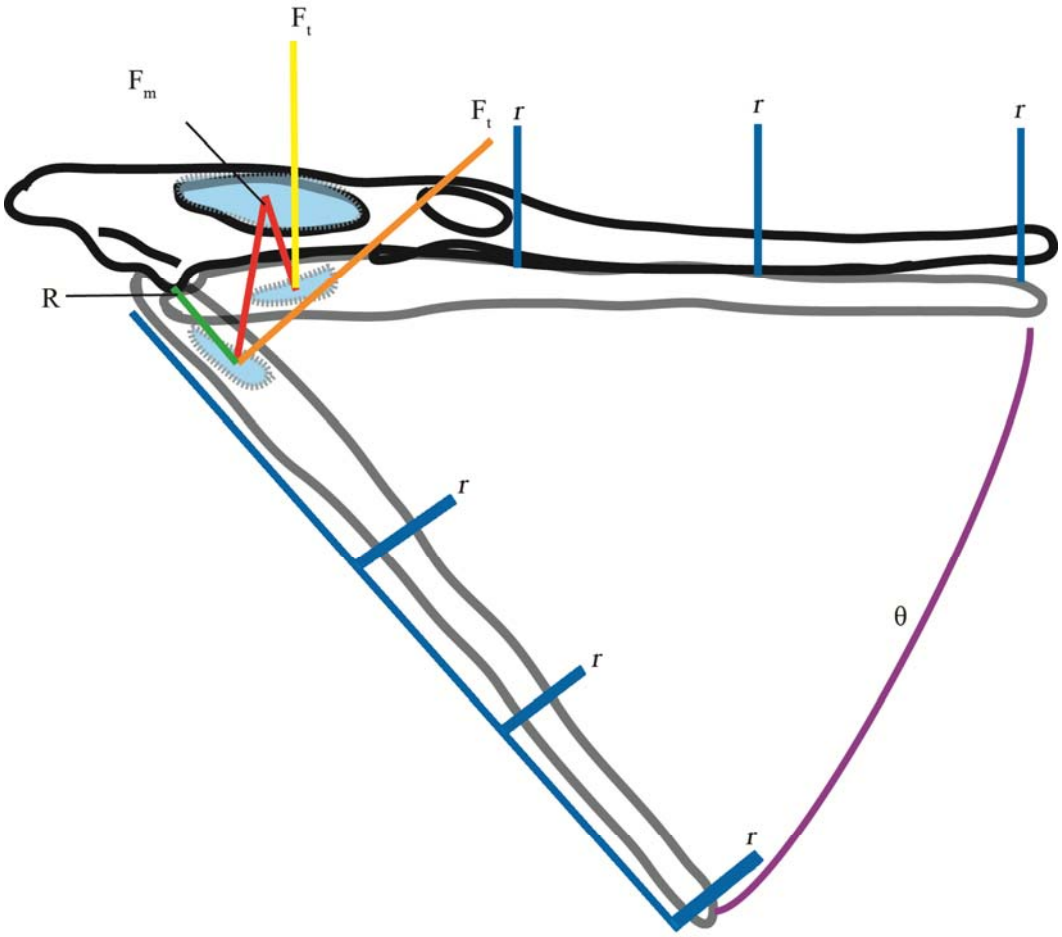

Figure 3.3: Measurements used to calculate torque, bite force, angular and tangential accelerations, and angular and tangential velocities. F_m equals the muscle force, F_t is tangential force, R is the distance between the axis of rotation and the muscle insertion, *r* is the distance between the axis of rotation and a point on the jaws, θ is the gape angle.

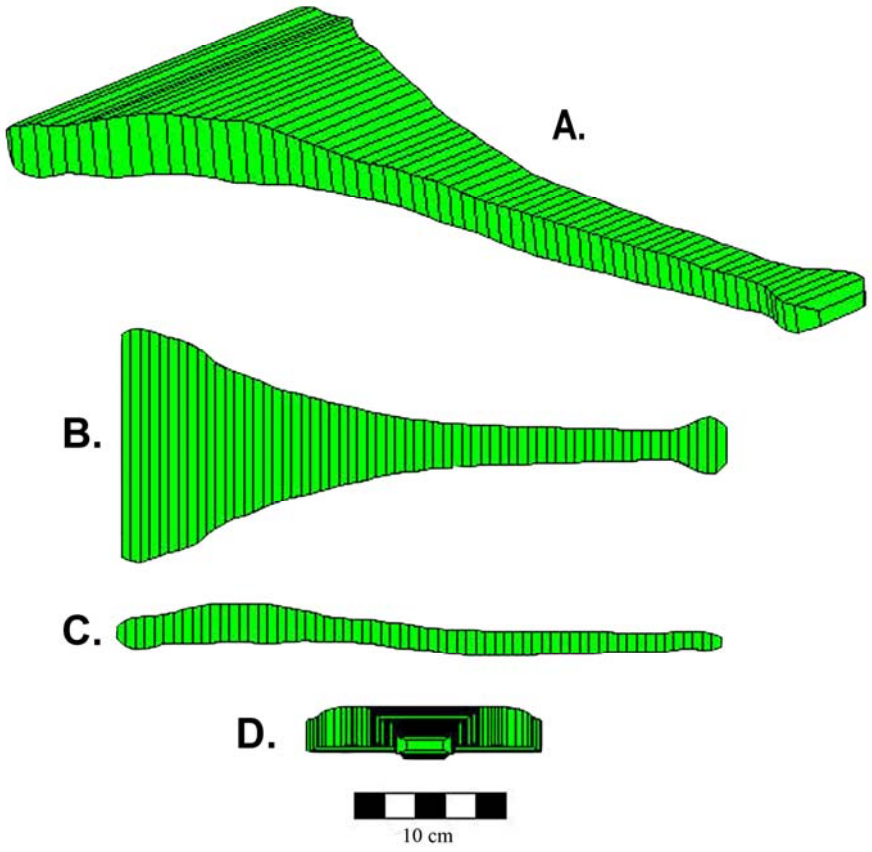

Figure 3.4: Model used to calculate the rotational inertia (RI) of the lower jaws of Champsosaurus lindoei. A. isometric view. B. dorsal view. C. lateral view. D. anterior view.

CHAPTER 4: MECHANICAL AND HYDRODYNAMIC PEFORMANCE OF NEOCHORISTODERE AND EXTANT CROCODILIAN SKULLS

Introduction

As computer technology has improved over the past decade it has become incorporated into greater numbers of palaeontological studies. Advances in computing have allowed systematic studies to incorporate larger data sets, imaging technology has given greater clarity when studying the internal anatomy of extinct animals, and the chemical makeup of fossils can more easily be determined. The most prevalent studies are those that investigate the biomechanics and mechanical functions of fossil vertebrates (Rayfield et al., 2001; Henderson, 2002; Rayfield, 2004, 2005; Snively et al, 2006; Snively and Russell, 2007), studies involving range of motion (Wilhite, 2003), and intraspecific variation (Wilhite, 2005).

The finite element methodology (FEM) is a relatively young, but heavily utilized research tool in vertebrate palaeontology. Traditionally the FEM has been used in engineering (Zienkiewicz, 1971) and orthopaedic medicine (Huiskes and Chao, 1983; Huiskes and Hollister, 1993) to test mechanical strength/performance in a wide range of structures and products. The benefits of using the FEM are that it is noninvasive and thus does not damage fragile specimens, it is not limited to extant taxa, fragmentary specimens can be reconstructed, and the models can be modified to test the effect of a particular structure (Rayfield, 2007).

The predominant area of palaeontological research using finite element analysis (FEA) is the investigation of feeding mechanics in extinct vertebrates (Rayfield, 2001, 2004, 2005; Henderson, 2002; Wroe et al., 2007; Bell et al., 2009). Because studies regarding feeding mechanics often seek to compare fossil and extant taxa, the FEM has resulted in a rich collection of studies that also investigate modern crocodilians and other large carnivores (McHenry et al., 2006; Wroe et al., 2007; Moazen et al., 2008; Moreno et al., 2008; Pierce et al., 2008; Tseng, 2009). The FEM has also allowed researchers to test hypotheses regarding the function of structures only seen in extinct taxa such as the nasals of theropod dinosaurs, the thickened dome in pachycephalosaurs, the tail club of ankylosaurids, and the pneumaticity of sauropod cervical vertebrae (Snively et al., 2006; Snively and Cox, 2008; Arbour and Snively, 2009; Schwarz-Wings et al., 2009).

The FEM began as a mathematical technique whereby the structure of interest was represented as a series of solvable discrete problems by combining mathematical difference equations and engineering elastic continuum problems (Richardson, 1910; Turner et al., 1956; Clough, 1960; Zienkiewicz et al., 2005; Rayfield, 2007). Now, the FEM is conducted using computer software such as Strand7®.

Applying a force (measured in Newtons [N]) to a structure generates stress within the structure. Stress is defined as the force per unit area ($N \cdot m^{-2}$) and can be divided into two types, tensile and compressive stress. Tensile stress results from an object, or part of an object, being stretched, whereas compressive stress is the

converse. Both can occur within the same object, such as when a beam is bent and the molecules on one surface are pulled apart and on the other surface are pushed together. Stress and strain can elicit an osteological response such as bone remodelling or deposition.

Bone shape and evolution

Traditionally it has been thought that bones are structures optimally formed to provide the maximum amount of strength with a minimum of material (Wolff, 1892, translated in 1986; Rayfield, 2007). Later authors have argued that bone growth is an adaptive self-regulating mechanism (Huiskes, 2000). Osteocytes detect strain within the bone and signal the deposition, removal, or realignment of bone (Currey, 2002). The cause of bone remodelling is typically thought to be epigenetic, but also occurs at a genetic level in that the shape, material properties, mineral content, and the controls for bone remodelling lie within the genetic level, and therefore can be selected for (Rayfield, 2007).

Because bone remodelling is controlled by genetic factors that respond to stress and strain, it is possible to investigate questions about how a structure functioned and why it evolved in a particular way (Rayfield, 2007). There are two interpretations regarding the structure of bones and how they relate to loading (Rayfield, 2007). The first is an adaptationist approach whereby a structure, or bone, is assumed to be optimally adapted and evolved for a particular function. In the second case, a structure is tested for how optimally it performs, with the

assumption that other considerations, such as phylogenetic, ontogenetic, or constructional constraints, contribute to the shape of the structure under investigation. The approach used in this investigation is that of the second interpretation.

The broader implications of the FEM in vertebrate palaeontology are not limited to questions regarding the evolution of a structure. Questions about the palaeoecology of extinct animals can be investigated using the FEM. For example, FEA of the dome of pachycephalosaurs supports the hypothesis that the thickened dome could be used for head butting behaviour (Snively and Cox, 2008). However, if the FEM revealed that dome impacts resulted in stress greater than the yield strength of bone the interpretation regarding the function, and thus our views about the ecology of pachycephalosaurs would be altered.

The morphology of the neochoristodere skull is remarkable because the adductor chamber contains powerful jaw adductor muscles supported by a gracile external framework. The jaw adductor muscles were capable of producing bite forces comparable to crocodilians of equal size. The ability of the musculature contained within the adductor chamber to close the jaws has been examined in the previous chapter, but does not resolve questions regarding how the stress generated by those muscles was distributed throughout the skull. The purpose of using the FEM upon the feeding apparatus of neochoristoderes is to compare them to their ecological analogues, and determine how their palaeoecology was influenced by the stresses generated by feeding. It is hypothesized that neochoristodere skulls were able to withstand the stress produced by the muscles

within the adductor chamber and the stress produced by a bite. However, because the skulls of neochoristoderes are delicate, it is thought that the peak and average stress in the skull will be greater than that a crocodilian of similar size.

Hydrodynamics

Previous studies regarding *Champsosaurus* have made the observation the skull is dorsoventrally flattened, even more so than that of crocodilians (Erickson, 1972; Erickson, 1985). The hypothesised functional advantage is that it would have hydrodynamic advantages during lateral striking (Erickson, 1972; Erickson, 1985). Furthermore, longirostry has been suggested as being adapted to optimize hydrodynamic performance at the expense of mechanical performance (McHenry et al., 2006). The criteria used to compare the hydrodynamic performance of the various skulls to one another (neochoristodere versus crocodilian, and longirostrine versus brevirostrine) in this study are the fluid velocity, fluid pressure, and Reynolds number calculated from computer simulations of skull cross sections through the specimens.

Reynolds number is a dimensionless value that is defined as the ratio of fluid inertial forces to fluid viscous forces. Reynolds numbers below a range of 500 to 2000 often result in laminar flow, whereas values above result in turbulent flow. Laminar flow occurs when individual molecules move uniformly as subparallel sheets and is characteristic of slow moving water. Turbulent flow is generally seen in higher velocity water and the molecules move in random patterns. Induced drag generally increases with turbulence due to friction between

the boundary layer and the surface of the object. The boundary layer is defined as the thin layer of fluid flow over the surface of the object where the fluid velocity changes from zero (on the surface of the object) to ninety nine percent of the remaining fluid. Pressure drag is related to the velocity and pressure of the water immediately in front of and behind the object. Observations of the flow velocity, fluid pressure, and Reynolds numbers will be used to infer which specimens are subject to the least drag and have better hydrodynamic performance during lateral strikes.

Materials and Methods

Equipment and Software

The Immersion™ Microscribe 3D (microscribe/digitizer) was connected to a laptop with a 1.73GHz Intel® Pentium® dual-core processor with 2GB DDR2 RAM. For the digitizer to function the appropriate software is needed. Rhinoceros© 4.0 was used to collect the data generated by the digitizer. Rhinoceros© 4.0 is a NURBS (Non uniform rational b-spline) based CAD program. Rhinoceros© 4.0 is also used as a 3D modelling program capable of creating shapes and editing models. Geomagic Studio 10.0® is a similar program to Rhinoceros©, but with improved features. Like Rhinoceros©, Geomagic Studio 10.0® can be used with the digitizer, and is capable of creating objects and editing. Mimics© 12.0 is used to view and edit data collected from CT scans, but can edit most 3D models through the use of an additional module. Strand7® was

used to conduct FEA of biting. To test hydrodynamic performance the cylinder fluid dynamics template in COMSOL Multiphysics® was chosen.

Specimens

The following specimens were digitized for the purpose of finite element analysis:

TMP 1984.3.9 – Idealized skull cast of *Champsosaurus natator*.

UALVP 33928 – Incomplete cranium of *Champsosaurus lindoei* missing the anterior half of the snout.

UALVP 47243 – Incomplete cranium of *Champsosaurus natator*, missing the left temporal arch, and braincase.

UAMZ HER-R800 – complete skull of *Alligator mississippiensis.*

UAMZ HER-R803 – complete skull of *Crocodylus cataphractus.*

UAMZ HER-R802 – complete skull of *Gavialis gangeticus.*

UAMZ HER-R805 – complete skull of *Tomistoma schlegelii.*

3D Modelling

A digital representation of the specimen or structure of interest is required to conduct FEA. The prerequisites for determining whether or not a specimen is suitable for digitizing are the completeness and extent of deformity for each specimen (Mallison et al., 2009). There are two aims for digitizing a fossil specimen, constructing an "ideal" specimen, or making an exact digital replica of the fossil (Mallison et al., 2009). In the latter case, completeness and the extent of

deformation does not matter. Digitizing for the purpose of obtaining an exact replica would be more applicable in museums, or digital databases. Studies examining biomechanics require that the model being used is ideal (Rayfield, 2007; Mallison et al., 2009). Therefore, the specimen must be complete and show little or no deformation. If a specimen is missing extensive areas far too much data could be missing to make the model worth digitizing. For example, if one were to digitize a skull that was missing the entire snout, the model could be rendered useless because the data could not be recovered at all. Also, if a skull is dorso-ventrally crushed, it is assumed that the digitized specimen would not produce results that accurately reflect the way the skull performed during life. The criteria for determining completeness used in this study were whether or not the missing areas of the specimen could be reconstructed to make an idealized model of each specimen.

X-ray computed tomography (CT) is traditionally used in medicine to investigate the internal anatomy of a patient. A series of X-ray images are created, the number of which is dependent upon the size of the specimen and the desired resolution, with finer resolutions producing a greater number of images. Software, such as Amira®, Mimics®, or Osirix® can interpret the data generated by a CT scanner. CT scanning is advantageous because it's a non-destructive method to examine fossils. Any procedure that involves direct contact with the specimen has the potential to cause damage. CT data can be used to produce detailed digital models of specimens that preserve both small surface features and internal cavities. Studies that require accurate models of fossils, such as those that are

conducting FEA, most often turn to CT scanning as a means to generate their 3D models (Rayfield et al., 2001; Rayfield, 2004; Arbour and Snively, 2009; Schwarz-Wings et al., 2009). However, there are limitations with CT scanning. The first is the cost. Palaeontologists rely on the services of private companies or hospitals, both of which are generally expensive. Secondly, the time investment with CT scanning is much greater due to the high demand the facilities have. Other digitizing methods are far more lenient in this regard.

An alternative to CT scanning for obtaining 3D data is laser scanning. Laser scanners emit a beam of light that is reflected by the object and returned to the emitter. The scanner measures the distance to the object based on the time it takes for the beam to return. Emitters can come in a variety of forms; an immobile apparatus using a surround scan, portable mounted models, or hand-held emitters. Like CT scans, laser scanning results in a high resolution surface representation of a specimen. Depending on the distance, errors are minimal with at most a 5mm margin for error (Mallison et al., 2009). The drawback of laser scanning is that it cannot reproduce internal features.

A third method to recreate fossils digitally is to use mechanical digitizers. The Immersion™ Microscribe 3D (Microscribe, digitizer) is one such example. The Microscribe uses a stylus attached to a jointed mobile arm to collect 3D coordinate data. The data are generated by touching the stylus to the specimen and drawing it over the surface. The Microscribe measures the location of the tip of the stylus relative to the base of the unit and the specimen. The detail of this method is dependent upon the time investment, with greater amounts of time

producing far more accurate models. The advantages of using a Microscribe versus CT scanning are that mechanically digitizing a specimen is far less expensive, faster, and allows researchers to digitize specimens at their leisure. The Microscribe is portable and therefore researchers do not have to take specimens out of collections (increasing the potential for damage during transit).

The Microscribe does have drawbacks when compared to CT scans. The biggest is perhaps the resolution of the digital model. CT scans can preserve even the smallest of details, such as the ornamentation on the surface of the bone, whereas digital models created using the Microscribe tend to be smooth and lack surface textures. Also, CT scans will recreate internal features as well, such as cavities or bone histology. The Microscribe is only able to recreate the surface of an object.

Ultimately, the Microscribe was chosen to digitize the specimens used in this study regardless of the perceived superiority of CT scanning (Rayfield, 2007). Although the Microscribe is unable to reproduce the level the detail of a CT scan, surface ornamentation does not affect FEA results. As discussed earlier, only CT scanning is able to reproduce any internal features. However, internal cavities can be simulated when processing the Microscribe data, using computer aided design (CAD) software.

The Microscribe was placed so that the arm could easily access the entire specimen. The specimens were placed with the dorsal surface facing up and the specimens and digitizer were stabilized. Any movement of either the base of the digitizer or specimen can cause major errors. For example, if the base were moved

even slightly when digitizing, the data collected would shift the same way. Three dots (arranged in x, y, and z axes) were placed on the specimen so that the Microscribe could be calibrated. Once calibrated, the digitizer can then be used to "sketch" the specimen. The stylus was dragged over the surface of the specimen in a manner reminiscent of shading a drawing using a pencil. Mechanical digitizers measure the location of the stylus in 3-dimensional space and produce coordinate data. The coordinates are then displayed in Rhinoceros© 4.0 as individual points, with large numbers creating a point cloud in the shape of the specimen.

The most efficient method to digitize each specimen was to only sketch one half. For the crocodilians the right half of the skull was digitized. Because the fossil specimens were incomplete, the most complete half of the skull was sketched. The dorsal surface was digitized first and once complete the specimen was flipped and the Microscribe was recalibrated. Sketching the specimens then continued until the ventral surface was filled in. Wilhite (2003) and Mallison et al, (2009) have suggested that using NURBS (non-uniform rational b-spline) is far more accurate. NURBS uses curves, rather than points, to directly create a surface model.

Rhinoceros© was then used to manipulate the point cloud. The point cloud was mirrored along its length and the two halves were joined together to construct a complete specimen. Both Rhinoceros© and Geomagic Studio® can then use the point cloud data to render a closed surface mesh representing the specimen. The mesh is comprised of triangular plates joined together. With both modelling

programs the initial mesh is created with errors, such as holes that are the result of low density point sampling. On thin structures (such as the quadrate of *Champsosaurus*) too little point sampling can also cause the program to render only one side. It was found that Rhinoceros© was consistently more error-prone, creating many holes, and other random errors. Geomagic Studio® produced fewer errors at this stage and so was used to render each specimen. Any errors that occur after the point cloud was rendered were manually corrected. The "fill holes" tool in Geomagic Studio® can fill in most holes automatically, but complex or large holes have to be corrected manually.

The largest difference between CT scanning and mechanical digitizing is that CT scans can be used to render the internal cavities and vessels present in a fossil specimen. The Microscribe cannot collect coordinate data from areas the stylus cannot reach, such as any internal cavities. However, there is a way to reconstruct most internal features. CAD software can generate and manipulate entirely new geometric shapes as well. Because this study aims to determine the biomechanical properties of neochoristodere and crocodilian skulls, accurate models were needed and therefore required the presence of the nasal passage, braincase, and other major cavities.

The shapes of the nasal passages, auditory canals, and braincases in the crocodilians specimens were determined via visual inspections and CT images. Lu et al. (1999) studied the internal details of *Ikechosaurus sunailinae* and the results were applied to *Champsosaurus*. CT scans were collected and used to verify the distribution of the internal cavities in *Champsosaurus* (Figure 4.1). Internal

cavities were added by first importing the models into Rhinoceros© and two shapes were used to represent the major cavities, a cylinder for the nasal passage, and a sphere for the braincase. Each shape upon creation would then be moved into the appropriate position within the current model. Then, using the 'bend', 'taper', and 'scale' tools in Rhinoceros© the shapes were moulded into the shape of the cavities found in the specimens. The models were imported into Geomagic® Studio and were connected to their external openings (Figure 4.2 *Champsosaurus*; Figure 4.3, *Crocodylus*).

UALVP 47243 was chosen for digitizing because it has a complete snout and one complete temporal arch. Other specimens housed at the University of Alberta Laboratory for Vertebrate Palaeontology were either missing large areas that could not easily be reconstructed or were considerably deformed. A second representative of *Champsosaurus natator* was digitized as well using TMP 1984.3.9, a cast of an idealized reconstruction. UALVP 47243 is missing the left temporal arch and the braincase was eroded prior to collection and could only be partially recovered. Using Rhinoceros© the left temporal area was created using a mirror image of the right temporal arch. The mirror was then attached to the rest of the skull. The braincase was omitted from the digitizing process, and a facsimile was created in Rhinoceros©.

UALVP 33928 was chosen to represent *C. lindoei* as a digital model because it is a nearly complete skull and with little deformation. There were only two problems during the digitizing process. The first is that beyond the internal nares the snout is missing and the remainder of the snout was reconstructed using

the snout from UALVP 47243. The anterior half, up to the internal nares was copied, and then was pasted on to UALVP 33928. The new snout was then scaled to fit the specimen and the tip of the snout was expanded slightly to better represent the condition described in *C. lindoei* by Gao and Fox (1998). The second problem was that metal bars had been adhered to the temporal bars to provide greater support (thereby unnaturally increasing the size of the temporal bars). Using the 'smooth' and 'sandpaper' tools in Geomagic® Studio removed all traces of the metal supports.

Digital representations of fossils are not limited to those that can be scanned with CT scans, lasers, or the Microscribe. McHenry (2009) in his reconstruction of *Kronosaurus* did not have fossil material suitable for digitizing. The solution was to make a digital model of a *Kronosaurus* skull from scratch using Geomagic® Studio. It is conceivable that any animal can be reconstructed in this way. This is the premise behind the reconstruction of *Simoedosaurus* in this study. No suitable specimens of *Simoedosaurus* for digitization could be located and like McHenry (2009) a digital model was made without using any specimen of *Simoedosaurus*. However, rather than making a *Simoedosaurus* skull from scratch, the model of TMP 1984.9.3 (*Champsosaurus natator*) was transformed to resemble *Simoedosaurus* (Erickson, 1987). To morph the model of TMP 1984.3.9 into *Simoedosaurus* the measurements described in Erickson (1987) were used as a guide when transforming the different areas of the original model. In Geomagic® Studio the 'deform region' tool was used to highlight an area and stretch it The 'bend' and 'scale' tools in Rhinoceros© were also useful.

The snout was shortened and widened to match the proportions described by Erickson (1987). The lower temporal bar was adjusted so that in dorsal view the skull was triangular. The fenestrae between the parietals and squamosals were closed, and the posterior border of the parietal was raised. The temporal bar formed by the postorbital and the squamosal was rotated and bent to resemble the condition figured in Erickson (1987).

Four extant genera of crocodilians were chosen to be digitized so that the results of the FEM conducted on the neochoristoderes could be compared to extant morphological analogues. Cranial specimens of *Alligator mississipiensis*, *Crocodylus cataphractus*, *Gavialis gangeticus*, and *Tomistoma schlegelii* were digitized. All four crocodilians were complete specimens and therefore did not require any editing beyond fixing the errors after the specimens were rendered.

Finite Element Analysis and Hydrodynamics

Once the model is completed it can then be imported into Strand7®, a 3D finite element program. Strand7® cannot conduct FEA on a hollow shell, the initial product of the preprocessing phase of Rhinoceros© and Geomagic® Studio. Converting the shell to a solid, also known as a volume mesh, was completed in the remeshing module of Mimics©. At this point, the digital models were ready to be imported into Strand7®, and the next phase of processing, adding the musculature, commenced. Strand7® is designed primarily for use in engineering problems, and therefore does not contain algorithms that define how muscles work. Boneload (Grosse et al., 2007) is an additional program that works

with Strand7 to provide algorithms that accurately model how a muscle pulls on the bone surface. The Boneload methods described here are summarized from Dumont et al. (2009).

The first step is to create the attachment surfaces for the muscles so that Boneload may calculate the stress each muscle generates upon the surface of the bone. The surfaces of each of the solid meshes were exported from Strand7® as binary stereolithography (STL) files. Only the surface, versus the entire solid mesh, of the final solid mesh must be exported from Strand7® to ensure that the geometry of the plates remains constant. The STL files were then imported into Geomagic® Studio. The muscle attachment surfaces were outlined and each muscle was exported as its own STL file. Boneload also requires the coordinates of the centroid of each muscle attachment area, both origins and insertions, to be input into a Microsoft Excel file.

The muscle attachment files were imported and attached to the original solid mesh. At this point the solid mesh and the muscle attachment sites were given the material properties of compact bone in crocodilians (McHenry et al., 2006). Young's modulus, which is the measure of how elastic a material is, was set at 10 gigapascals (GPa) for all models. Poisson's ratio, which is the ratio between how much an object is stretched and how much it contracts in the direction perpendicular to the direction it is being stretched, was set at 0.4 for all models.

Once the muscle attachment sites are connected to the solid mesh and material properties have been applied, the muscles are exported as a single

NASTRAN file and imported into Boneload with the Excel file containing the coordinate and force data for each muscle. Boneload has three solvers that attempt to model how muscles interact with the bones that they are attached to. The differences between the solvers are the speed at which they are able to solve problems and how accurately the solver emulates how muscles function. The first is the Ad Hoc Uniform Traction Solver that models the muscle force vector proceeding directly to its insertion. This is the fastest of the three solvers, but is the least accurate. The second is the Tangential Traction Solver that models the force vector of the muscles as being perpendicular to the surface of the bone, but accounts for the muscles curving to their insertions. The Tangential Traction Solver strikes a balance between processing time and accuracy. The final solver is the most accurate, but the slowest of the three solvers. The Tangential Plus Normal Traction solver models the musculature similar to that of the Tangential Traction Solver, but mimics the stacking of muscle fibres that occurs as muscles increase in thickness towards their insertion. For this study the Tangential Traction Solver was used on all of the models. It was found that the Tangential Plus Normal Traction Solver was unable to process the data of the thirty muscle attachment sites, and Boneload would cease to function as a result.

The original solid mesh was then opened in Strand7® once again and the NASTRAN file created by Boneload was imported and attached to the solid mesh. The load case generated by Boneload was selected and restraints were added. Restraints are points (nodes) that restrict the movement of the model. Movement can be restricted in any or all directions of translation or rotation. In all models six

nodes were selected as restraints on each of the articular surfaces of the mandibles and the quadrate condyles and movement was restricted in all directions. The assumption was that during jaw adduction, both the mandible and the cranium would be unable to translate or rotate in any direction.

Grasping behaviour was modelled by adding additional restraints on tooth positions at the end of the snout, middle of the snout, and directly below the orbits. Because the teeth are embedded in prey, the jaw would be restricted from translating in all directions and rotation about the x- and y-axis. The restraints placed on the snout were allowed to rotate about the z-axis because it is assumed that during grasping the jaw is still able to rotate. When modeling strikes, force vectors, calculated in the previous chapter, were added. When striking at prey the teeth are initially subject to the force of the impact. In both grasping and striking models the restraints and loads were placed bilaterally.

Different muscle force calculations were used depending on whether striking or grasping behaviour was being modelled. When grasping the jaw musculature is undergoing isometric contraction, because although the muscles are contracting the mandible is not rotating. During a strike the jaw rotates. Isometric contraction, and therefore grasping, has the greater specific tension, and thus muscle forces of the two (Snively and Russell, 2007). For grasping, the muscle force calculations using a specific tension of 30 were used. A specific tension of 24 was used for striking.

The final step was to run the analyses and view the results in Strand7®. The linear static solver was selected and von Mises stress was used to determine

the magnitude of stress observed in the specimens. The von Mises stress is a function of the three principal stresses σ_1, σ_2, and σ_3 that measures how stress distorts a material (Rayfield, 2007). It is a good predictor of failure of bone due to bone being susceptible to ductile fracturing (Rayfield 2007). The breaking point of bone is reached when the von Mises stress exceeds the yield strength of bone in uniaxial tension, which has been measured at 104 MPa (Rayfield, 2007).

To verify the hypotheses of Erickson (1972, 1985) that the skulls of *Champsosaurus* are functionally optimized for hydrodynamic performance, cross sections of the models used in the FEA were imported into the multiphysics program COMSOL®. It has been demonstrated that crocodilians, particularly *Gavialis gangeticus*, capture prey using lateral striking (Thorbjarnarson, 1990). Therefore, it is assumed that *Champsosaurus* feeds by lateral striking as well. Four cross sections were taken from each specimen: through the middle of the temporal region, in the orbits, the middle of the snout, and at the terminus of the snout. Each cross section was imported into the cylinder fluid dynamics template in COMSOL®, a 2D fluid tank that simulates water flowing at a velocity of 1.5 m/s in the center of the cylinder. When the cross section is imported and placed within the tank COMSOL® is able to calculate how the water flows around the specimen. To judge the ability of each specimen to perform lateral striking under water the fluid velocity, fluid pressure, and Reynolds number for each trial were collected. Lower values for peak velocity, fluid pressure, and Reynolds number indicates better performance during lateral striking.

Results

Finite element analysis

FEA results are figured as colour plots measured as von Mises stress (Figures 4.4 – 4.23). The neochoristoderes, when compared with crocodilians, have greater peaks and higher average von Mises stress throughout both the crania and mandibles. The most pervasive trend observed in all of the specimens is that the stress generated by both grasping and striking behaviour decreases as the restraint or load is placed further posteriorly on the snout. Secondly, the crania have lower peaks and average stresses in all specimens when compared to the stress observed in their respective mandibles. Lastly, lower stress is observed in the models of grasping behaviour in all specimens.

For the grasping models in the neochoristoderes, UALVP 47243 (Figure 4.8) has the highest stress observed in the skull, followed by UALVP 33928 (Figure 4.4). TMP 1984.3.9 (Figure 4.10) and the model of *Simoedosaurus* (Figure 4.12) have the lowest stresses during grasping behaviour. The order differs during striking behaviour. The highest stress is observed in TMP 1984.3.9 (Figure 4.11), followed by UALVP 47243 (Figure 4.9), and *Simoedosaurus* (Figure 4.13), and the lowest stress is observed in UALVP 33928 (Figure 4.6). The areas that have the greatest stresses on the crania are the dorsal and ventral surfaces of the rostrum, which experience compressive and tensile stress respectively. Compressive stress is found in the area between the orbits, tensile stress on the upper and lower temporal bars, and tensile stress on the dorsal surface on the quadrate. The posttemporal bar in UALVP 47243 and TMP

1984.3.9 experiences tensile stress as well, however, the same is not observed in UALVP 33928. The stresses on the mandibles tends to be more uniformly distributed, but are greater where the jaw musculature insert generating tensile stress, and on the dorsal and ventral surfaces of the lower jaw (experiencing tensile and compressive stresses respectively). The magnitude of stress in the lower jaw spikes immediately posterior to the point at which the two rami of the lower jaw connect.

Of the crocodilians, the greatest stress during grasping is observed in *Tomistoma schlegelii* (Figure 4.22), followed by *Gavialis gangeticus* (Figure 4.20), *Crocodylus cataphractus* (Figure 4.18), and finally *Alligator mississipiensis* (Figure 4.15). In each grasping trial the specimens all have stress concentrated between the orbits, on the ventral surface of the palatine, around the area immediately anterior to the articulation between the quadrate and articular, and on the ventral surface of the angular ventral to the mandibular fenestra. The longirostrine specimens have greater stresses throughout the snout when compared to brevirostrine morphologies.

In the striking trials the observed stress generally increases in magnitude and changes in its distribution compared to what is observed in the grasping trials. In the striking trials of *Alligator mississippiensis* (Figure 4.17) stresses are concentrated on the dorsomedial, dorsal, and dorsolateral surfaces of the surangular, the anterior margin of the mandibulae fenestra, and the dorsal and ventral surfaces of the anterior dentary immediately posterior to the terminus of the lower jaw. For the longirostrine specimens (Figures 4.19. 4.21, 4.23) the

distribution of stress remains consistent to that observed in the trials modelling grasping behaviour, the only difference being that the magnitude of stress increases.

Hydrodynamics

The parameters measured in the hydrodynamic analyses were fluid velocity, fluid pressure, and peak Reynolds number. Fluid velocities (Table 4.1; Figures 4.24 – 4.30) are lower in the neochoristoderes and tend to decrease from the cross sections through the temporal region to the end of the snout (posteriorly to anteriorly). As the fluid approaches the cross section in each trial the flow is deflected over the dorsal and ventral surfaces of the specimen resulting in low velocity water on the leading edge and trailing the specimen. In the longirostrine specimens in the snout cross sections the area of low velocity water on the leading edge is smaller than that of the brevirostrine specimens. The area of the low velocity water trailing the snout cross sections has a greater length in UAVLP 33928, UALVP 47243, and *Alligator mississippiensis*. In the orbital and temporal cross sections the neochoristoderes have less low velocity water on the leading edge, and a greater length of low velocity trailing each section. The flow around the orbital and temporal cross sections appears to be significantly more streamlined that those of the crocodilians.

The distribution and magnitude of fluid pressure (Table 4.2; Figures 4.31 – 4.37) roughly correlates to the low velocity fluid flow observed on the leading and trailing edges of each cross section. In all of the cross sections pressure

differential between the leading and trailing edges is lower in neochoristoderes than those observed in the crocodilian specimens. The longirostrine crocodilians have lower pressure than brevirostrine specimens. There is no consistent trend in the change in fluid pressure between the temporal cross sections and the end of the snout.

The cell Reynolds number (Table 4.3; Figures 4.38 – 3.44) was measured for each cross section as well. Generally the neochoristoderes have lower peak Reynolds numbers than the crocodilian cross sections. In the temporal cross sections the neochoristoderes have the lowest Reynolds numbers, followed closely by *Gavialis gangeticus*, *Crocodylus cataphractus*, *Alligator mississippiensis*, and lastly *Tomistoma schlegelii*. In the orbital cross sections there is no consistent trend in the change in Reynolds number. The Reynolds number decreases in UALVP 47243, *Simoedosaurus*, and *Gavialis gangeticus*, whereas the remaining specimens show increases. In the snout cross sections the neochoristoderes have the lowest peak Reynolds numbers. When comparing the snout cross sections of the crocodilians to one another the longirostrine specimens have the lowest Reynolds numbers at the end of the snout. But in the mid-snout sections *Alligator mississippiensis* has the lowest number. Of the crocodilians, the highest Reynolds numbers in the snout cross sections are those of *Crocodylus cataphractus*.

Discussion

The most striking result of the FEA is the difference in magnitude of the stress experienced between neochoristoderes and the crocodilians. The peak and average stresses throughout the crania and mandibles of neochoristoderes are considerably greater in both the grasping and striking models. The crocodilians have a negligible number of brick elements that exceed 104 MPa, whereas several regions of the neochoristodere skulls do exceed the yield strength of bone in the striking trials. There are several factors that have an effect on the stress seen throughout the skull. The first is the load placed upon the mandibles. Because neochoristoderes have larger jaw musculature, and thus the greater calculated bite forces, it is not unexpected that they would have greater stress throughout the skull. Secondly, neochoristodere skulls have less mass to dissipate the stress generated during feeding than crocodilians of similar size, especially in the lower jaw and in the temporal region. Lastly, the overall shape of the crania and mandibles are considerably different between neochoristoderes and crocodilians. The crania and mandibles of crocodilians are taller than they are wide in profiles and cross sections when compared to those of neochoristoderes. According to mechanical first principles, skull height, or any object where the height is greater than width, decreases the potential for bending in the dorsoventral direction (Herrel et al., 2002; Verwaijen et al., 2002; Herrel et al., 2005; McHenry et al., 2006). It is thought that the significantly greater stresses observed in the neochoristoderes are the result of being dorsoventrally flattened and that crocodilians benefit from the mechanical advantage of having tall crania and

mandibles. The greater mass of bone and the construction of the crocodilian skull provides a mechanical advantage over neochoristoderes that allows crocodilians to process larger, stronger prey.

The stress differs considerably between the models of grasping behaviour and those emulating striking. The average stress is lower in the models of grasping and is generally confined to the temporal area, the posterior half of the mandibles, and the area immediately surrounding the restraints on the snout. The stresses in the temporal region and the posterior mandibles are the result of tension being applied to the surface of the bones when the jaw muscles contracts. Grasping produces less stress throughout the temporal region and the posterior mandibles, despite the greater muscle forces being exerted as a result of isometric contraction.

In all of the striking models the peak and average stress was higher throughout the skull, especially in the areas posterior to the points on the snout where loading was applied. The stress generated during a strike differs from that of grasping behaviour in that the stress experienced is instantaneous rather than the prolonged stress of grasping. Therefore during a full cycle of prey acquisition the skull first experiences the stress associated with the impact of a strike immediately followed by the sustained stress as seen in the results of the grasping models.

Not only do the results of the striking models give insight as to how stress is distributed throughout the skull during the initial impact of the jaw closing about a prey item but they may also model the stress generated by struggling prey

(during grasping). For example, not all prey is immediately incapacitated by the initial strike of any predator and struggles while being held. When prey is struggling it would exert force upon the jaws, and thus result in stress. The stress resulting from struggling prey would be dependent upon prey size and therefore influence prey choice. With respect to neochoristoderes, the striking models have stresses that approach or in several areas exceed the yield strength of bone. The implication is that were *Champsosaurus* to bite prey too large then the ensuing struggle would have had potential to generate stress beyond the yield strength of bone, and thus may have caused damage.

Results of the striking trials conducted at the terminus of the snout in the neochoristoderes generate the highest stress of all of the remaining trials. The resulting stress on the dorsal and ventral surfaces of the rostrum and mandibles approach 104 MPa, and even exceeds the yield strength of bone in some areas. As the load is moved further posteriorly the stress throughout the skull decreases in all specimens. According to beam mechanics, specifically those of cantilever (a beam in which one end is stationary) systems, the moment of bending increases the closer a load is applied to the fixed end of the beam. In the case of the crania and lower jaw, if the bite force remains constant as the force is applied further posteriorly it results in less stress. However, in the striking models the bite force is calculated to increase further posteriorly, but the rate of the increase is significantly lower than that of the bending moment. The functional significance is that during lateral striking neochoristoderes and crocodilians would likely prefer to utilize the middle of the snout to balance bite force with the resulting

stresses. Thorbjarnarson (1990) supports this interpretation in finding that during lateral striking in *Gavialis gangeticus* the number of prey items caught was highest in the middle third of the snout, followed by the anterior third, and the posterior third of the snout.

Other notable areas where stress is concentrated in neochoristoderes are in the frontals, specifically between the orbits, and the upper temporal bar. The frontals are thickened compared to the remainder of the skull roof. Repeated compression of the frontals due to feeding would result in the deposition of additional bone (Gregory and Adams, 1915; Adams, 1919; Case, 1924; Olsen, 1961). Therefore, it is likely that the frontals have become adapted to absorb stress transmitted from the snout. The source of the stress in the upper temporal bar in the grasping trials is the tensile forces exerted by the powerful M. adductor mandibulae superficialis (mAMES) and is also a factor contributing to the large size of the neochoristodere lateral temporal fenestra. Previous authors have suggested that fenestrae in bone and the formation of membranes within are causally linked to tensile stress (Oxnard et al.,1995; Witzel and Preuschoft, 2005). The remaining borders of the lateral temporal fenestra do not exhibit the same magnitude of stress during grasping. It is likely that the lower stress observed in the posterior, ventral, and anterior margins of the lateral temporal fenestra are due to inadequacies in regards to representing the membrane of the mAMES. Further studies creating more accurate representations of the membranous origin of the mAMES could give more detailed representations of the distribution of the stress throughout this area.

In the models of grasping the temporal region and the braincase experience stress lower than that of the mandibles in all specimens. During striking behaviour however, the stress throughout the temporal chamber increases dramatically in UALVP 47243, TMP 1984.3.9, and *Simoedosaurus*. Stress generated by the load upon the snout is transmitted through the palatines, pterygoids, jugals, and frontals. Despite the striking trials that show stress transmission from the snout to the temporal chamber, the magnitude of that stress falls well below the yield strength of bone. Previous authors have been unable to reconcile the large jaw musculature with the gracility of the bones where those muscles attach (Vandermark et al., 2007). The results suggest however, that the gracile bones of the temporal chamber are not the limiting factor in determining prey choice, and were well able to withstand typical bite forces during prey acquisition and processing.

There are differences in the distribution of stress between the longirostrine and brevirostrine specimens. The peak stress observed on the rostrum is greater in the slender snouted specimens and is similar to that observed by Pierce et al. (2008). The adaptive significance of this difference has been suggested to be the result of a functional compromise between hydrodynamic performance versus mechanical performance (McHenry et al., 2006). The hypothesis of McHenry et al. (2006) suggests the brevirostrine specimens place greater emphasis upon mechanical advantages. This is likely because their preferred prey is larger and thus a stronger skull is needed to resist forces that may be exerted by the struggling prey (Pierce et al., 2008). McHenry et al. (2006) suggested that the

longirostrine morphology is adapted for hydrodynamic performance at the expense of mechanical performance. The results of the FEA contained herein support the interpretation of McHenry et al. (2006). However, there is a third aspect to be considered in the functional compromises between longirostrine and brevirostrine morphologies. The analyses of jaw muscle function of the specimens resulted in the jaws of the longirostrine specimens having greater angular acceleration and velocity than their brevirostrine specimens. Therefore, rather than there being only a compromise between mechanical and hydrodynamic performance, there appears to be a functional triad between the two aforementioned variables and angular acceleration of the lower jaw (Pierce et al., 2008).

McHenry et al. (2006) suggested that the longirostrine morphology is adapted for hydrodynamic performance. The primary prey item of longirostrine crocodilians, especially *Gavialis gangeticus*, is fish (Thorbjarnarson, 1990), and the same has been interpreted for *Champsosaurus* (Russell, 1956). Furthermore, the shape of the neochoristodere skull is dorsoventrally flattened when compared with crocodilians, and it has been previously hypothesized to be adapted for hydrodynamic performance when the head is swung laterally through the water (Erickson, 1972, 1985). The results of the hydrodynamic analyses generally support the hypothesis of McHenry et al. (2006). The greatest Reynolds numbers were observed in the crocodilian specimens, and therefore greater turbulence is produced when they laterally swing their heads through water. Turbulence can result in greater friction between the surface of the specimen and the boundary

layer, thus increasing induced drag. Generally, *Gavialis gangeticus* has the lowest Reynolds numbers of the crocodilians, whereas it and *Tomistoma schlegelii* have the lowest Reynolds numbers at the end of the snout which supports the conclusions of McHenry et al. (2006).

Fluid pressure differentials and the fluid velocities around the specimens influence how much pressure drag the specimen is subjected to during lateral striking. The lower peak velocities and fluid pressure observed in the neochoristoderes suggest that they experience less pressure drag than crocodilians. The same parameters were observed to be lower in longirostrine crocodilians compared to brevirostrine forms, suggesting lower pressure drag. It would seem that induced and pressure drag are lower in longirostrine crocodilians, which means that they have greater hydrodynamic performance as suggested by McHenry et al. (2006). Specimens of *Champsosaurus* have better hydrodynamic performance compared to all of the crocodilians, which in turn result in strike speeds (in water) that would be faster than their modern analogues. The findings support Erickson (1972, 1985) in that the dorsoventrally flattened skull is an adaptation for hydrodynamic performance in lateral striking.

The models used in the hydrodynamic analyses were conducted with the lower jaw in a closed position. During striking it is far more likely that the mandibles would be lowered in anticipation for prey capture. The likely effect would be that the separation of the upper and lower jaws would lower pressure drag, because the height of the skull would in effect be reduced. Secondly,

opening the jaws would expose the teeth which may serve to break up the boundary layer around the teeth and would lower the effects of induced drag.

Regardless of the specimen, it is important to note that the forces used herein are likely the maximum, or near maximum forces that the jaw musculature could exert. In other words, the specimens are modeled as biting as hard as they could. It is likely that when grasping or striking prey the force exerted by the muscles, and thus the stress throughout the skull would be lower in most cases where the prey has ceased to struggle, or did not require the full effort of the jaw musculature to subdue.

It has been suggested that rugosity may also affect stress distribution throughout skulls (Rayfield, 2004). Observations of neochoristodere specimens do not indicate any prominent rugosity. However, the surface of the crocodilian skull roof and the posterolateral surfaces of the surangular and angular displays considerable rugosity. All of the models used in this study were smooth and preserved little of the surface texture in the original specimens. Rayfield (2004) suggested that rugose bone texture in tyrannosaurid nasals and postorbitals are optimized to resist compressive, shearing, and bending stresses. The implication of Rayfield (2004) is that the rugose areas in crocodilians may have lower stress than indicated by the analyses contained herein.

Rayfield (2004, 2005) have suggested that the presence of sutures in finite element models can also affect the distribution and magnitude of stress. All of the models in this study were not modelled with the prominent sutures present in their respective skulls and were completely fused. Complex, interlacing suture

morphologies have been claimed to accommodate compressive stress (Jaslow, 1990), whereas grooved suture morphology is meant to accommodate tensile stresses (Rayfield, 2004). Rayfield (2004) found that addition of the suture along the border of the maxilla and jugal redirected compressive stresses away from the lacrimal, illustrating the effect that sutures can have upon the results of FEA. Future studies recreating sutures in neochoristodere and crocodilian skulls could refine the FEA conducted in this study.

The addition of soft tissues in the models would also affect the magnitude of stress seen throughout the specimens. Soft tissues have been reported *in vivo* to absorb strain and transmit loads across sutures, indicating their effect upon mechanical performance (Buckland-Wright, 1978; Thomason et al., 2001). It is thought that in the specimens modelled herein that the reconstruction of the soft tissues, particularly those of the lower jaw such as the intermandibularis, would reduce the magnitude of stress observed throughout the crania and mandibles. It is generally concluded by many FEA studies, including this one, that the addition of soft tissues is needed to gain a more accurate understanding of stress in biological FEA (Rayfield, 2004; Tseng, 2009).

When comparing the results of the muscle force calculations to those of the FEA there is an incongruity. As discussed in the previous chapter, the method used to calculate the muscle forces, and the resulting bite forces, results in forces that are far lower than those observed in extant crocodilians (Erickson et al., 2003). However, in the neochoristoderes those bite forces generate stress that is near the yield strength of bone, which supports the accuracy of the dry skull

method used on the neochoristoderes, and may even suggest that the estimates of the ASCA were too high.

Conclusion

The purpose of this study was to investigate the mechanical and hydrodynamic properties of neochoristodere skulls, specifically that of *Champsosaurus*, and compare the results to four species of crocodilians. It was found that in models of grasping and striking behaviour that the neochoristoderes experienced higher peaks and average stresses than all of the crocodilian specimens. The causes of the difference in stress between the two groups are the greater bite forces calculated for neochoristoderes, the lower mass of the neochoristodere skull, and the dorsoventrally flattened morphology in the neochoristoderes. The stress observed in the neochoristoderes in most of the trials tends to be well below the yield strength of bone, but does approach it, or even exceed it in the striking models at the terminus and in the middle of the snout. The implication is that neochoristoderes likely preferred to strike and grasp prey with the middle of the snout, as seen in observations of extant feeding in *Gavialis gangeticus* (Thorbjarnarson, 1990). Also, it is believed that the greater stress in neochoristoderes restricted them to hunting smaller prey than crocodilians of similar size, because larger, more powerful prey could potentially exert forces upon the jaws as they struggle that would damage the skull.

The dorsoventrally flattened skulls of neochoristoderes have been shown to be exhibit higher stresses than those of crocodilians. Previous studies have

suggested that this is an adaptation to improve hydrodynamic performance (Erickson, 1972, 1985). The results of the hydrodynamic models support this hypothesis. The models of *Champsosaurus natator* and *Champsosaurus lindoei* have lower Reynolds numbers when compared to the remaining specimens. It was also found that the snouts of longirostrine animals had lower Reynolds numbers than their brevirostrine relatives. The findings support the hypothesis of McHenry et al. (2006) that longirostry is functionally adapted for hydrodynamic performance at the expense of mechanical performance. The greater hydrodynamic performance of *Champsosaurus* supports the interpretation of the previous chapter that they were adapted for preying upon small fish, amphibians, reptiles, and soft invertebrates.

This is the first FEA analysis involving neochoristoderes, and the first study to analyse hydrodynamic performance in neochoristoderes and crocodilians. The results of this study illustrate the potential for FEA to provide insight into extinct taxa through comparisons with extant analogues using techniques previously unavailable to palaeontologists. The ability to compare results across extinct and extant taxa, and to compare a variety of performance variables results in a better understanding of the feeding behaviours and palaeoecology of neochoristoderes.

CHAPTER 4: TABLES

Specimen	Temporal	Orbital	Mid snout	Snout terminus
UALVP 33928	2.038	2.078	1.788	1.776
UALVP 47243	1.839	1.892	1.791	1.835
Simoedosaurus dakotensis	1.877	1.920	1.882	1.932
Alligator mississippiensis	2.073	2.114	1.874	1.906
Crocodylus cataphractus	2.127	2.177	1.964	1.956
Gavialis gangeticus	2.121	2.122	1.869	1.995
Tomistoma schlegelii	2.090	2.075	1.981	1.932

Table 4.1: Peak fluid velocity (m/s) in cross sections at four points on the skull: through the temporal chamber, orbits, middle of the snout, and at the tip of the snout.

	Temporal		Orbital		Mid snout		Snout terminus	
Specimen	Min	Max	Min	Max	Min	Max	Min	Max
UALVP 33928	-1.345	1.410	-1.819	1.341	-1.312	1.104	-1.037	1.308
UALVP 47243	-1.084	1.319	-1.286	1.394	-0.996	1.348	-1.174	1.395
Simoedosaurus dakotensis	-0.914	1.449	-1.619	1.358	-1.165	1.324	-1.511	1.327
Alligator mississippiensis	-1.382	1.484	-1.416	1.460	-1.393	1.346	-1.039	1.423
Crocodylus cataphractus	-2.176	1.503	-1.340	1.476	-1.356	1.358	-1.548	1.366
Gavialis gangeticus	-1.729	1.434	-1.451	1.407	-1.406	1.436	-1.672	1.132
Tomistoma schlegelii	-1.350	1.483	-1.557	1.447	-1.487	1.372	-1.569	1.381

Table 4.2: Minimum and maximum fluid pressure (Pa) in cross sections at four points on the skull: through the temporal chamber, orbits, middle of the snout, and at the tip of the snout.

Specimen	Temporal	Orbital	Mid snout	Snout terminus
UALVP 33928	56.529	58.794	50.290	50.160
UALVP 47243	53.538	52.514	49.849	49.690
Simoedosaurus dakotensis	54.670	53.199	52.346	49.908
Alligator mississippiensis	61.001	71.397	52.183	55.035
Crocodylus cataphractus	57.288	58.764	57.551	60.014
Gavialis gangeticus	56.427	55.931	54.993	52.864
Tomistoma schlegelii	61.475	63.455	52.871	50.581

Table 4.3: Peak cell Reynolds number in cross sections at four points on the skull: through the temporal chamber, orbits, middle of the snout, and at the tip of the snout.

CHAPTER 4: FIGURES

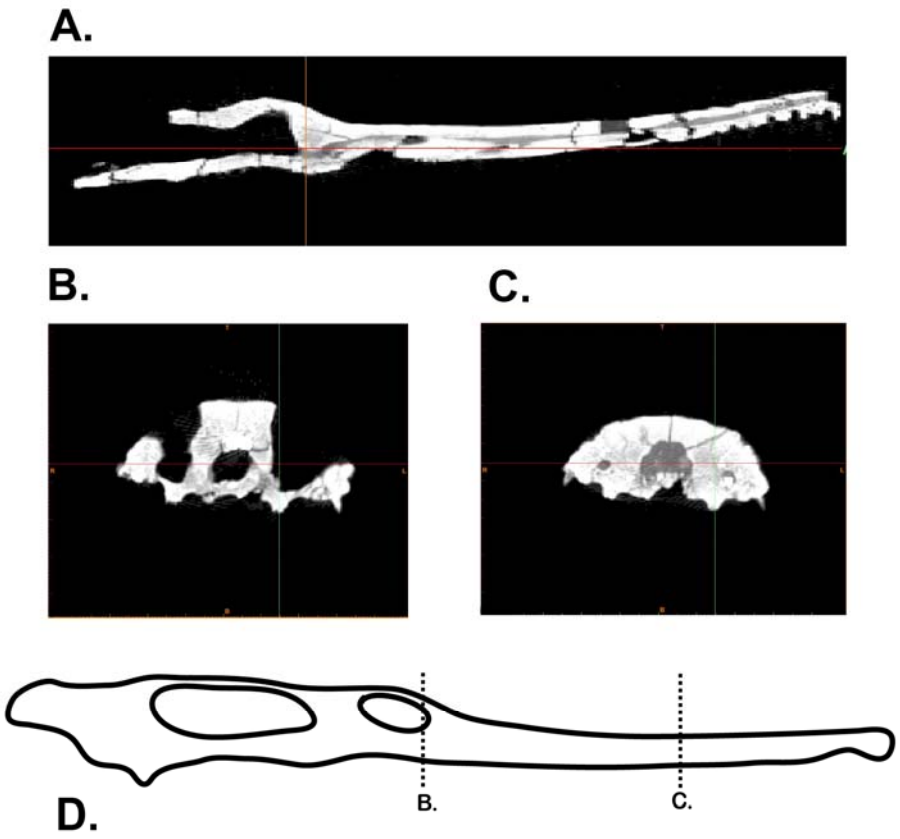

Figure 4.1: CT scans of UALVP 47243 (*Champsosaurus natator*). A, sagittal section. B, cross section through the anterior margin of the orbit. C. cross section through the snout anterior to the internal choanae. D, diagram indicating the locations of B and C.

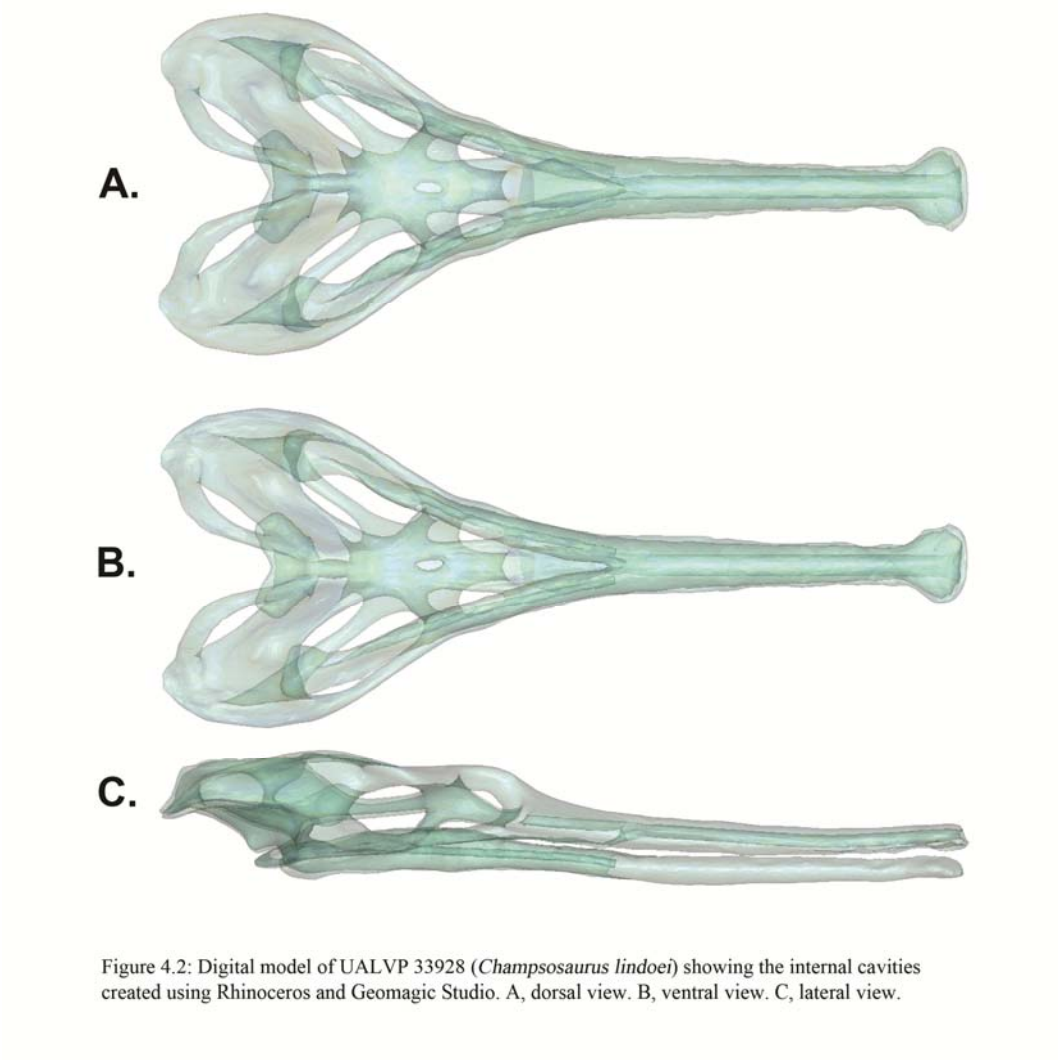

Figure 4.2: Digital model of UALVP 33928 (*Champsosaurus lindoei*) showing the internal cavities created using Rhinoceros and Geomagic Studio. A, dorsal view. B, ventral view. C, lateral view.

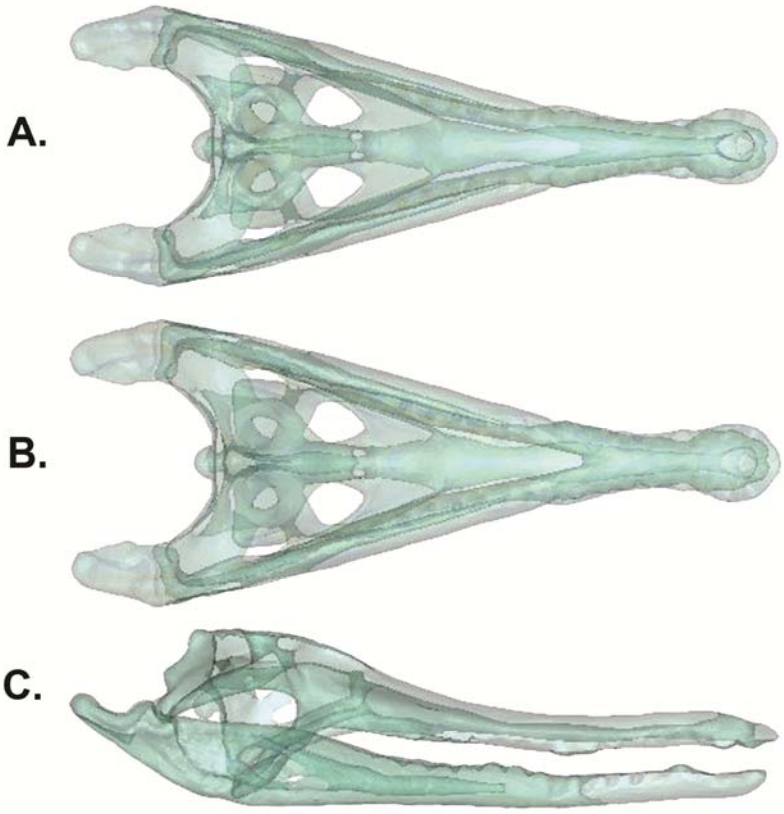

Figure 4.3: Digital model of UAMZ HER-R803 (*Crocodylus cataphractus*) showing the internal cavities reconstructed using Rhinoceros and Geomagic Studio. A, dorsal view. B, ventral view. C, lateral view.

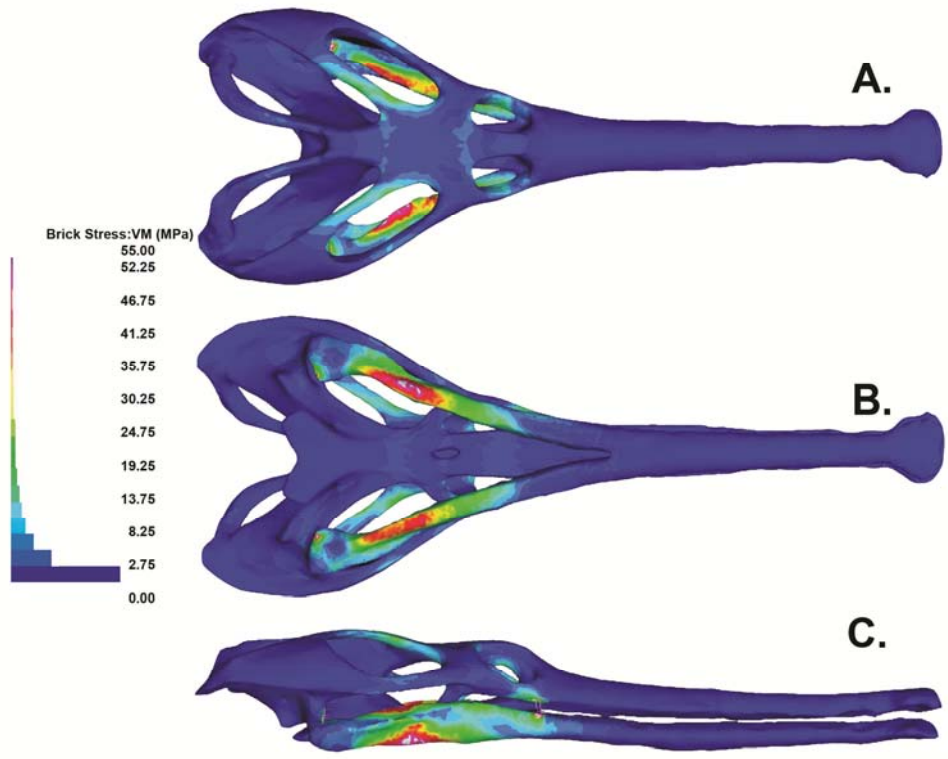

Figure 4.4: Von Mises (VM) brick stress in UALVP 33928 (*Champsosaurus lindoei*) during grasping ventral to the orbits. A, dorsal view. B, ventral view. C, lateral view.

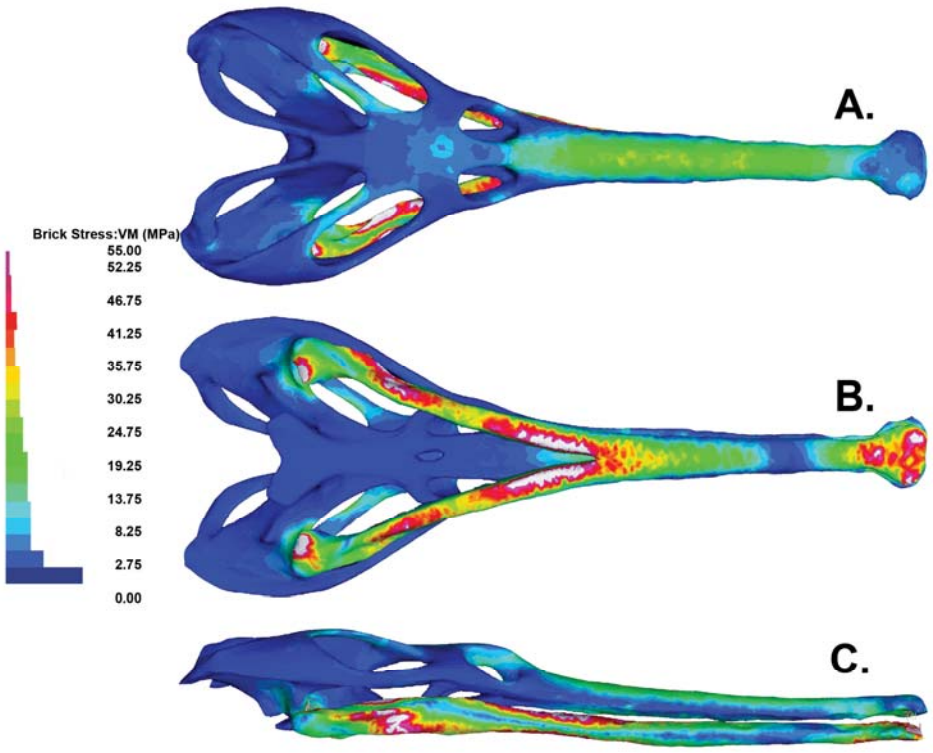

Figure 4.5: Brick stress during grasping at the terminus of the jaws in UALVP 33928. A, dorsal view. B, ventral view. C, lateral view.

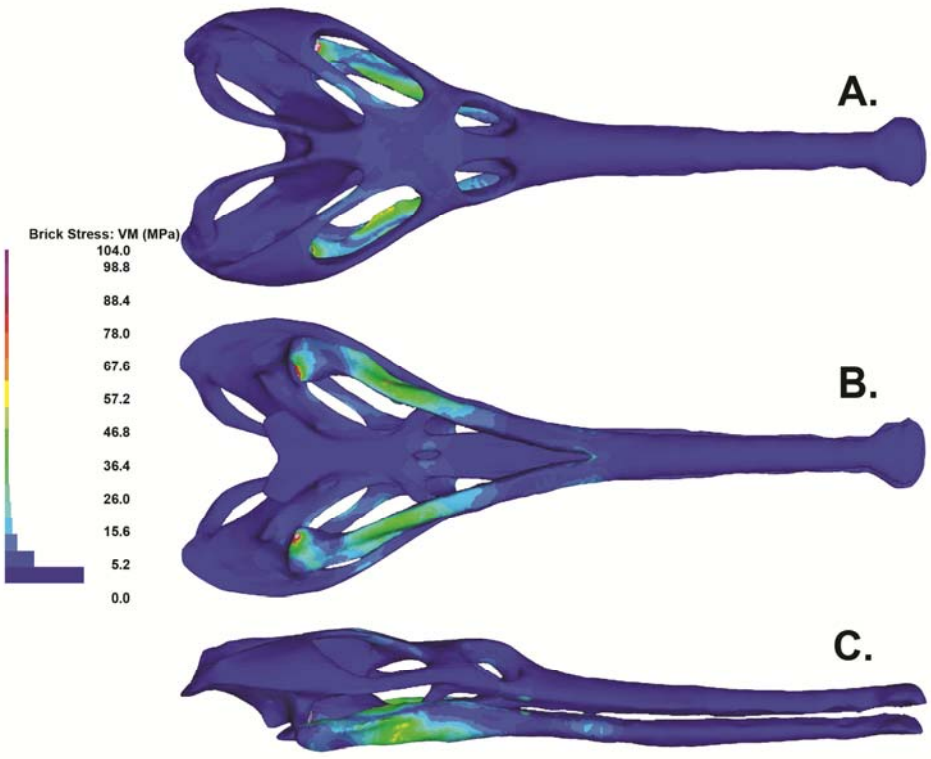

Figure 4.6: Brick stress during striking ventral to the orbits in UALVP 33928. A, dorsal view. B, ventral view. C, lateral view.

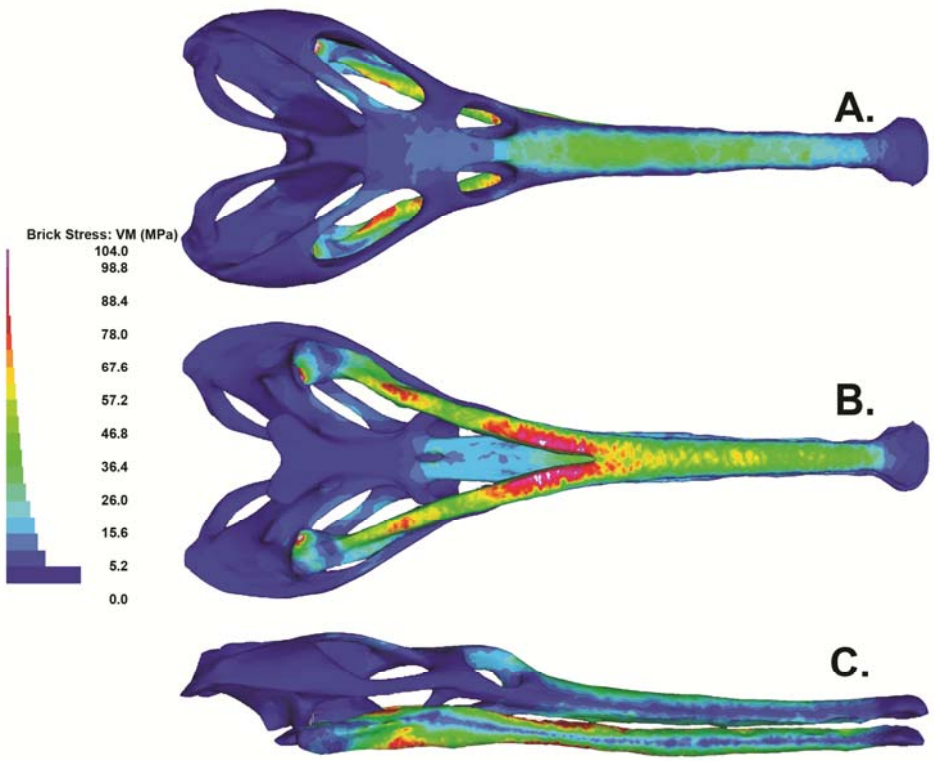

Figure 4.7: Brick stress in UALVP 33928 when striking with the terminus of the snout. A, dorsal view. B, ventral view. C, lateral view.

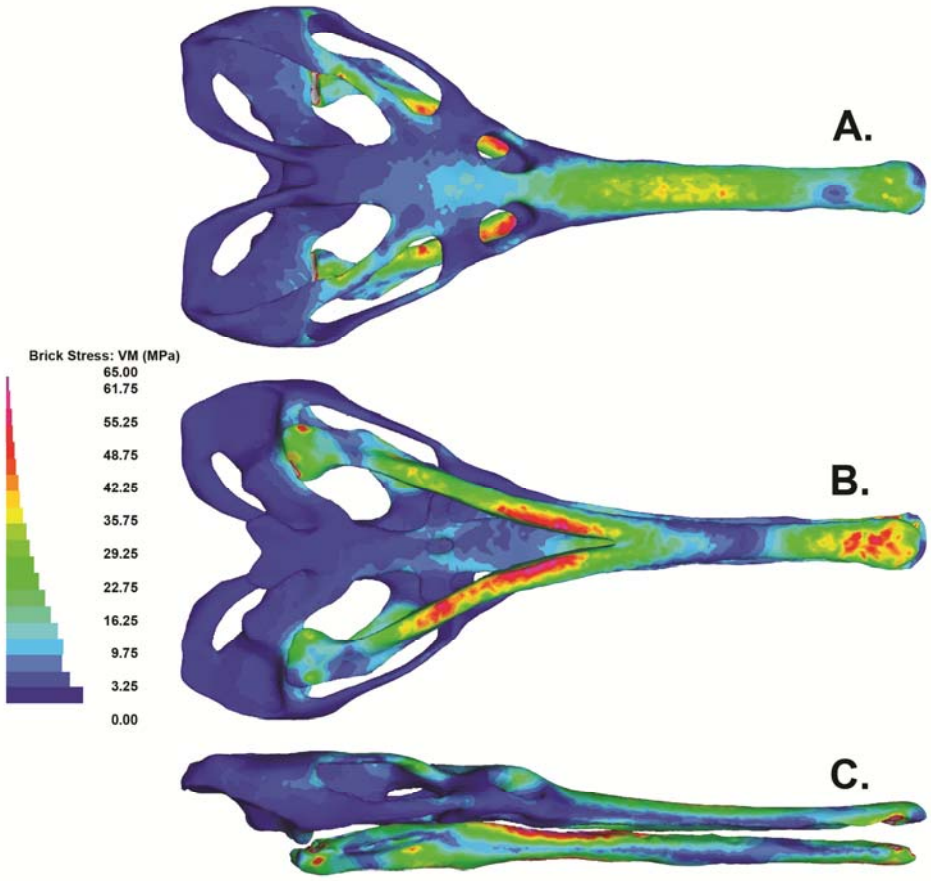

Figure 4.8: Brick stress in UALVP 47243 (*Champsosaurus natator*) when grasping with the terminus of the snout. A, dorsal view. B, ventral view. C, lateral view.

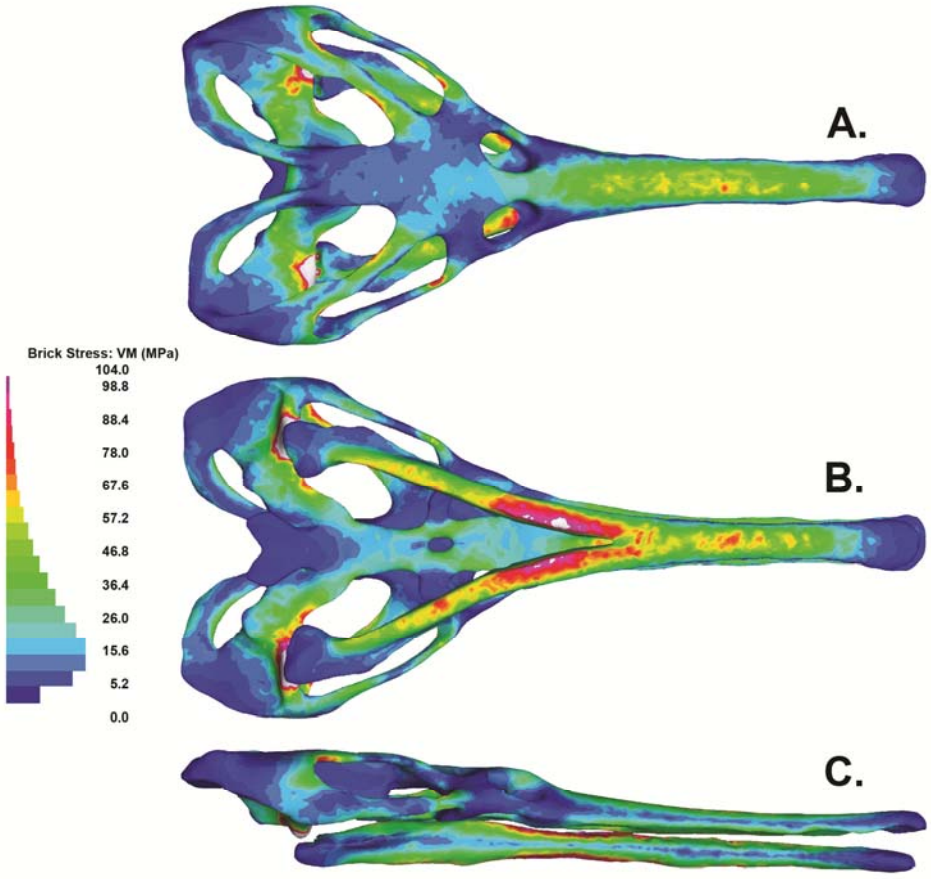

Figure 4.9: Brick stress in UALVP 47243 when striking with the terminus of the snout. A, dorsal view. B, ventral view. C, lateral view.

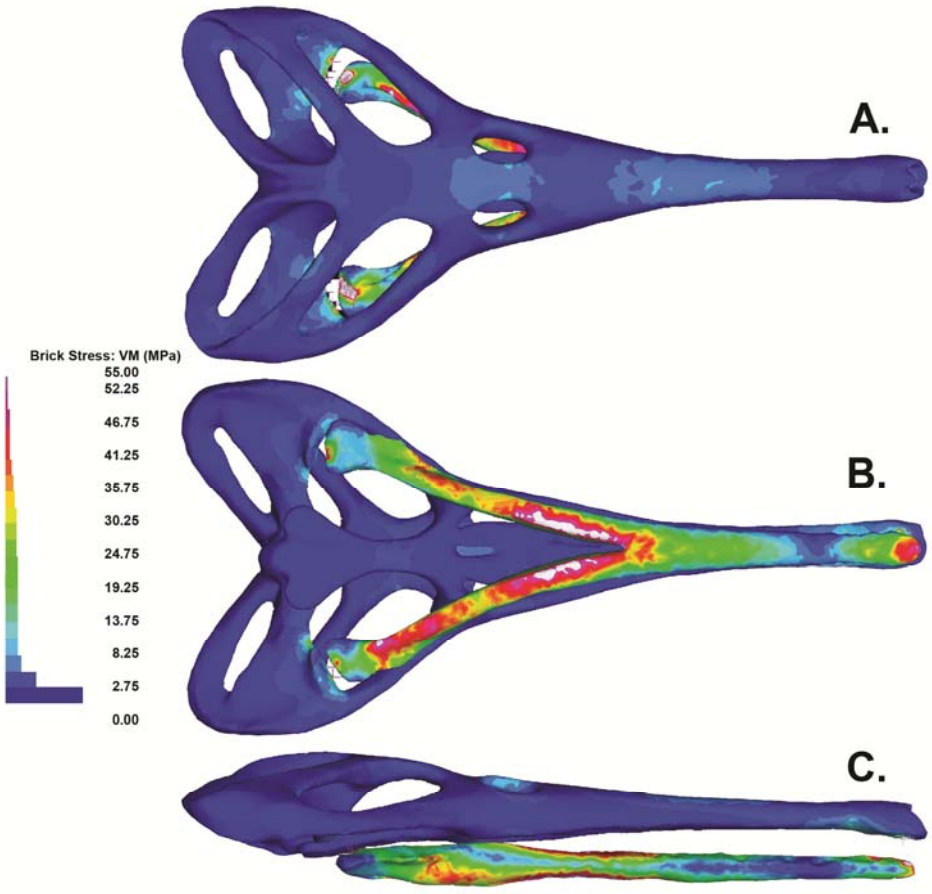

Figure 4.10: Brick stress in TMP 1984.3.9 when grasping with the terminus of the snout. A, dorsal view. B, ventral view. C, lateral view.

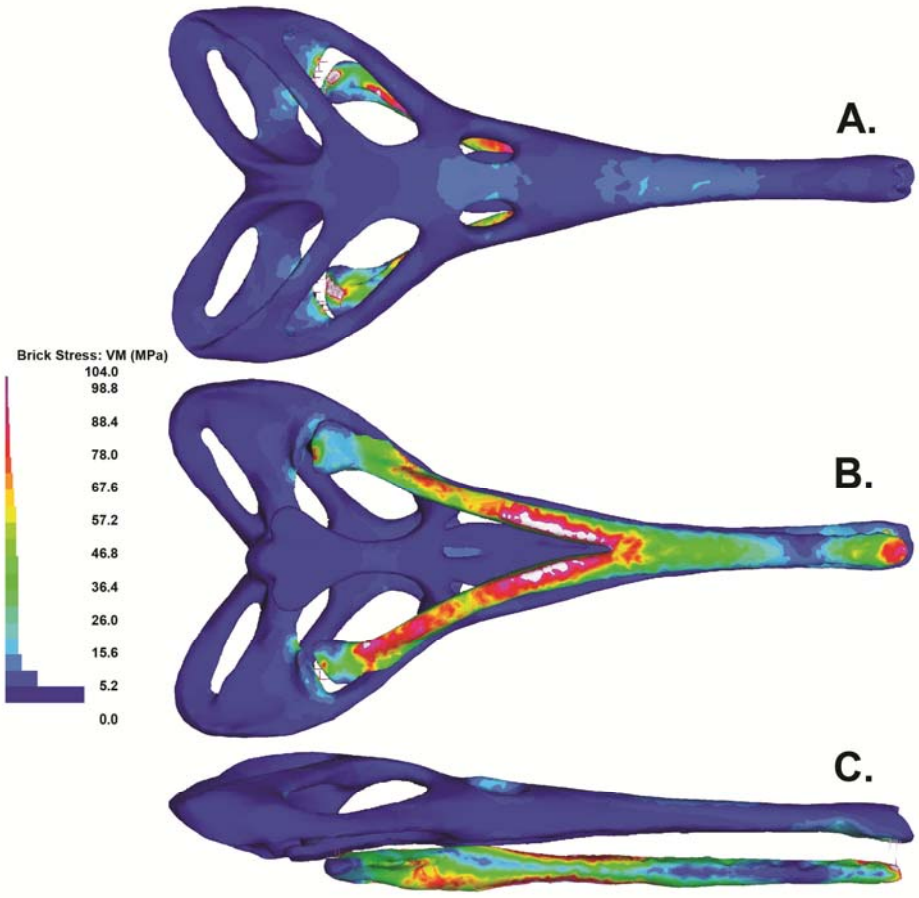

Figure 4.11: Brick Stress in TMP 1984.3.9 when striking with the terminus of the snout. A, dorsal view. B, ventral view. C, lateral view.

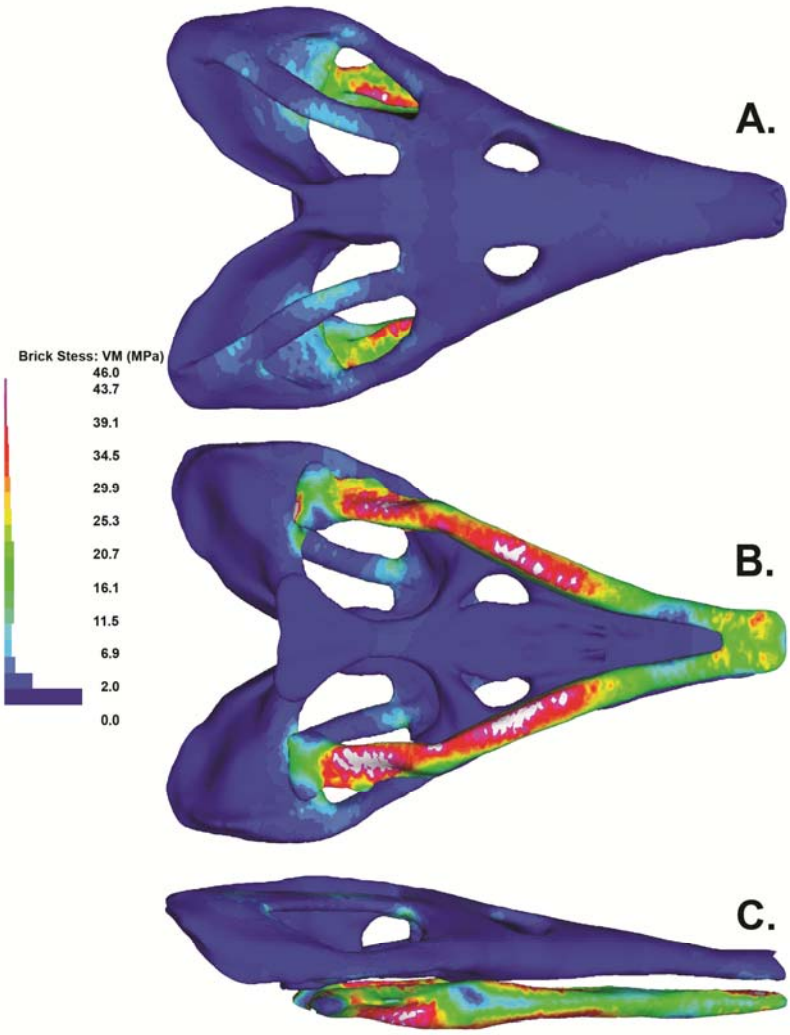

Figure 4.12: Brick stress in *Simoedosaurus dakotensis* when grasping with the terminus of the snout. A, dorsal view. B, ventral view. C, lateral view.

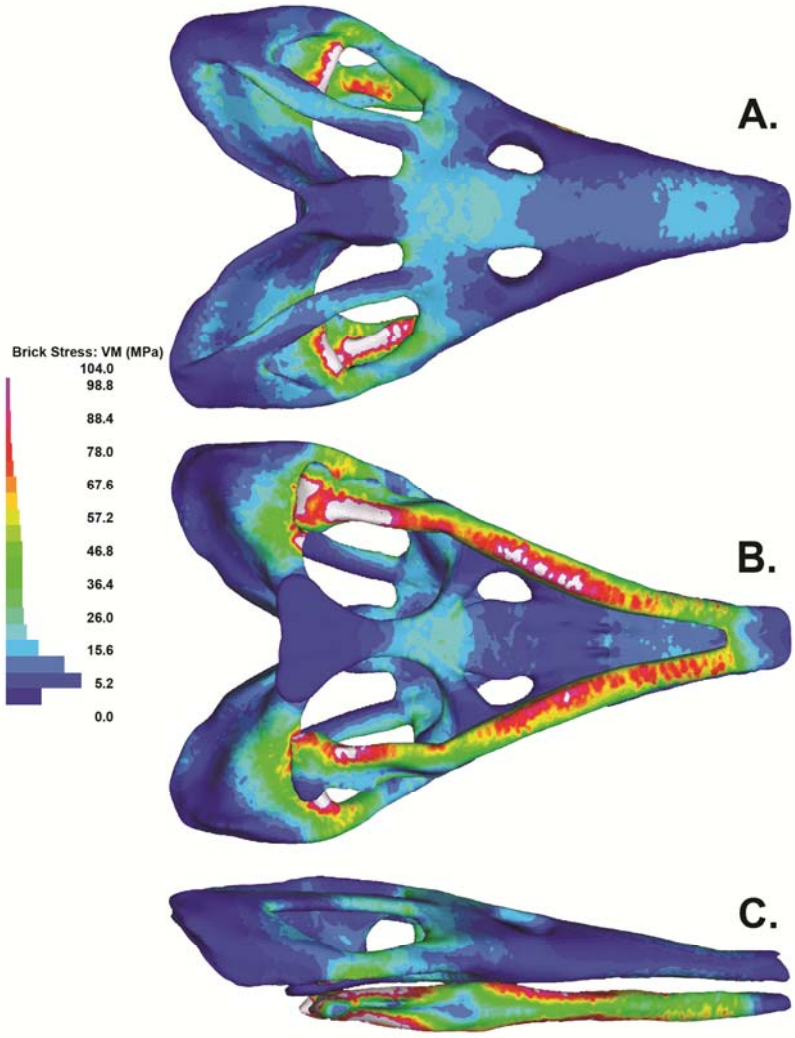

Figure 4.13: Brick stress in *Simoedosaurus dakotensis* when striking with the terminus of the snout. A, dorsal view. B, ventral view. C, lateral view.

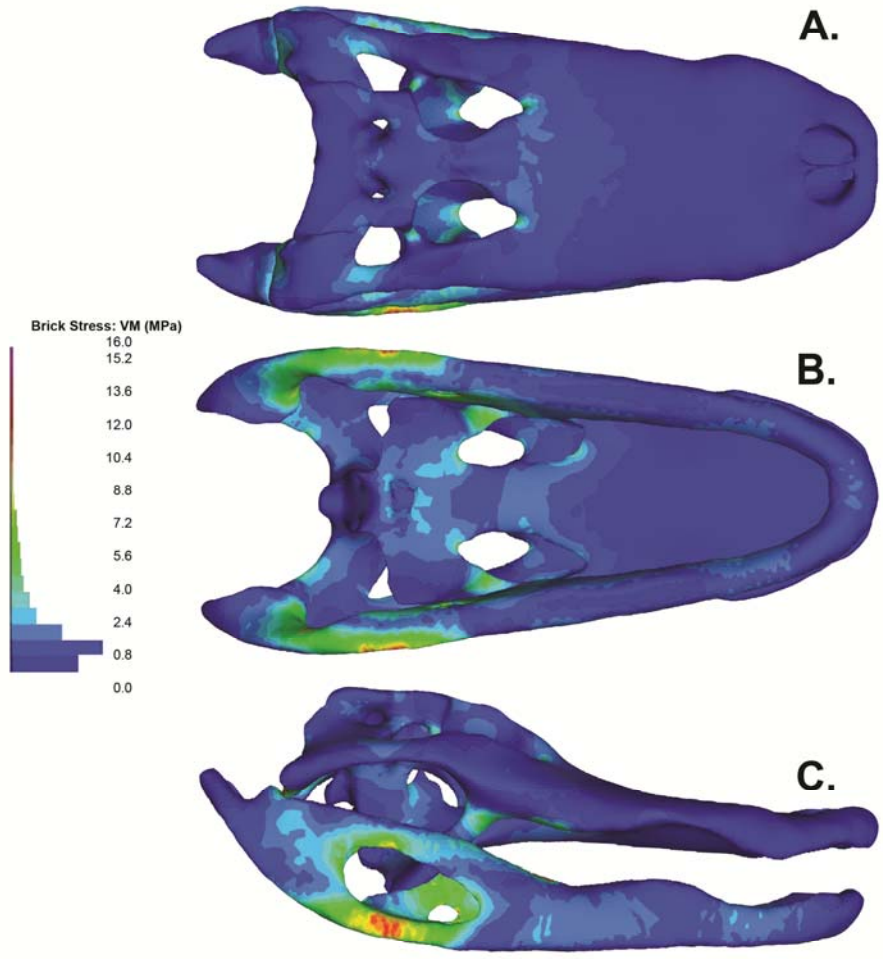

Figure 4.14: Brick stress in *Alligator mississippiensis* when grasping with the most posterior tooth.. A, dorsal view. B, ventral view. C, lateral view.

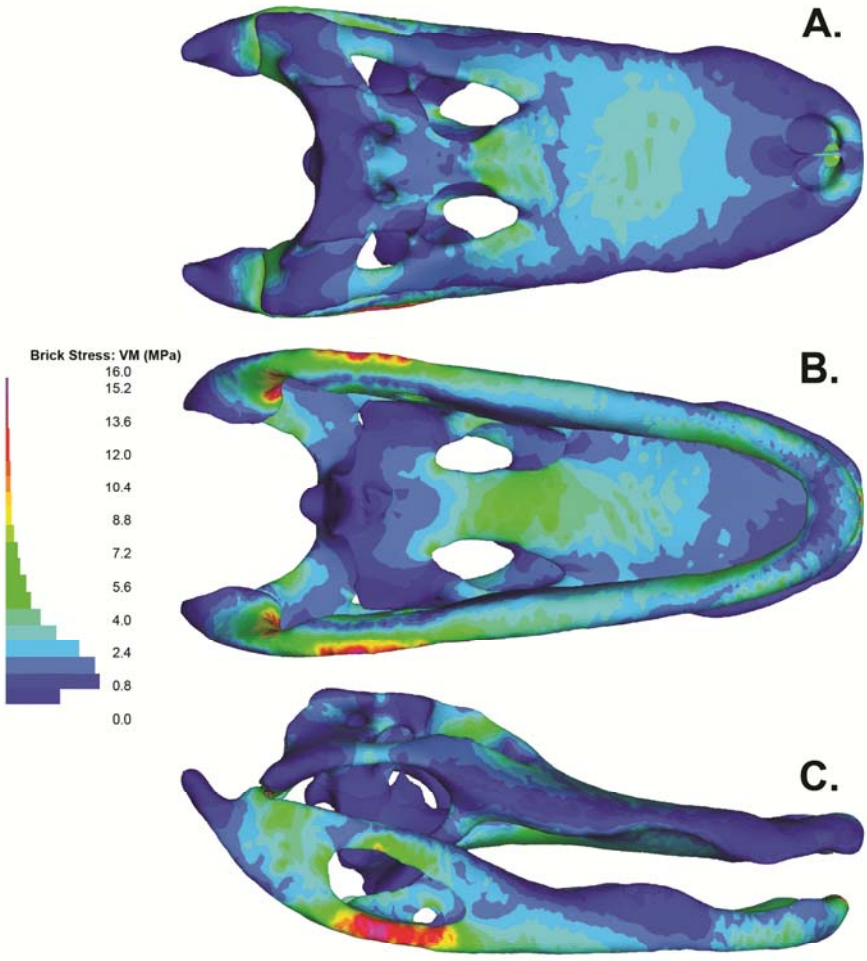

Figure 4.15: Brick stress in *Alligator mississippiensis* when grasping with the terminus of the snout. A, dorsal view. B, ventral view. C, lateral view.

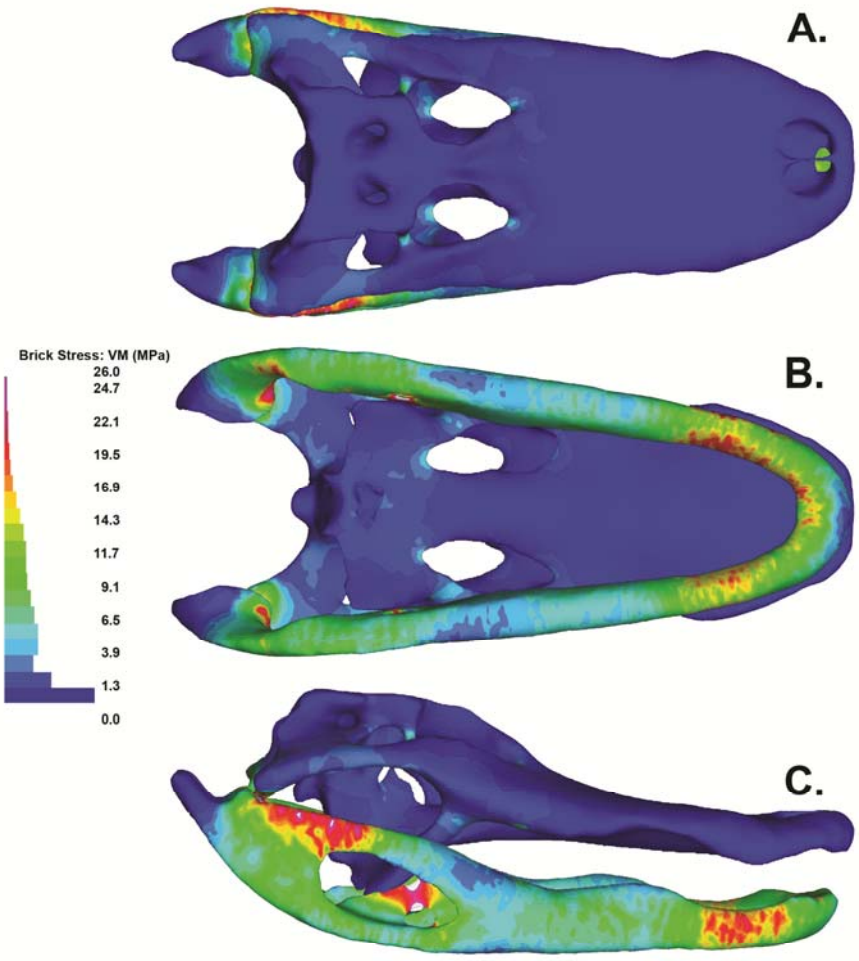

Figure 4.16: Brick stress in *Alligator mississippiensis* when striking with the most posterior tooth position. A, dorsal view. B, ventral view. C, lateral view.

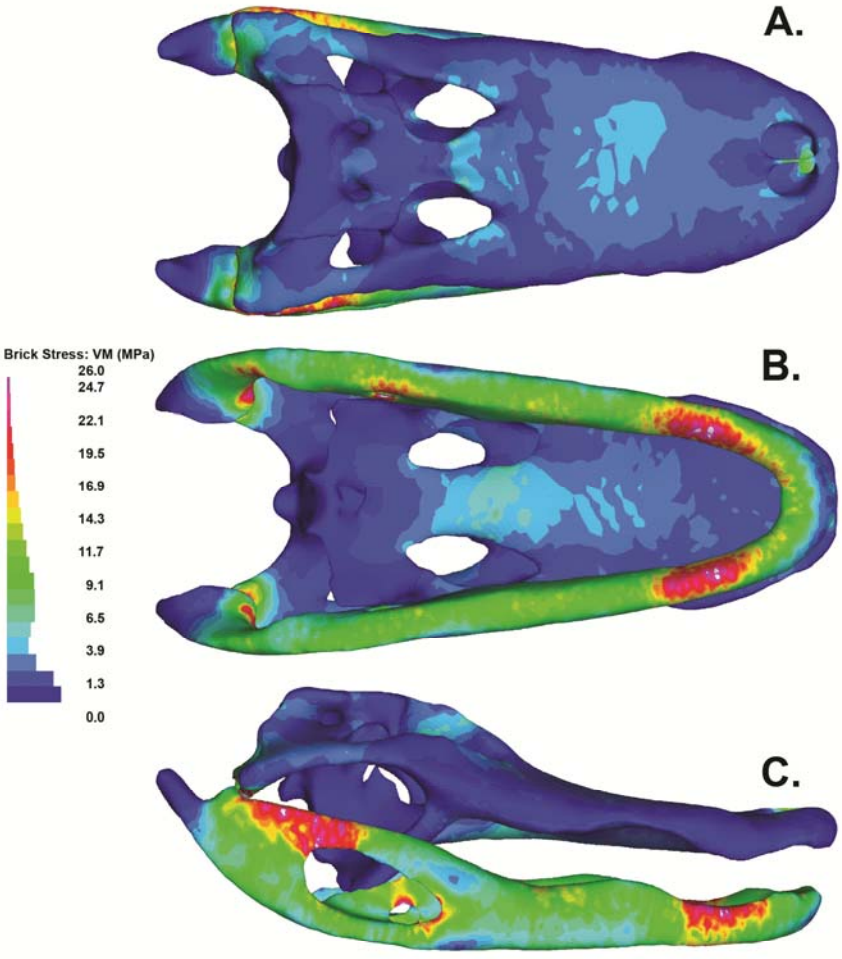

Figure 4.17: Brick stress in *Alligator mississippiensis* when striking with the terminus of the snout. A, dorsal view. B, ventral view. C, lateral view.

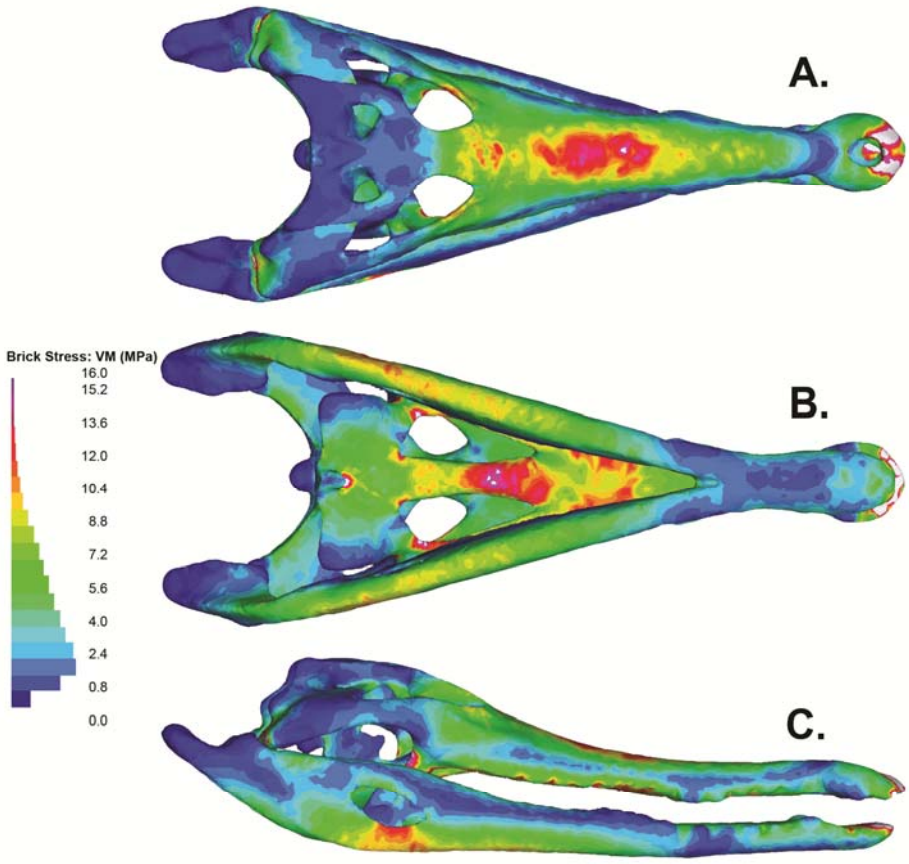

Figure 4.18: Brick stress in *Crocodylus cataphractus* when grapsing with the terminus of the snout. A, dorsal view. B, ventral view. C, lateral view.

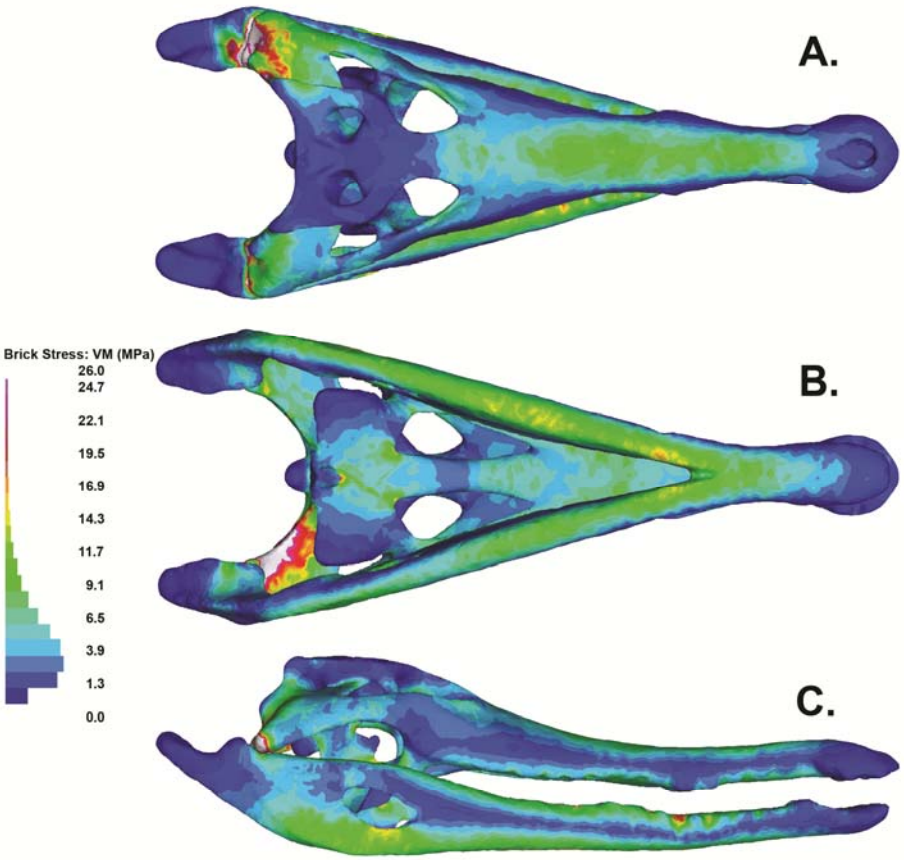

Figure 4.19: Brick stress in *Crocodylus cataphractus* when striking with the terminus of the snout. A, dorsal view. B, ventral view. C, lateral.

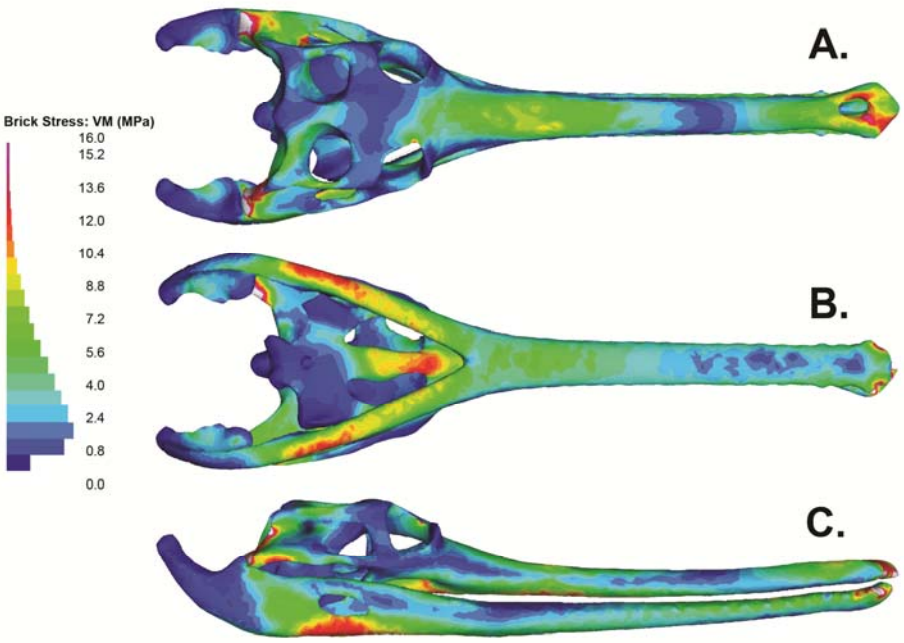

Figure 4.20: Brick stress in *Gavialis gangeticus* when grasping with the terminus of the snout. A, dorsal view. B, ventral view. C, lateral view.

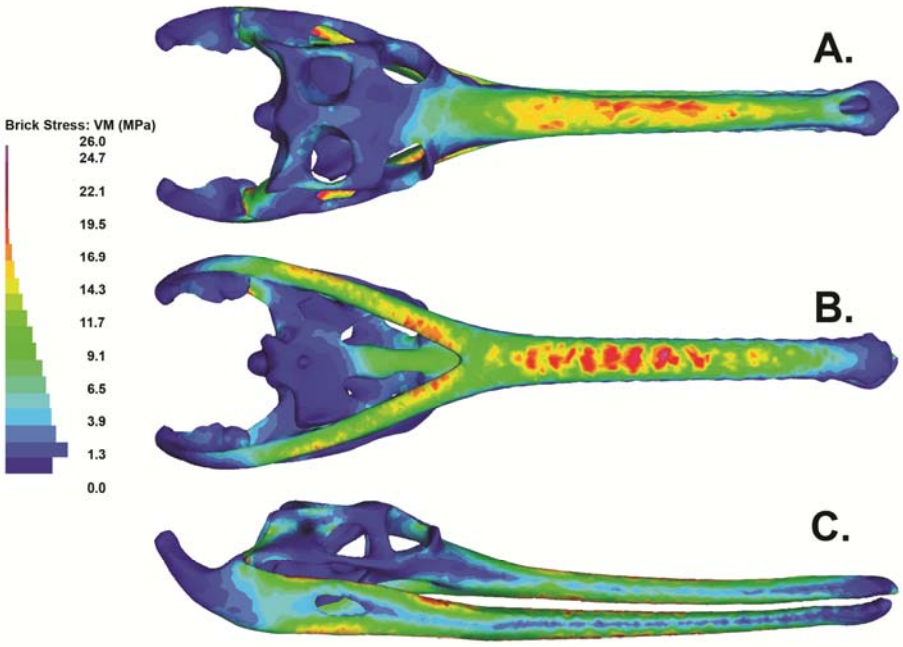

Figure 4.21: Brick stress in *Gavialis gangeticus* when striking with the terminus of the snout. A, dorsal. B, ventral. C, lateral.

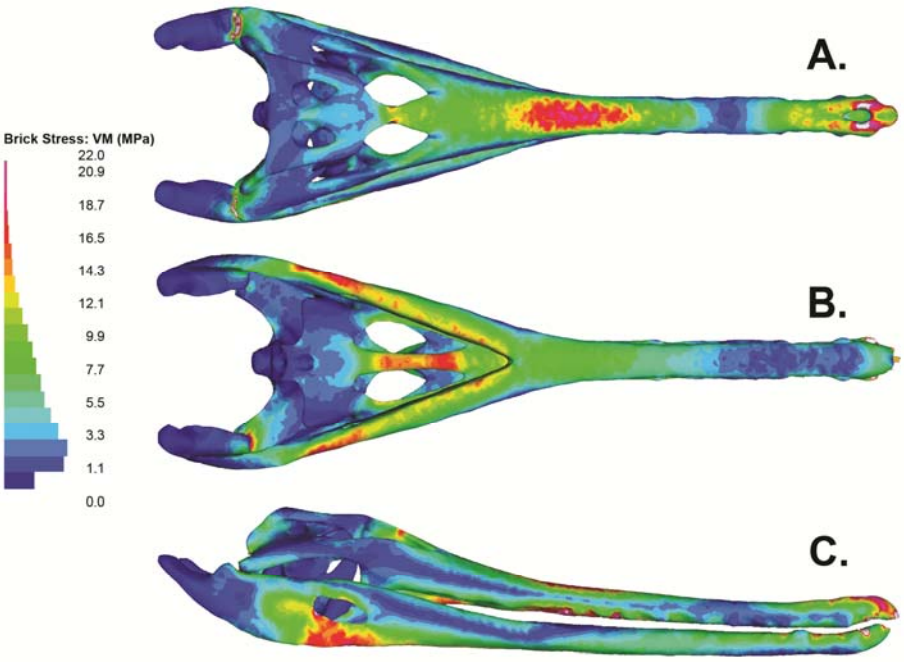

Figure 4.22: Brick stress in *Tomistoma schlegelii* when grasping with the terminus of the snout. A, dorsal view. B, ventral view. C, lateral view.

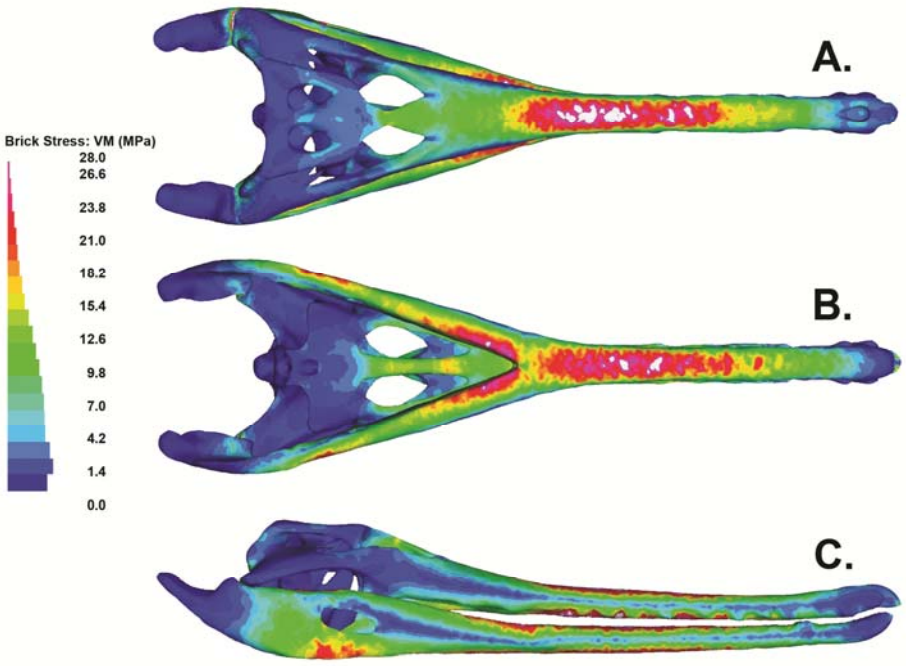

Figure 4.23: Brick stress in *Tomistoma schlegelii* when striking with the terminus of the snout. A, dorsal view. B, ventral view. C, lateral view.

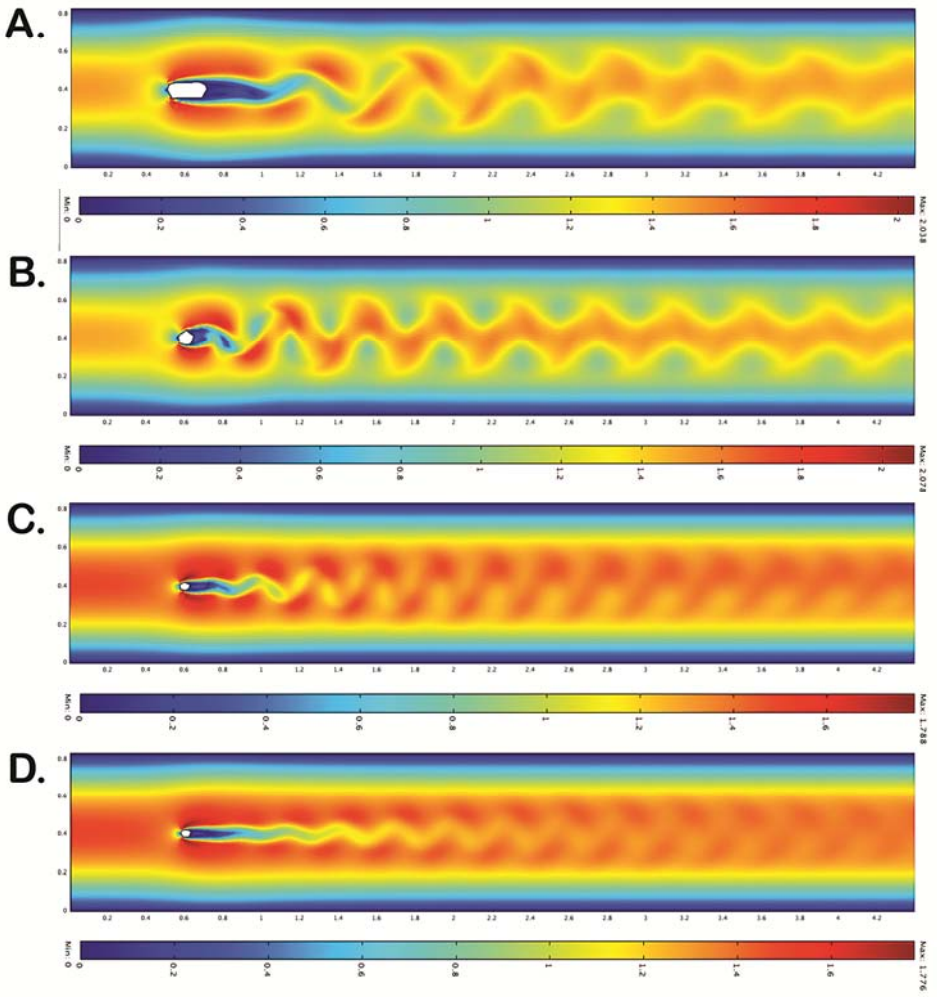

Figure 4.24: Fluid velocity in UALVP 33928. A, temporal cross section. B, orbital cross section. C, mid snout cross section. D, snout terminus cross section.

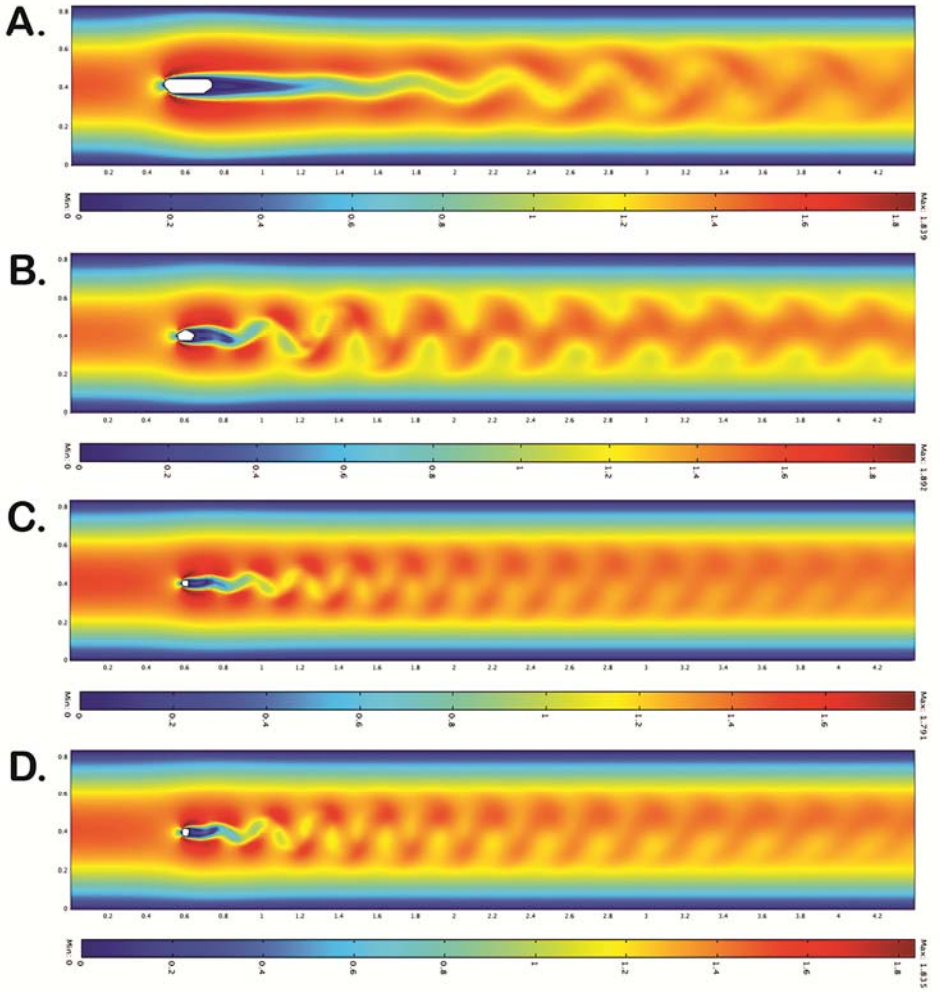

Figure 4.25: Fluid velocity in UALVP 47243. A, temporal cross section. B, orbital cross section. C, mid snout cross section. D, snout terminus cross section.

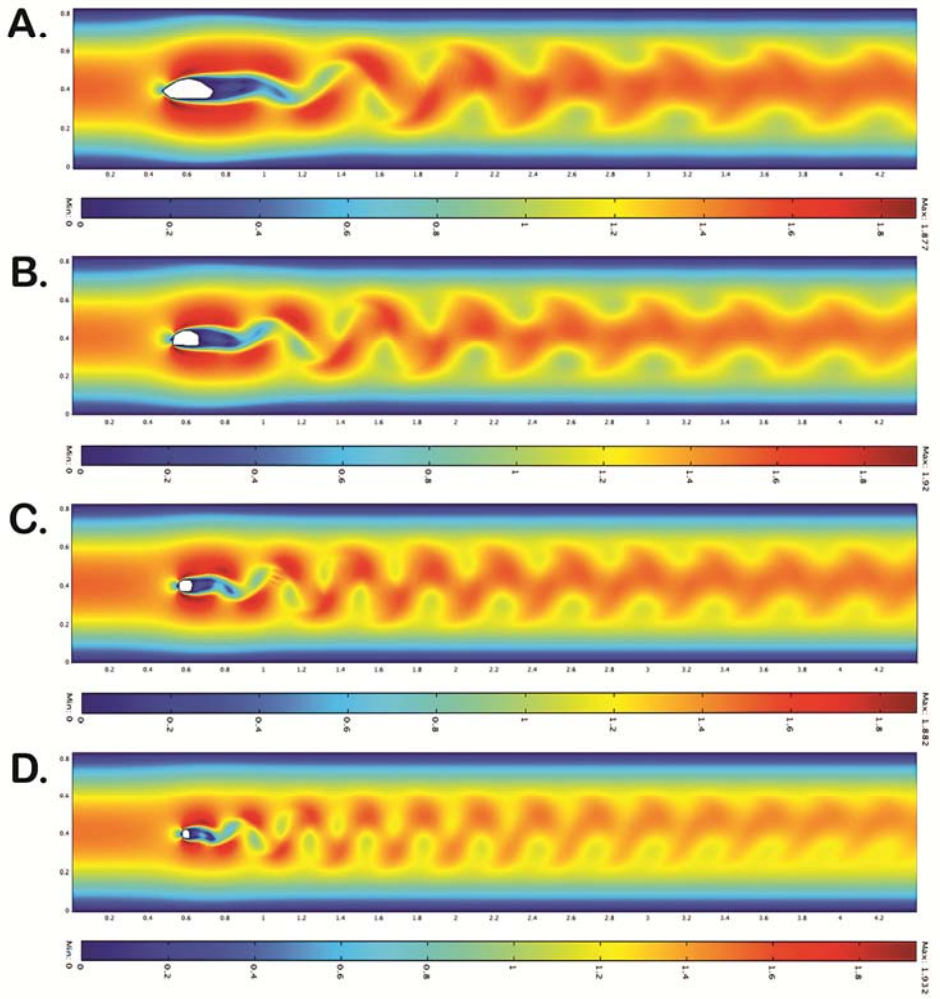

Figure 4.26: Fluid velocity in *Simoedosaurus dakotensis*. A, temporal cross section. B, orbital cross section. C, mid snout cross section. D, snout terminus cross section.

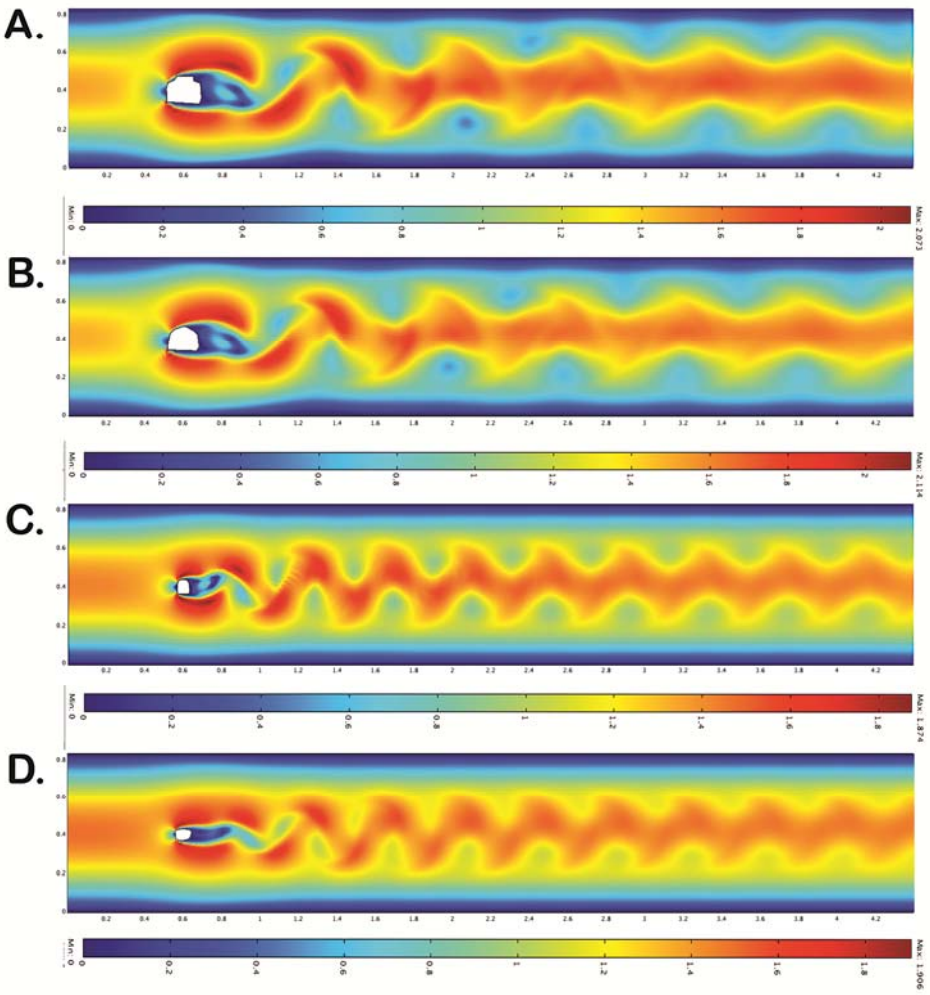

Figure 4.27: Fluid velocity in *Alligator mississippiensis*. A, temporal cross section. B, orbital cross section. C, mid snout cross section. D, snout terminus cross section.

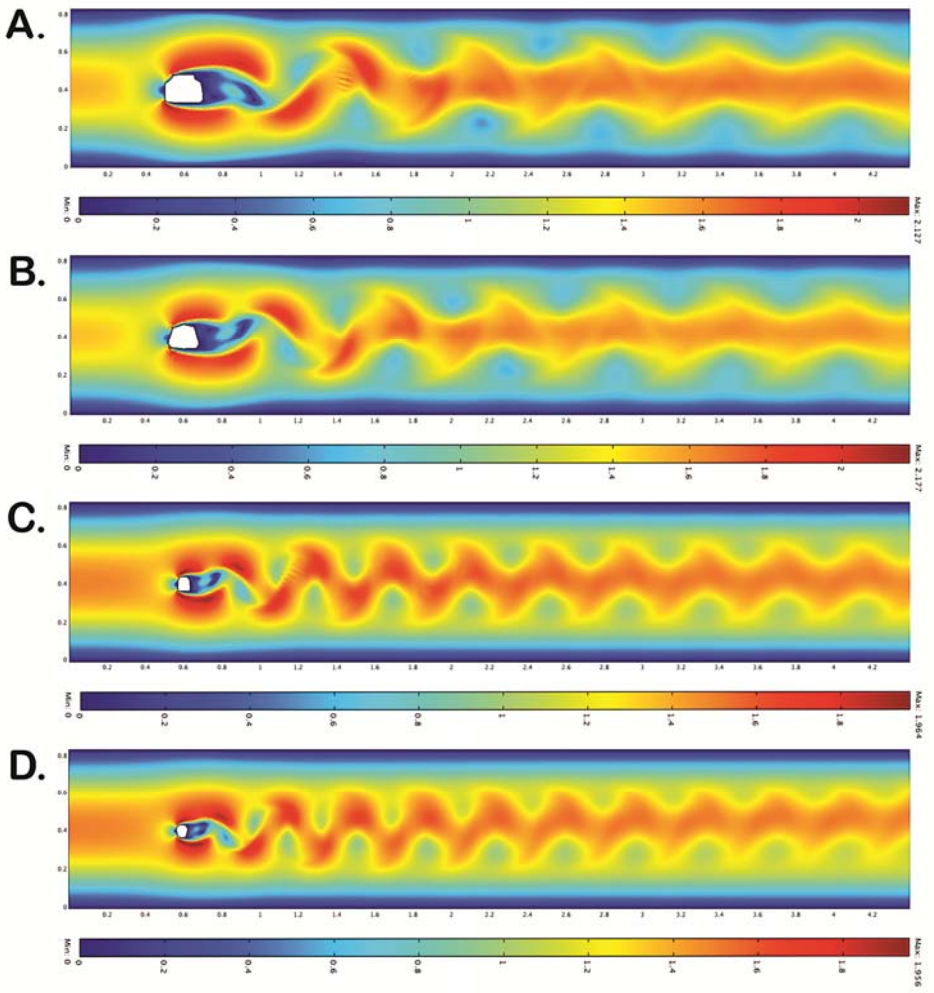

Figure 4.28: Fluid velocity in *Crocodylus cataphractus*. A, temporal cross section. B, orbital cross section. C, mid snout cross section. D, snout terminus cross section.

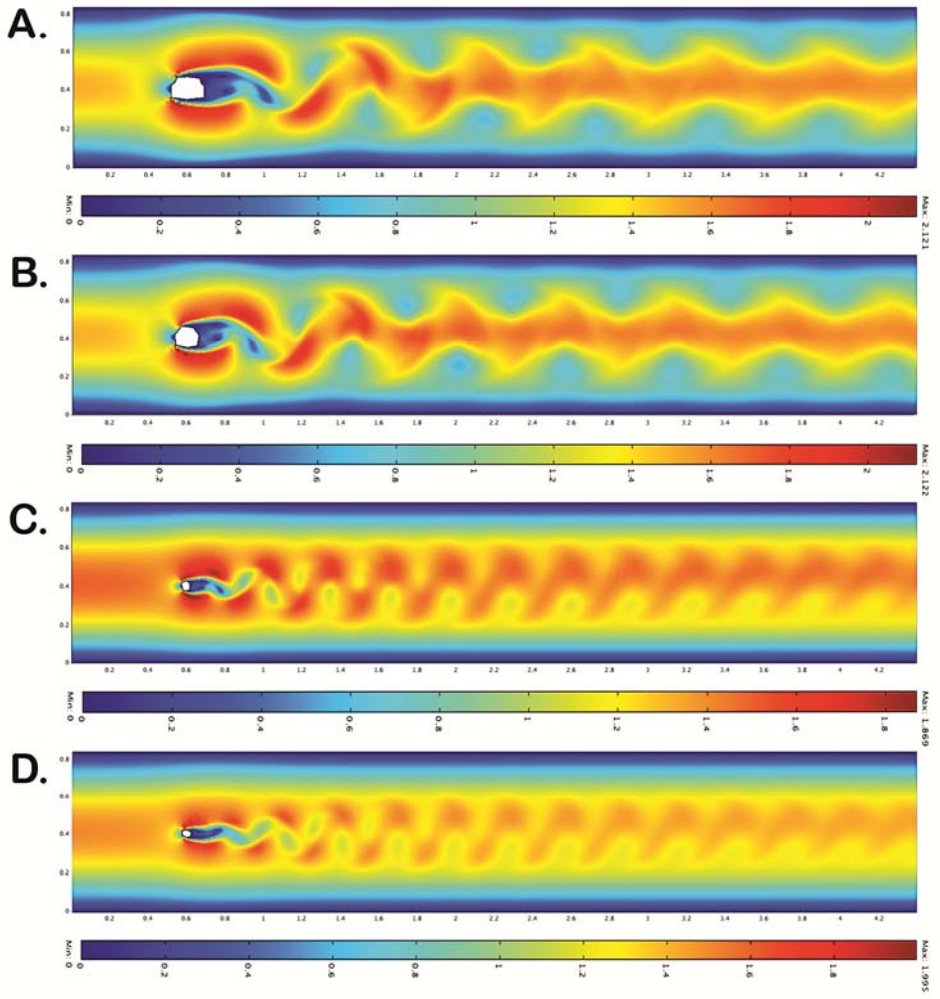

Figure 4.29: Fluid velocity in *Gavialis gangeticus*. A, temporal cross section. B, orbital cross section. C, mid snout cross section. D, snout terminus cross section.

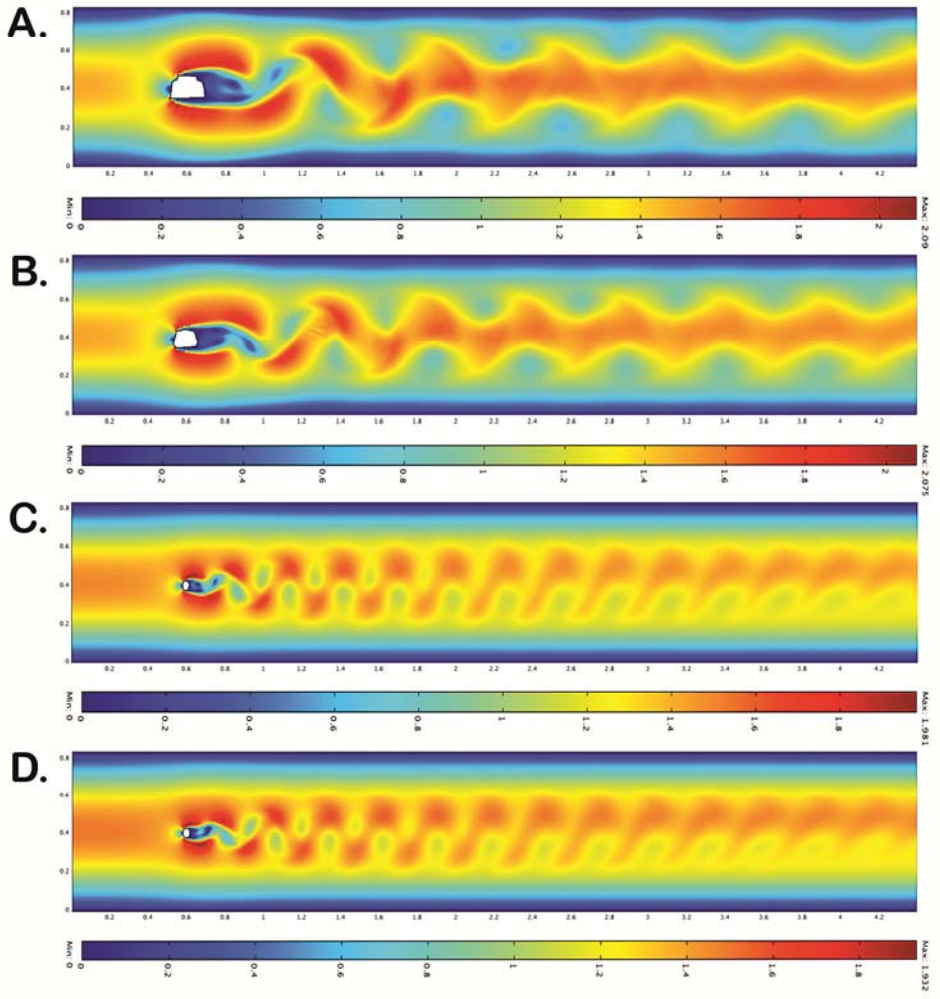

Figure 4.30: Fluid velocity in *Tomistoma schlegelii*. A, temporal cross section. B, orbital cross section. C, mid snout cross section. D, snout terminus cross section.

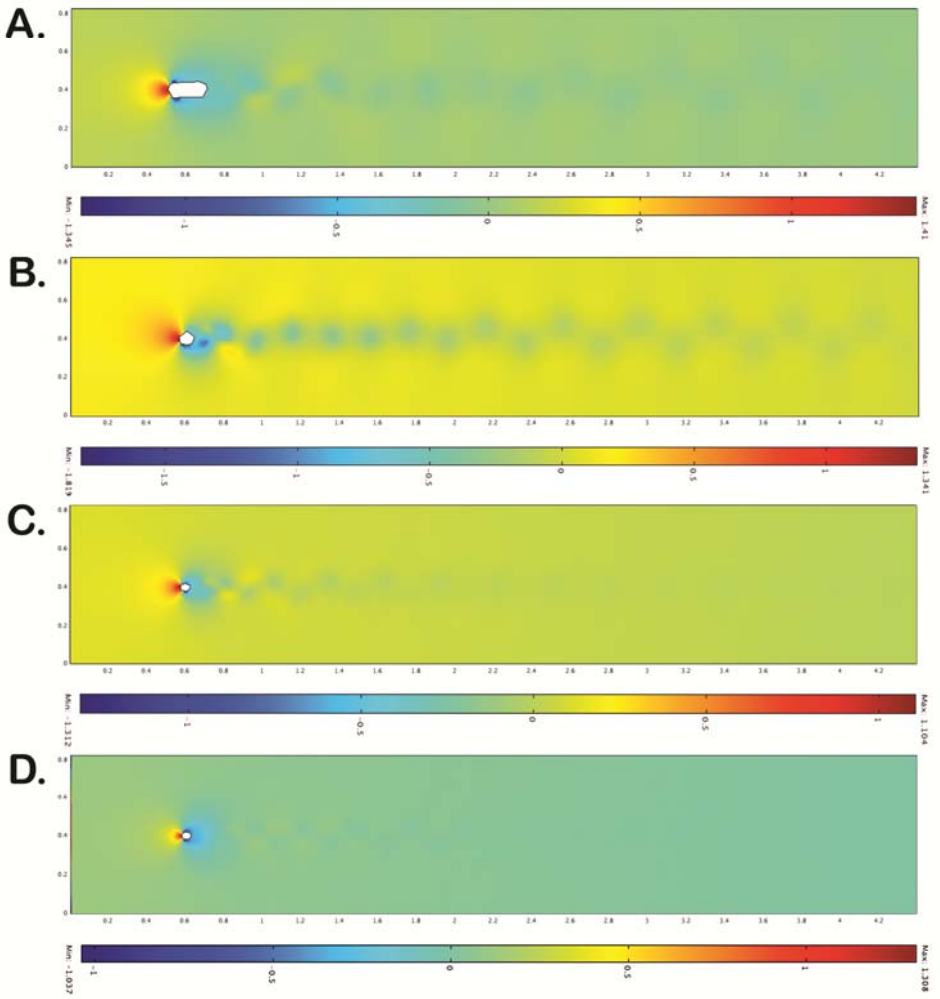

Figure 4.31: Fluid pressure in UALVP 33928. A, temporal cross section. B, orbital cross section. C, mid snout cross section. D, snout terminus cross section.

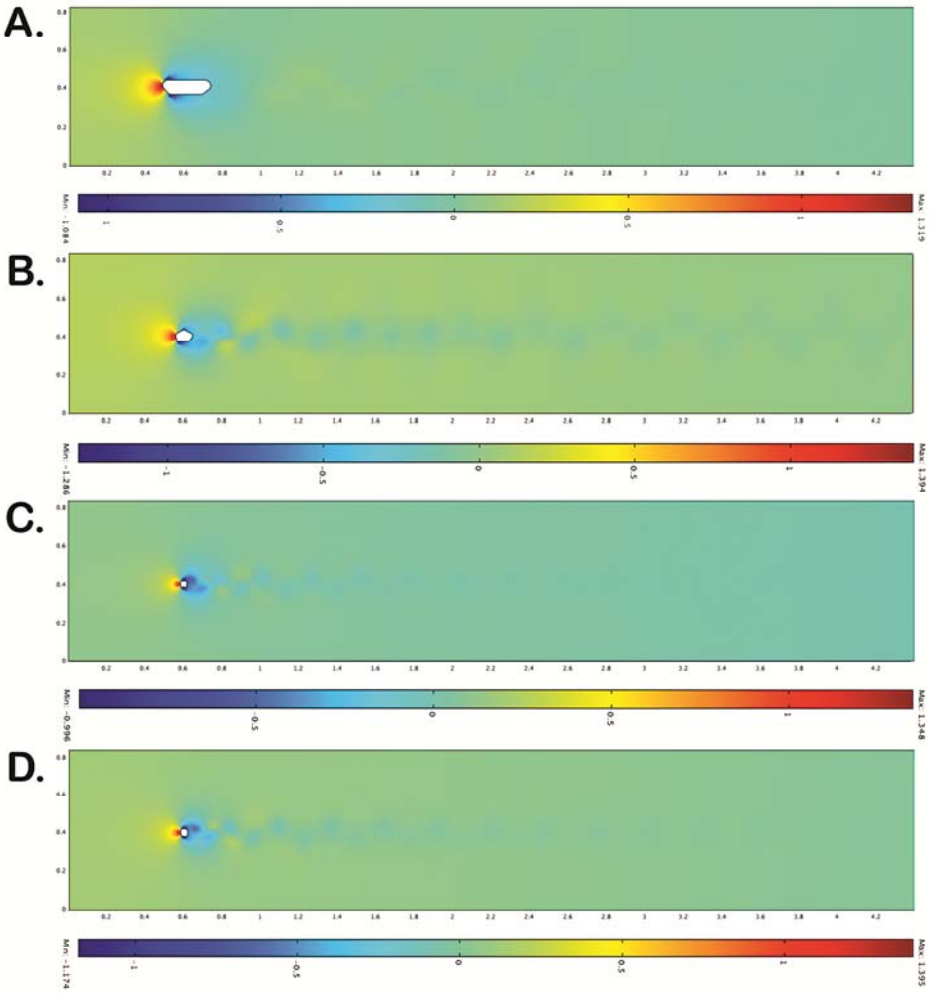

Figure 4.32: Fluid pressure in UALVP 47243. A, temporal cross section. B, orbital cross section. C, mid snout cross section. D, snout terminus cross section.

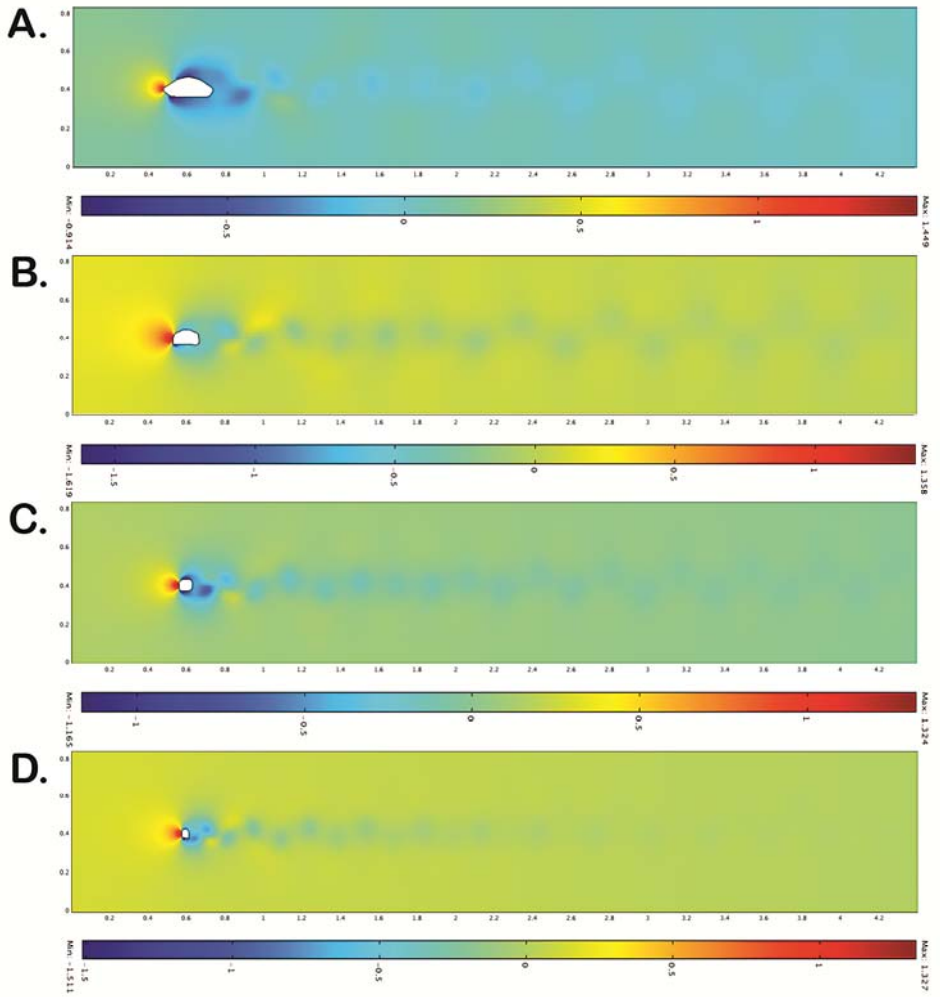

Figure 4.33: Fluid pressure in *Simoedosaurus dakotensis*. A, temporal cross section. B, orbital cross section. C, mid snout cross section. D, snout terminus cross section.

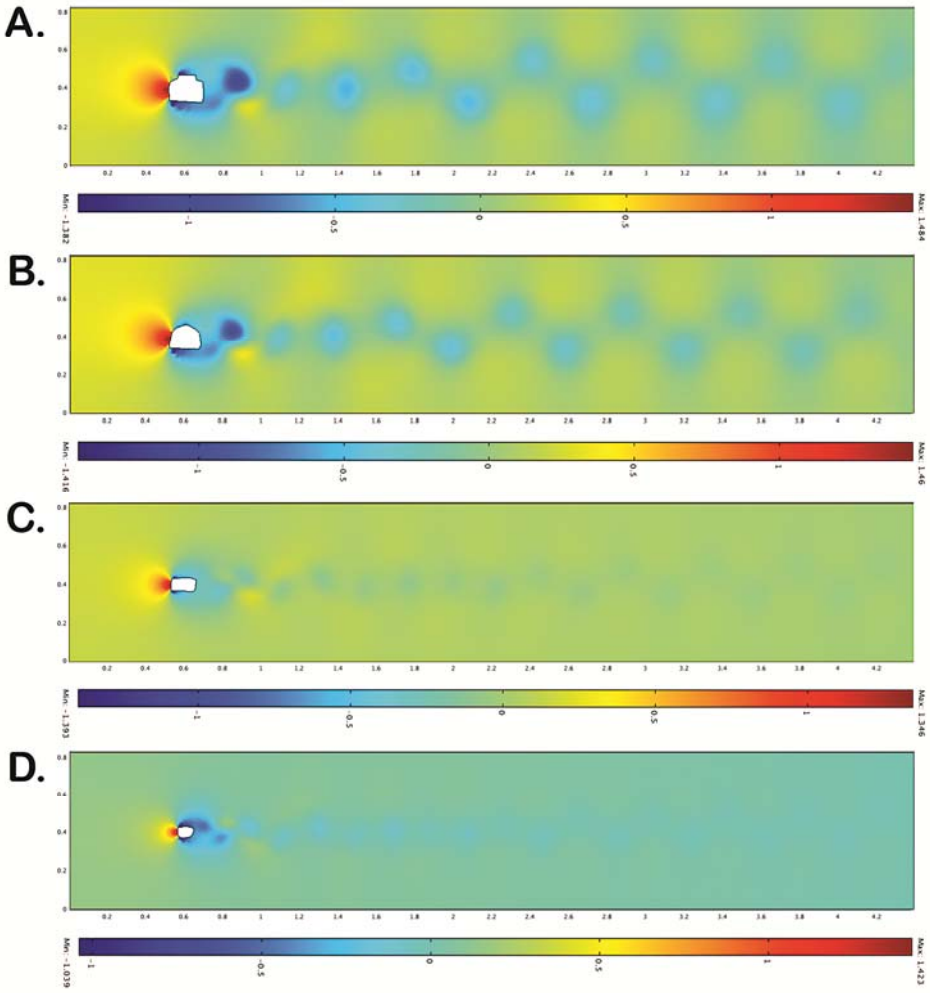

Figure 4.34: Fluid pressure in *Alligator mississippiensis*. A, temporal cross section. B, orbital cross section. C, mid snout cross section. D, snout terminus cross section.

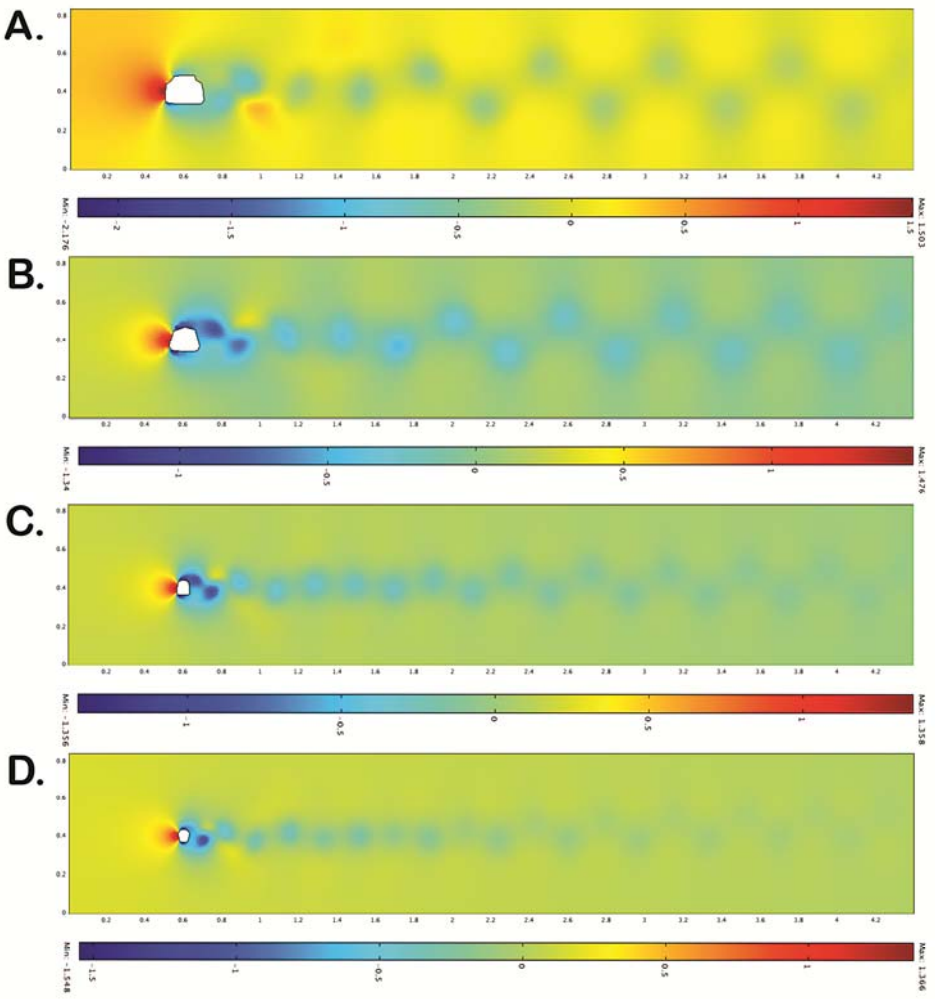

Figure 4.35: Fluid pressure in *Crocodylus cataphractus*. A, temporal cross section. B, orbital cross section. C, mid snout cross section. D, snout terminus cross section.

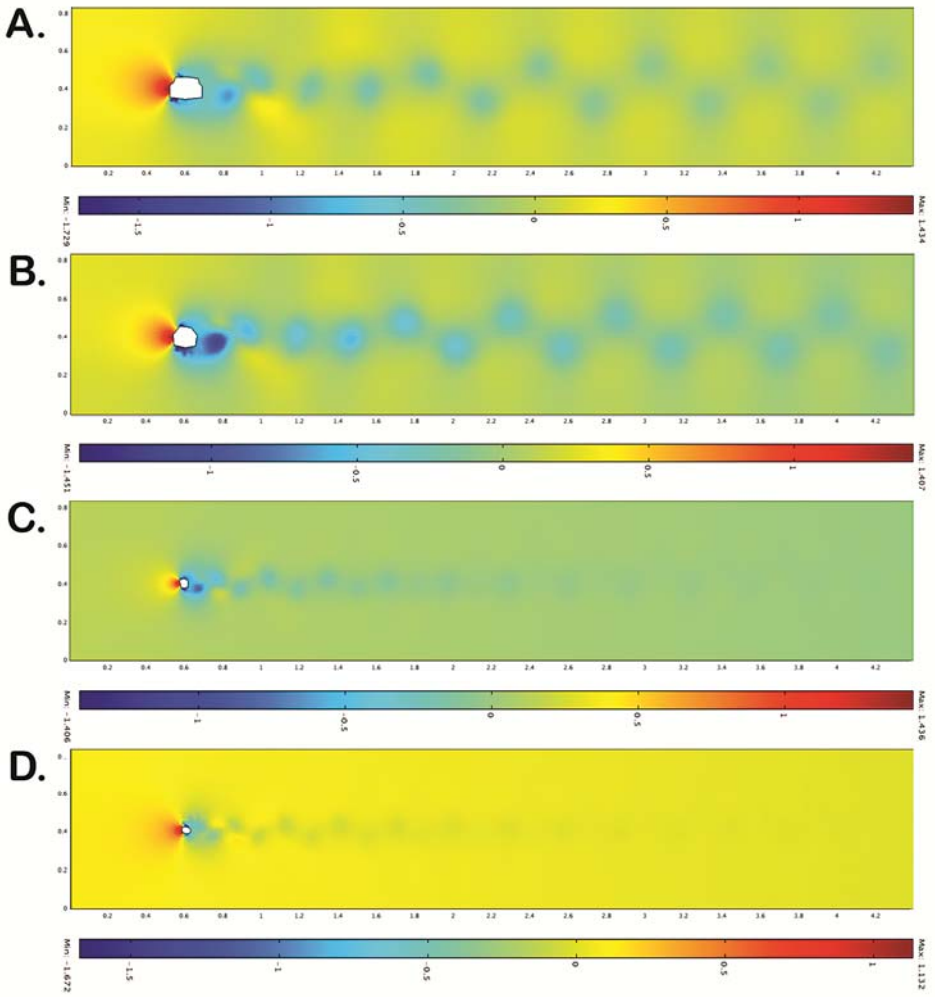

Figure 4.36: Fluid pressure in *Gavialis gangeticus*. A, temporal cross section. B, orbital cross section. C, mid snout cross section. D, snout terminus cross section.

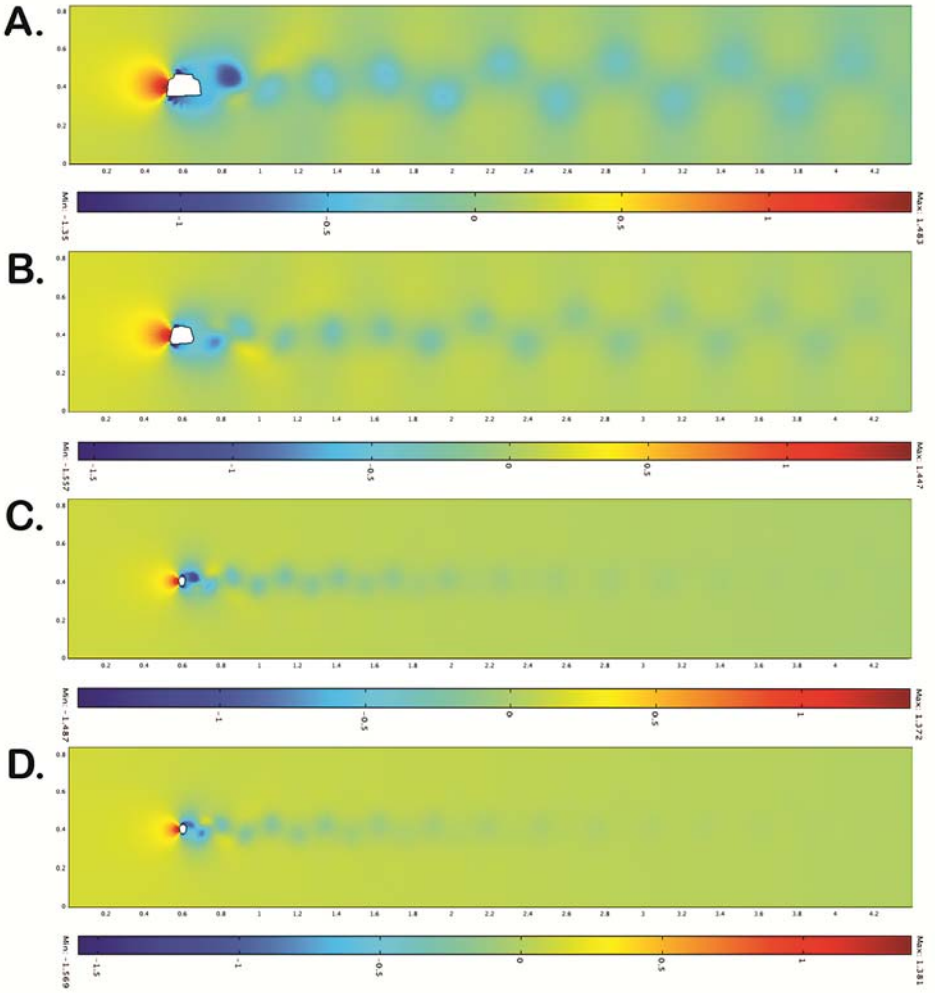

Figure 4.37: Fluid pressure in *Tomistoma schlegelii*. A, temporal cross section. B, orbital cross section. C, mid snout cross section. D, snout terminus cross section.

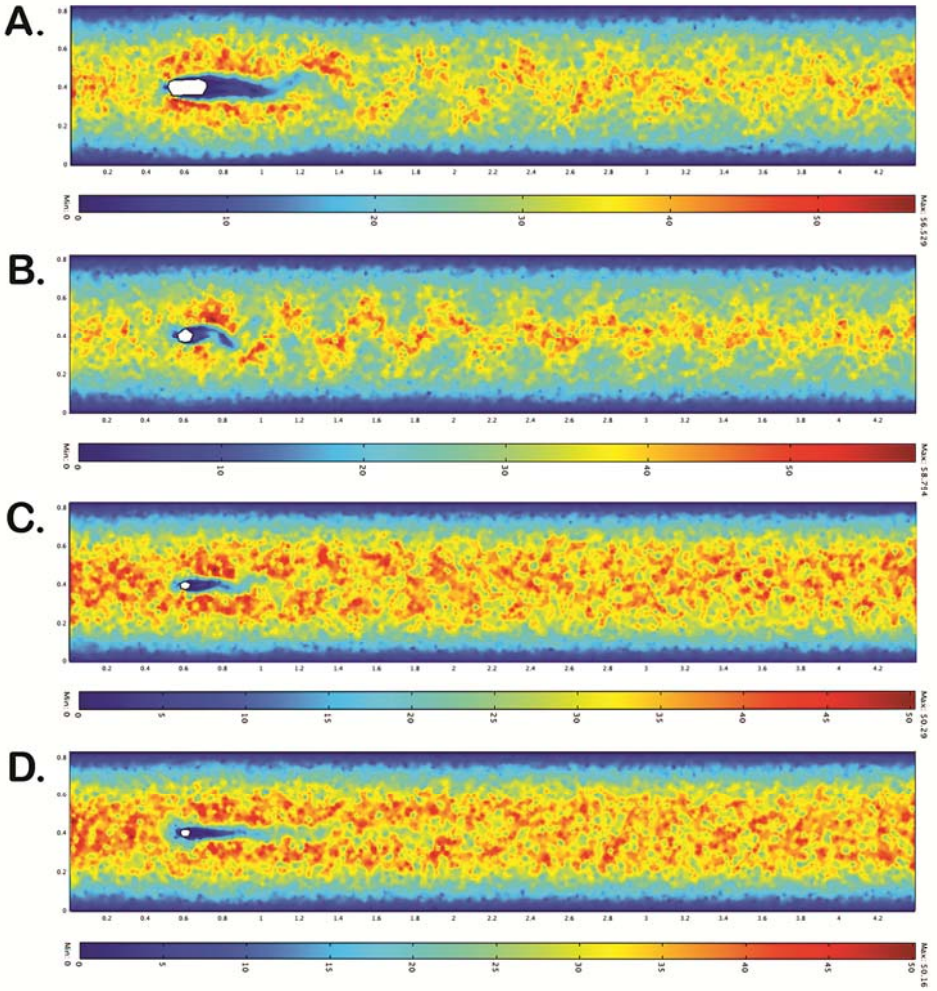

Figure 4.38: Cell Reynolds number in UALVP 33928. A, temporal cross section. B, orbital cross section. C, mid snout cross section. D, snout terminus cross section.

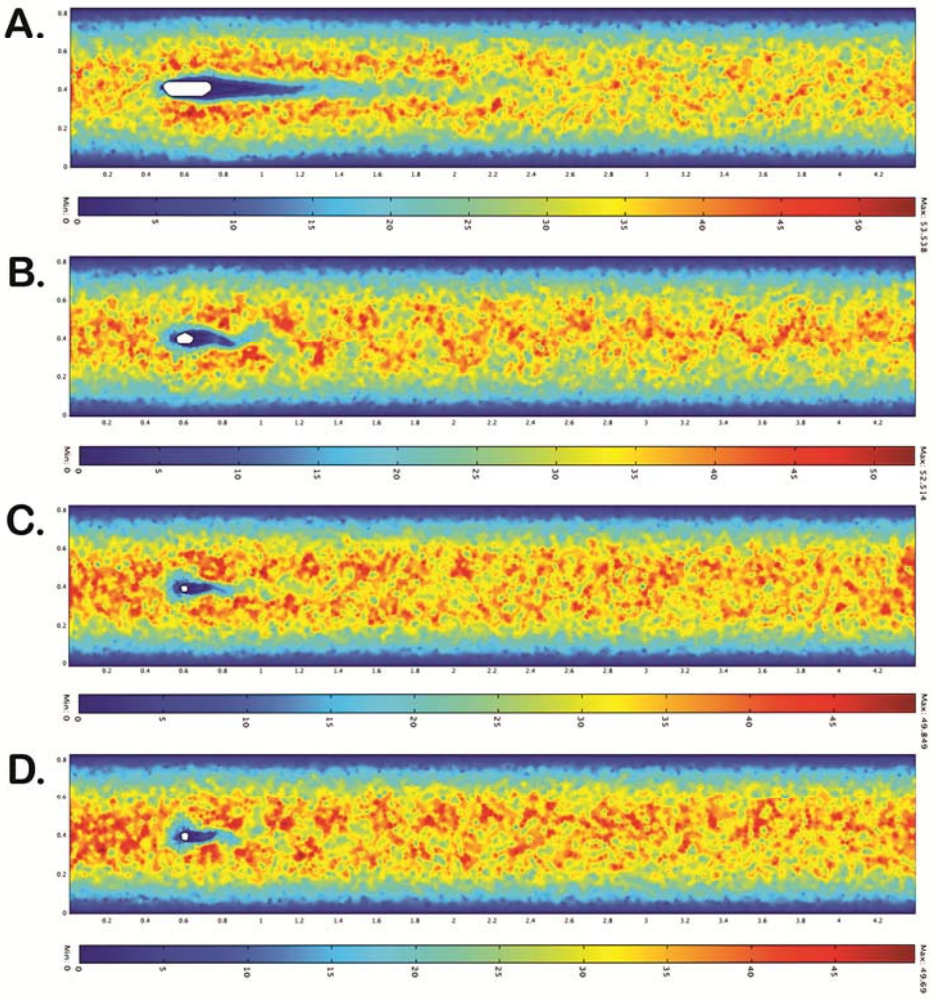

Figure 4.39: Cell Reynolds number in UALVP 47243. A, temporal cross section. B, orbital cross section. C, mid snout cross section. D, snout terminus cross section.

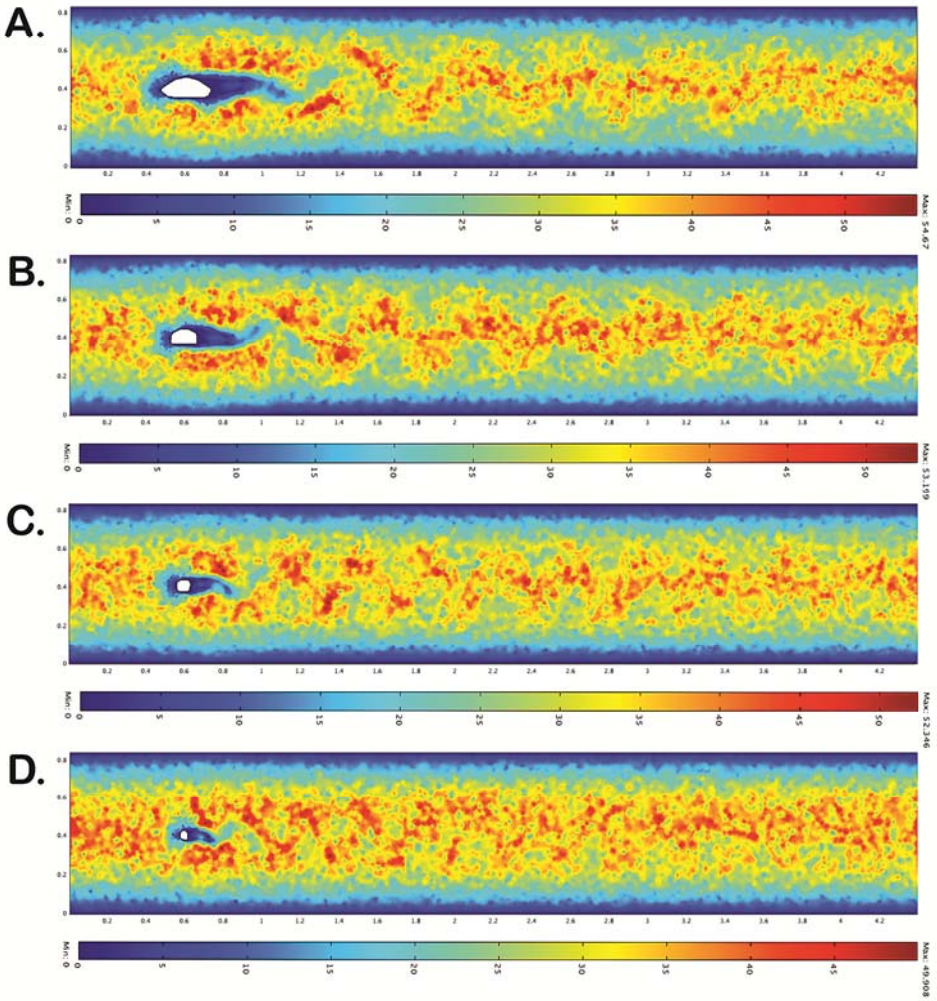

Figure 4.40: Cell Reynolds number in *Simoedosaurus dakotensis*. A, temporal cross section. B, orbital cross section. C, mid snout cross section. D, snout terminus cross section.

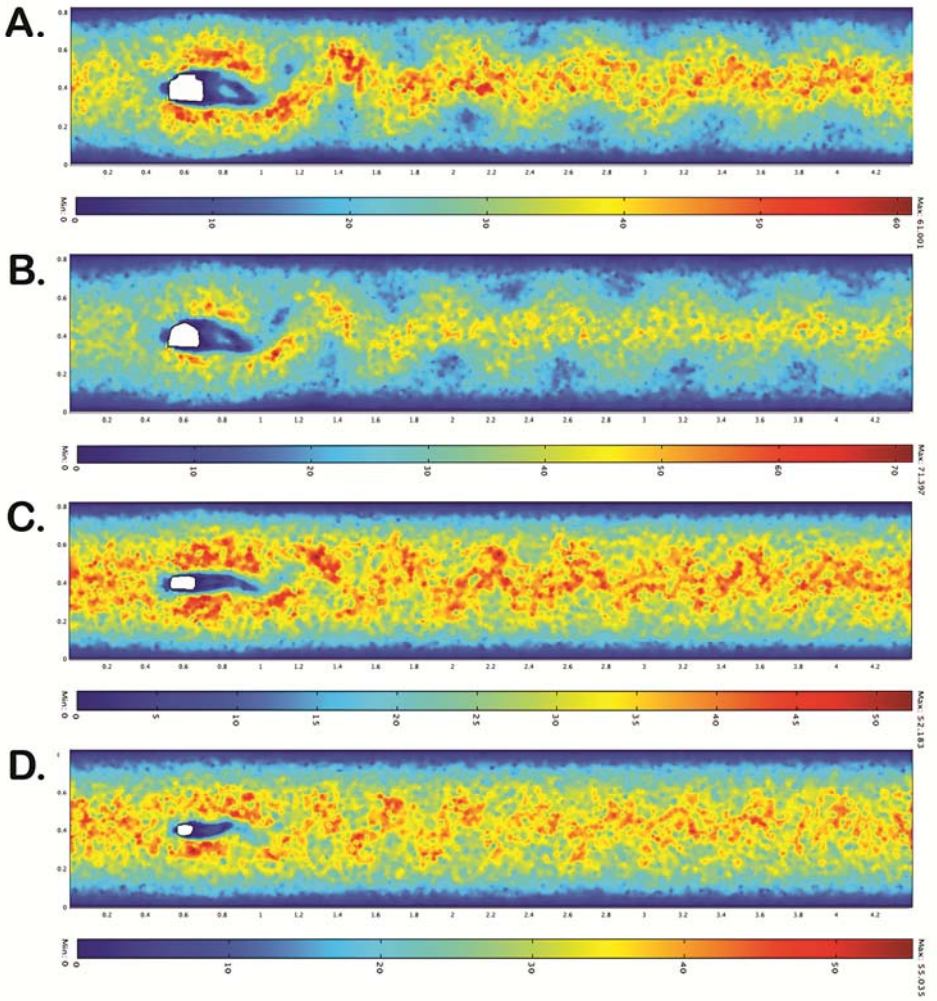

Figure 4.41: Cell Reynolds number in *Alligator mississippiensis*. A, temporal cross section. B, orbital cross section. C, mid snout cross section. D, snout terminus cross section.

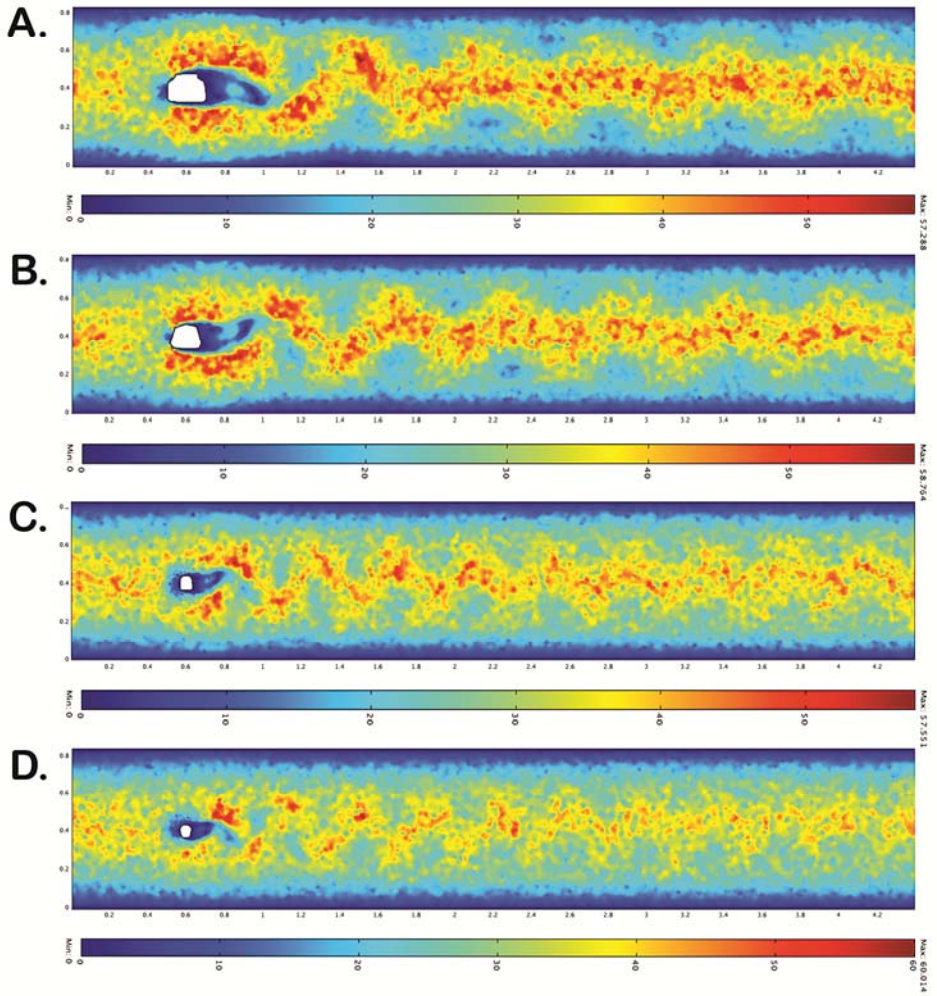

Figure 4.42: Cell Reynolds number in *Crocodylus cataphractus*. A, temporal cross section. B, orbital cross section. C, mid snout cross section. D, snout terminus cross section.

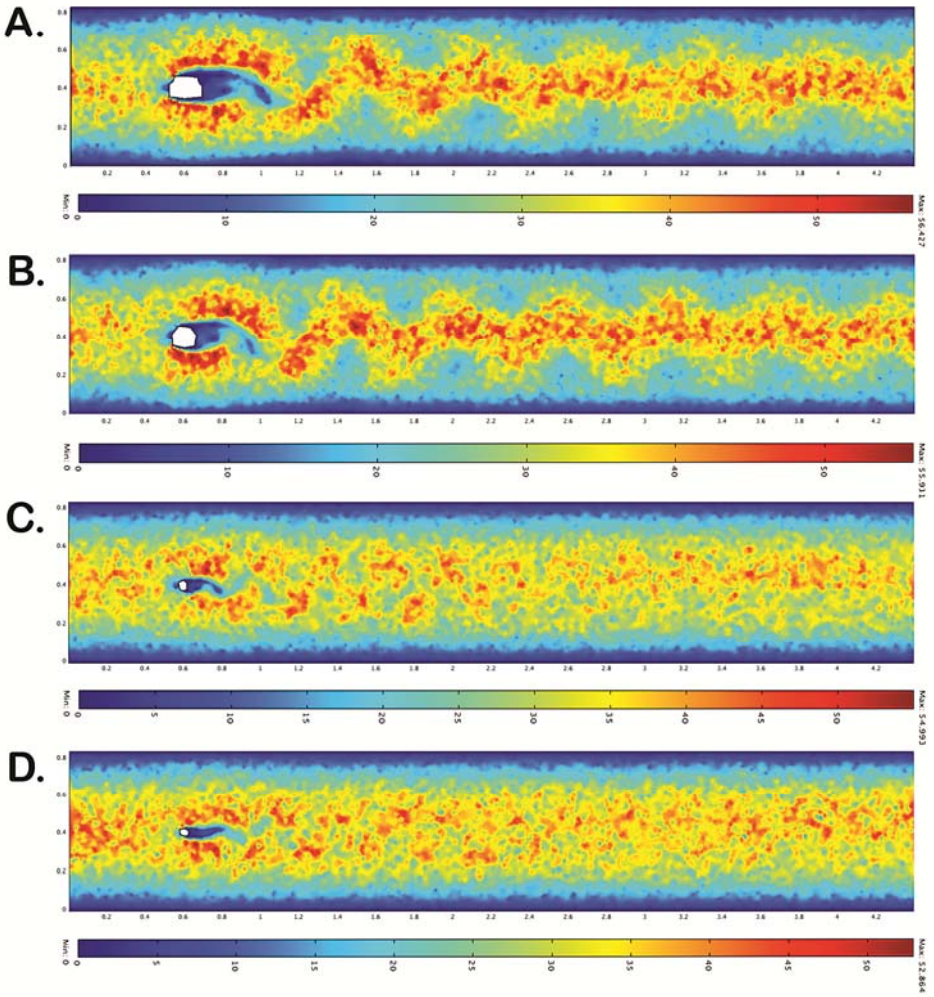

Figure 4.43: Cell Reynolds number in *Gavialis gangeticus*. A, temporal cross section. B, orbital cross section. C, mid snout cross section. D, snout terminus cross section.

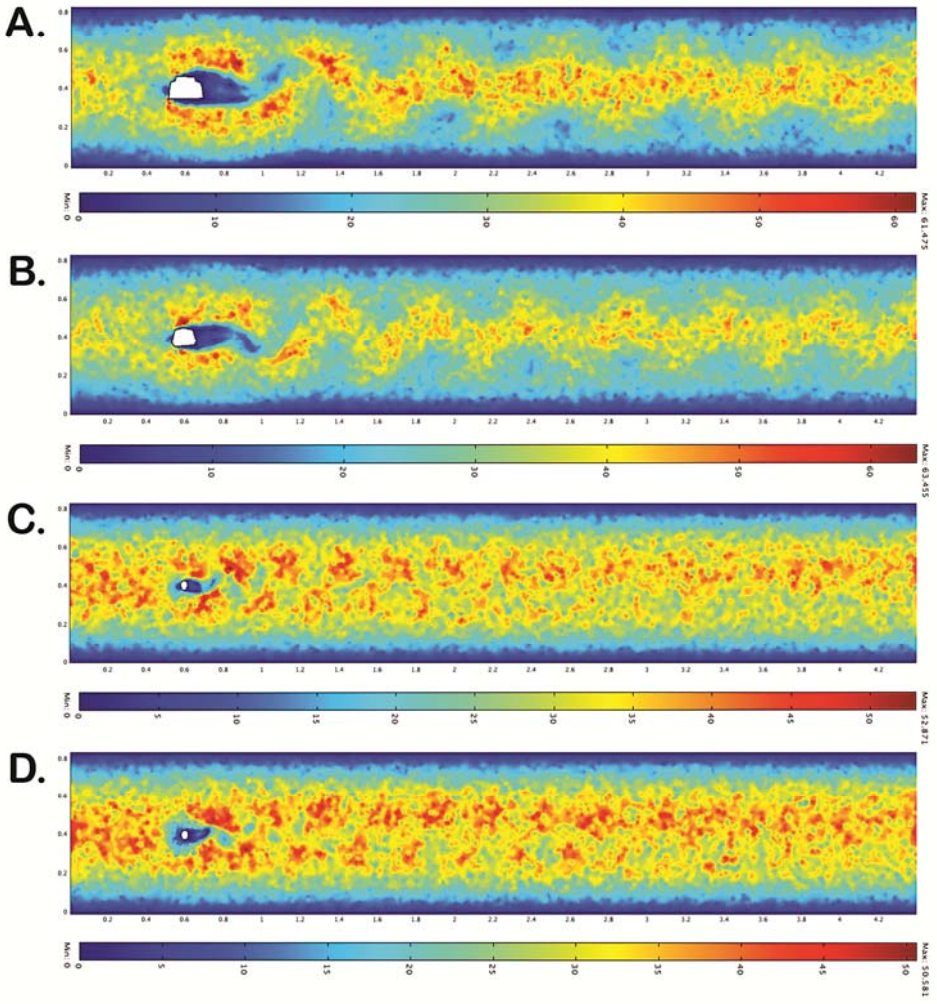

Figure 4.44: Cell Reynolds number in *Tomistoma schlegelii*. A, temporal cross section. B, orbital cross section. C, mid snout cross section. D, snout terminus cross section.

CHAPTER 5: CONCLUSIONS AND PALAEOECOLOGICAL IMPLICATIONS

Throughout their long history between the Middle Jurassic (Evans, 1990; Averianov et al., 2006) to the Miocene (Hecht, 1992; Evans and Klembara, 2005) they exhibit a range of morphologies from the lizard-like *Cteniogenys*, *Monjurosuchus*, and *Philydrosaurus*, to the long necked *Hyphalosaurus* and *Shokawa*, and the crocodiliform Neochoristodera. The Neochoristodera converge upon the skull morphologies seen in extant crocodilians: *Simoedosaurus* and *Tchoiria* converge upon the brevirostrine or mesorostrine morphologies seen in *Alligator* and *Crocodylus*, whereas *Champsosaurus* and *Ikechosaurus* are more similar to the longirostrine *Gavialis* and *Tomistoma*. Because of the morphological similarity between the neochoristoderes and crocodilians it has been frequently hypothesized that neochoristoderes occupied similar ecological niches. *Simoedosaurus* and *Tchoiria* are thought to have the majority of their diet consist of tetrapods (Erickson, 1987), whereas the diet of *Champsosaurus* and *Ikechosaurus* is thought to be considerably more piscivorous (Russell, 1956).

Although neochoristoderes and crocodilians have similar cranial morphologies, they do differ in that the temporal chamber of neochoristoderes is larger relative to the size of the skull and the bones defining the chamber are gracile when compared to those of crocodilians. The enlarged temporal chamber undoubtedly contains a large mass of jaw musculature. Witmer (1995) outlined the importance of reconstructing soft tissues in extinct animals to make inferences

about phylogeny and paleoecology, and proposed a method called the extant phylogenetic bracket (EPB), which has been utilized in other reconstructions of musculature in extinct taxa (Snively et al., 2004; Snively and Russell, 2007). The EPB method reconstructs soft tissues by identifying the closest extant relatives to the taxon in question and compares the morphology of the soft tissues. The aim of the EPB is to identify soft tissues that share a 1:1 correspondence between the extant relatives, implying that the extinct taxon must also share the same morphology (Witmer, 1995). The EPB method was applied to neochoristoderes to determine the morphology of the jaw musculature present in their enlarged temporal chambers.

Even though the phylogenetic position of the Choristodera is ambiguous, it is assumed for the purposes of this study that the Choristodera is within the Archosauromorpha (Currie, 1981; Erickson, 1985; Gauthier et al., 1988; Evans, 1990; Rieppel, 1993; Storrs and Gower, 1993; Storrs et al., 1996; de Braga and Rieppel, 1997; Jalil, 1997), thus making the bracket taxa the Lepidosauria, and the Crocodylia. Three reconstructions were made, the first based on the descriptions of the jaw musculature of *Sphenodon* found in Wu (2003) and Jones et al. (2009), the second based on *Sphenodon* as described by Holliday and Witmer (2007), and the last based on crocodilians as described by Holliday and Witmer (2007).

The results of the EPB were only able to unequivocally identify muscle attachment sites for two muscles: the M. adductor mandibulae posterior, and the M. adductor mandible externus profundus. The remainder of the jaw musculature did not share the same origin sites among the three reconstructions. Witmer

(1995) states that in cases where a 1:1 correspondence cannot be made, compelling morphological evidence can justify a judgement as to the morphology of the soft tissue. It was concluded that crocodilian muscles are unsuitable as a model for neochoristodere jaw adductor musculature because the mAMES does not originate from the lateral temporal fenestra (unlike the models using *Sphenodon* jaw musculature). It has been suggested that the formation of fenestra is the result of repeated tensional forces being applied to the surfaces of bones (Oxnard et al.,1995; Witzel and Preuschoft, 2005). Therefore, from a functional perspective, the presence of the large lateral temporal fenestra is a mystery because there are no muscles originating from it. Secondly, the reconstruction based on crocodilian jaw musculature is unable to reconstruct the M. pseudotemporalis superficialis and profundus that arises from the surface of the laterosphenoid in crocodilians. The laterosphenoid has not been described or figured in neochoristoderes (Gao and Fox, 1998) likely because it does not ossify. When choosing between the two reconstructions based on *Sphenodon*, it was a matter of descriptive quality. Holliday and Witmer (2007) incorrectly describe and figure the M. adductor mandibulae externus profundus as being superficial to the M. adductor mandibulae medialis, a relationship that has traditionally been reversed. The descriptions of Wu (2003) and Jones et al. (2009) are by comparison far more comprehensive, and thus were the preferred model for the jaw musculature of neochoristoderes.

Reconstructing the jaw musculature allowed for analyses of the jaw muscle function in both neochoristoderes and crocodilians. Models of specimens

of *Champsosaurus natator*, *Champsosaurus lindoei*, and *Simoedosaurus dakotensis* were compared to *Alligator mississippiensis*, *Crocodylus cataphractus*, *Gavialis gangeticus*, and *Tomistoma schlegelii*. The dry skull method was used to calculate the cross sectional area (CSA) of the two major muscle groups in each specimen, and it was found that neochoristoderes have the larger CSA, and thus the larger muscle forces. It was found that the jaw musculature in neochoristoderes was dominated by the mAMES and mAMP, and to a lesser extent by the mAMEM, mAMEP, and mPSTS. In crocodilians the largest muscles are the mPTD, mPTV, mAMP, and in *Gavialis gangeticus* the mAMEP. The jaw musculature of the neochoristoderes was found to exceed the tangential force, torque, bite force, angular acceleration, and angular velocity produced by crocodilians. The ability of the jaw musculature in neochoristoderes to rotate the jaw decreases as gape is increased, whereas in crocodilians the situation is reversed.

The jaw musculature of neochoristoderes exceeds that of crocodilians in terms of both size and force generated. The finite element method was used to determine the effect of such powerful muscles on the magnitude and distribution of stress produced during feeding. For each specimen two models of feeding were investigated. The first was a model of grasping behaviour in which the snout was restrained to simulate teeth embedded in prey. The second was a model simulating striking in which the restraints on the snout were replaced with bite forces calculated in Chapter 3. In both the grasping and striking models the neochoristoderes had more stress when compared to the crocodilians. The stress

observed in the neochoristoderes generally fell below the tensile yield strength of bone, 104 MPa. However, in the models of striking at the terminus of the snout the peak stress in the mandibles exceeded the yield strength. It was also found that the stress in the mandibles greatly exceeded that of the temporal chamber. This suggests that despite the gracile nature of the neochoristodere temporal arcade, it was the strength of the mandibles that were the limiting factor.

It was also found that longirostrine animals had greater stress throughout the skull, especially on the snout, when compared to their brevirostrine relatives. McHenry et al. (2006) suggested that longirostrine animals have a hydrodynamic advantage compared to brevirostrine forms, and sacrifice mechanical strength. To further investigate the differences between longirostrine and brevirostrine animals, and to determine if the dorsoventrally flattened skulls of neochoristoderes are adapted for hydrodynamic performance as suggested by Erickson (1972, 1985), cross sections of the digital models were imported into a simulated flow tank. The fluid velocity, fluid pressure, and Reynolds number of cross sections through the skulls of the neochoristodere and crocodilian specimens were compared to one another to determine which specimens were better adapted for hydrodynamic performance during lateral striking. Neochoristoderes had lower peak fluid velocities, less difference in fluid pressure, and lower Reynolds numbers than crocodilians, suggesting that they are subject to less induced and pressure drag. The same pattern was found when comparing sections of the snouts of the longirostrine specimens to their brevirostrine relatives, supporting McHenry et al. (2006).

The findings of the biomechanical, finite element, and hydrodynamic analyses suggest that rather than there being only a compromise between hydrodynamic and mechanical performance as stated by McHenry et al. (2006), that there is a third element, muscle performance, to consider. The skulls of *Champsosaurus* are adapted for hydrodynamic performance and for fast jaw adduction at the expense of mechanical performance. Longirostrine crocodilians have a similar pattern, except that they seem to sacrifice some hydrodynamic performance and jaw angular acceleration for mechanical performance. Brevirostrine specimens such as *Alligator mississipiensis* and *Simoedosaurus dakotensis* are the reverse. Compared to their slender snouted relatives their snouts are broad, absorbing stress generated from biting, at the expense of hydrodynamic performance and jaw closing speed. The implication for *Champsosaurus* is that it supports previous hypotheses that their primary diet included small fish, tetrapods, and invertebrates (Russell, 1956), and *Simoedosaurus* fed upon larger prey such as slow fish and tetrapods (Erickson, 1987).

The results of the analyses in this study may help reconcile how crocodilians and neochoristoderes shared ecosystems. Generally both crocodilian and neochoristodere fossil material are present in the faunas of the late Cretaceous to Paleocene of North America. For example, the Dinosaur Park Formation of Alberta contains high concentrations of *Champsosaurus*, *Leidyosuchus*, and *Albertochampsa* fossil material. Reconstructing the jaw musculature of *Champsosaurus* and comparing its morphology and function to crocodilians

provides support for the hypothesis that it was better adapted for the acquisition and handling of small fish, amphibians, reptiles, and soft invertebrates (Russell, 1956). Sympatric crocodilians would have been better able to prey upon larger food such as tetrapods, larger fish, and invertebrates. The result would be that *Champsosaurus* and the crocodilians sharing the ecosystem may have partitioned their niches based on the prey size. In the Dinosaur Park Formation, the prey of the two species of *Champsosaurus* may have included the small unnamed teleosts described by Brinkman and Neuman (2002). Larger fish such as *Myledaphus*, sturgeon, *Acipenser*, *Belanostomus*, *Lepisosteus*, amiids, holosteans A and B, *Paratarpon*, and *Cretophareodus* would have been too large as adults, and only juveniles would have been suitable prey for *Champsosaurus*.

It has been suggested that *Champsosaurus* preferred areas of low crocodilian density due to competition with crocodilians (Erickson, 1972, 1985). The results of this study do not support this hypothesis because it is unlikely that *Champsosaurus* and any sympatric crocodilians were in direct competition. It is likely that the presence of crocodilians prevented *Champsosaurus* from expanding its morphospace to include mesorostrine and brevirostrine forms and thus expanding its niche to include larger aquatic or even terrestrial prey. As stated by Erickson (1972) divergent behaviour, specifically prey choice, contributed to the lengthy coexistence of *Champsosaurus* and crocodilians. It is likely that due to the little overlap in prey, that the extinction of large neochoristoderes in North America was due to climatic deterioration (cooling and drying) that was initiated in the late Eocene (Prothero, 1994), rather than competition as suggested by

Ksepka et al. (2005). It is more likely that *Champsosaurus* was in direct competition with piscivorous fish, such as gar, that shared the same habitat.

The results of this study do not help to resolve questions regarding how two species of *Champsosaurus* are able to coexist in various localities in North America. In the case of Dinosaur Provincial Park both *Champsosaurus natator* and *Champsosaurus lindoei* seem nearly equally capable of capturing small fish, and thus seemingly occupy the same habitat. Hypotheses of sexual dimorphism (Katsura, 2004) have been put forth, however adequate evidence has yet to be produced. This study scaled *Champsosaurus natator* and *Champsosaurus lindoei* to the same size, even though the latter is described as being the smaller of the two (Gao and Fox, 1998). Perhaps, even though both species were well adapted for capturing small fish, they were able to divide the niche further, *Champsosaurus lindoei* preying upon smaller fish than even *Champsosaurus natator*. To resolve this problem, further research into whether there is either a temporal or geographic separation between the two species is required.

Further avenues of research could examine the morphology and biomechanics of the neck musculature in neochoristoderes. The expanded temporal region not only allows for enlarged jaw adductor muscles, but it also increases the surface area on the posterior surface of the cranium for the attachment of the neck musculature. The results of this study suggest that *Champsosaurus* likely captured prey using lateral striking as seen in *Gavialis gangeticus* (Thorbjarnarson, 1990). Therefore, the neck muscles would be important factors in the feeding mechanics of *Champsosaurus*.

The expanded temporal chamber of neochoristoderes has been recognized to contain substantial jaw musculature, but no previous hypotheses have been made regarding the morphology of that musculature. The conclusion of the EPB method was that *Sphenodon* was the best model for reconstructing the jaw adductor muscles in neochoristoderes. Biomechanical analyses using rotational mathematics of the jaw musculature showed that the bite of a neochoristodere was stronger than that of a crocodilian of similar size, and that the jaw musculature of a neochoristodere accelerates the lower jaw faster than those of all examined crocodilians. FEA results show that the skulls of neochoristoderes were able to withstand grasping and striking in all modeled scenarios in that the breaking point of bone (104 MPa) was rarely exceeded. Hydrodynamic analyses show that *Champsosaurus* performed better hydrodynamically than the longirostrine crocodilians, because *Champsosaurus* had lower Reynolds numbers, maximum fluid velocities, and fluid pressure which contributes to lower drag during lateral striking. *Champsosaurus* seems to be adapted to maximize bite speed and hydrodynamic performance, which supports previous studies that suggest they were piscivorous due to the elongated snout and the small needle-like teeth (Russell, 1956; Erickson, 1985). Also, it has been suggested that *Champsosaurus* was in direct competition for food with the crocodilians that lived sympatrically with them, resulting in their extinction (Ksepka et al., 2005). The differences in biomechanics and FEA results suggest that the two groups did not compete significantly with one another. Niche partitioning was a consequence of differences in jaw muscle function, and the mechanical and hydrodynamic

performance of the skull, all of which contributed to the coexistence of *Champsosaurus* and crocodilians.

Literature Cited

Adams, L.A. 1919. A memoir on the phylogeny of the jaw muscles in recent and fossil vertebrates. Annals of the New York Academy of Science 28:51–166.

Akima, H., S. Kuno, H. Takahashi, T. Fukunaga, and S. Katsuta. 2000. The use of magnetic resonance images to investigate the influence of recruitment on the relationship between torque and cross-sectional area in human muscles. European Journal of Applied Physiology 83:475–480.

Al-Hassawi, A.M. 2007. Compartive anatomy of the neck region in lizards. Trafford publishing, Victoria, Canada.

Anderson, H.T. 1936. The jaw musculature of the phytosaur, *Machaeroprsopus*. Journal of Morphology 59:549–587.

Arbour, V.M., and E. Snively. 2009. Finite element analyses of ankylosaurid dinosaur tail club impacts. Anatomical Record 292:1412–1426.

Avernianov, A.O., T. Martin, S.E. Evans, and A.A. Bakirov. 2006. First Jurassic Choristodera from Asia. Naturwissenschaften 93:46–50.

Bamman, M.W., B.R. Newcomer, D. Larson-Meyer, R.L. Weisner, and G.R. Hunter. 2000. Evaluation of the strength-size relation *in vivo* using various muscle size indices. Medicine and Science in Sports and Exercise 32:1307–1313.

Barghusen, H.R. 1973. The adductor jaw musculature of *Dimetrodon* (Reptilia, Pelycosauria). Journal of Paleontology 47:823–834.

Bell, P.R., E. Snively, and L. Shychoski. 2009. A comparison of the jaw mechanics in hadrosaurid and ceratopsid dinosaurs using finite element analysis. Anatomical Record 292:1338–1351.

Brinkman, D.B., and Z.M. Dong. 1993. A new material of *Ikechosaurus sunailinae* (Reptilia: Choristodera) from the Early Cretaceous Langhongdong Formation, Ordos Basin, Inner Mongolia, and the interrelationships of the genus. Canadian Journal of Earth Sciences 30:2153–2162.

Brinkman, D.B., and A.G. Neuman. 2002. Teleost centra from uppermost Judith River Group (Dinosaur Park Formation, Campanian) of Alberta, Canada. Journal of Paleontology 76:138–155.

Brochu, C.A. 2001. Crocodylian snouts in space and time: phylogenetic approaches towards adaptive radiation. American Zoologist 41:564–585.

Brown, B. 1905. The osteology of *Champsosaurus* Cope. American Museum of Natural History, Memoirs 9:1–26.

Buckland-Wright, J.C. 1978. Bone structure and the patterns of force transmission in the cat skull (*Felis catus*). Journal of Morphology 155:35–62.

Busbey, A.B. 1989. Form and function of the feeding apparatus of *Alligator mississippiensis*. Journal of Morphology 202:99–127.

Busbey, A.B. 1995. The structural consequences of skull flattening in crocodilians. pp. 173–192 in J.J. Thomason (ed.), Functional Morphology in Vertebrate Paleontology. Cambridge University Press, Cambridge.

Byerly, T.C. 1925. The mycology of *Sphenodon punctatum*. University of Iowa Studies in Natural History 9:1–51.

Caldwell, M.W. 1996. Ichthyosauria: a preliminary phylogenetic analysis of diapsid affinities. Neus Jarhbuch für Geologie und Paläeontologie, Abhandlungen 200:361–386.

Carroll, R.L., and P.J. Currie. 1991. The early radiation of diapsid reptiles. pp. 354–424 in H.-P. Shultze, and L. Trueb (eds.), Origins of the Higher Groups of Tetrapods. Comstock Publishing Associates, Ithaca.

Carlson, B.M. 1981. Summary. pp. T.G. Connelly, L.L. Brinkley, and B.M. Carlson (eds.), Morphogenesis and Pattern Formation. Raven Press, New York.

Case, E.C. 1924. A possible explanation of fenestration in the primitive reptilian skull, with notes on the temporal region of the genus *Dimetrodon*. Contributions from the Museum of Geology, University of Michigan 2:1–12.

Cheng, E.J., S.H. Scott. Morphometry of *Macaca mulatta* forelimb: Shoulder and elbow muscles and segment inertial parameters. Journal of Morphology 245:206–224.

Cleuren, J., and F. De Vree. 1992. Kinematics of the jaw and hyolingual apparatus in *Caiman crocodilus*. Journal of morphology 212:141–154.

Cleuren, J., and F. De Vree. 2000. Feeding in crocodilians. pp. 337–358 in K. Schwenk (ed.), Feeding: form, function, and evolution in tetrapod vertebrates. Academic Press, San Diego.

Clough, R.W. 1960. The finite element in plane stress analysis. Conference on Electronic Computation, 2nd, Pittsburgh, PA.

Cope, E.D. 1876. On some extinct reptiles and Batrachia from the Judtih River and Fox Hills beds of Montana. Proceedings of the Academy of Natural Sciences Philadelphia 28:340–359.

Cope, E.D. 1884. The Choristodera. American Naturalist 17:815–817.

Currey, J.D. 2002. Bones: Structure and Mechanics. Princeton University Press, Princeton, 436 pp.

De Braga, M., and O. Rieppel. 1997. Reptile phylogeny and the interrelationships of turtles. Zoological Journal of the Linnean Society 120:281–354.

Densmore, L.D.I., and R.D. Owen. 1989. Molecular systematics of the Order Crocodylia. American Zoologist 29:831–841.

Dilkes, D.W. 1998. The Early Triassic rhynchosaur *Mesosuchus brownie* and the interrelationships of basal archosauromorph reptiles. Philosophical Transactions Biological Sciences 353:501–541.

Dumont, E.R., A. Herrel, R.A. Medellin, J.A. Vargas-Contreras, and S.E. Santana. 2009. Built to bite: cranial design and function in the wrinkle-faced bat. Journal of Morphology 279:329–337.

Edgeworth, F.H. 1935. The crainial muscles of vertebrates. Cambridge University Press, Cambridge.

Efimov, M.B. 1975. A champsosaurid from the Lower Cretaceous of Mongolia. In: Kramarenko NN, ed. Fossil Fauna and Flora of Mongolia. Transactions of the Joint Soviet-Mongolian Paleontological Expeditions 2:84–93.

Efimov, M.B. 1979. *Tchoiria* (Champsosauridae) from the Early Cretaceous of Khamaryn-Khural, MNR. Transactions of the Joint Soviet-Mongolian Paleontological Expeditions 8:56–57.

Efimov, M.B. 1983. Champsosaurs of Central Asia. Transactions of the Joint Soviet-Mongolian Paleontological Expeditions 24:67–75.

Endo, R. 1940. A new genus of Thecodontia from the *Lycoptera* beds of Manchoukuo. Bulletin of the Central National Museum Manchoukuo 2:1–14.

Endo, H., R. Aoki, H. Taru, J. Kimura, M. Sasaki, M. Yamamoto, K. Arishima, and Y. Hayashi. 2002. Comparative functional morphology of the masticatory apparatus in the long-snouted crocodiles. Anatomy, Histology, Embryology 31:206–213.

Erickson, B.R. 1972. The lepidosaurians reptile *Champsosaurus* in North America. Science Museum of Minnesota, Monograph 1:1–91.

Erickson, B.R. 1981. *Champsosaurus tenuis* (Reptilia: Eosuchia), a new species from the late Paleocene of North America. Science Museum of Minnesota, New Series 5:1–14.

Erickson, B.R. 1985. Aspects of some anatomical structures of *Champsosaurus* Cope (Reptilia: Eosuchia). Journal of Vertebrate Paleontology 5: 111–127.

Erickson, B.R. 1987. *Simoedosaurus dakotensis*, new species, a diapsid reptile (Archosauromorpha: Choristodera) from the Paleocene of North America. Journal of Vertebrate Paleontology 7: 237–251.

Erickson, G.M. 2001. The bite of *Allosaurus*. Nature 409:987–988.

Erickson, G.M., S.D. Van Kirk, J. Su, M.E. Levenston, W.E. Caler, and D.R. Carter. 1996. Bite-force estimation for *Tyrannosaurus rex* from tooth-marked bones. Nature 382:706–708.

Erickson, G.M., A.K. Lappin, and K.A. Vliet. 2003. The ontogeny of bite-force performance in American alligator (*Alligator mississippiensis*). Journal of Zoology 260:317–327.

Evans, S.E. 1988. The early history and relationships of the Diapsida; pp. 221–260 in M.J. Benton (ed.), The Phylogeny and Classification of the Tetrapods, Vol. 1: Amphibians, Reptiles, Birds. Clarendon Press, Oxford.

Evans, S.E. 1990. The skull of *Cteniogenys*, a choristodere (Reptilia: Archosauromorpha) from the Middle Jurassic of England. Geobios 24:187–199.

Evans, S.E., and M.K. Hecht. 1993. A history of an extinct reptilian clade, the Choristodera: longevity, Lazarus-taxa, and the fossil record. Evolutionary Biology 27:323–338.

Evans, S.E., and J. Klembara. 2005. A choristoderan reptile (Reptilia: Diapsida) from the Lower Miocene of Northwest Bohemia (Czech Republic). Journal of Vertebrate Paleontology 25:171–184.

Evans, S.E., and M. Manabe. 1999. A choristoderan reptile from the Lower Cretaceous of Japan. Special Papers in Paleontology 60:101–119.

Fox, R.C. 1968. Studies of Late Cretaeous vertebrates, 1. The braincase of *Champsosaurus* Cope (Reptilia: Eosuchia). Copeia 1968:100–109.

Gao, K., and R.C. Fox. 1998. New choristoderes (Reptilia: Diapsida) from the Upper Cretaceous and Palaeocene, Alberta and Saskatchewan, Canada, and phylogenetic relationships of the Choristodera. Zoological Journal of the Linnean Society 124:303–353.

Gao, K., and R.C. Fox. 2005. A new choristodere (Reptilia: Diapsida) from the Lower Cretaceous of western Liaoning Province, China, and phylogenetic relationships of Monjurosuchidae. Zoological Journal of the Linnean Society 145:427–444.

Gao, K., and D.T. Ksepka. 2008. Osteology and taxonomic revision of *Hyphalosaurus* (Diapsida: Choristodera) from the Lower Cretaceous of Liaoning, China. Journal of Anatomy 212:747–768.

Gao, K., S.E. Evans, Q. Ji, M. Norell, and S. Ji. 2000. Exceptional fossil material of a semi-aquatic reptile from China: the resolution of an enigma. Journal of Vertebrate Paleontology 20:417–421.

Gao, K., D.T. Ksepka, H. Lianhai, D. Ye, and H. Dongyu. 2007. Cranial morphology of an Early Cretaceous Monjurosuchid (Reptilia: Diapsida from Liaoning Province of China and evolution of the choristoderan palate. Historical Biology 19:215–224.

Gasc, J.P. 1981. Axial musculature. pp. 355–435 in C. Gans, and T.S. Parson (eds.), Biology of the Reptilia Volume 11. Academic Press, New York and London.

Gauthier, J.A., A. Kluge, and T. Rowe. 1988. Amniote phylogeny and the importance of fossils. Cladistics 4:105–209.

Gervais, P. 1887. Enumération de quelques ossements d'animaux vertébrés recueillis aux environs de Reims par M. Lemoine. Journal de Zoologie 6: 74–79.

Gorniak, G.C., H.I. Rosenberg, and C. Gans. 1982. Mastication in the tuatara, *Sphenodon punctatus* (Reptilia: Rhynchocephalia): structure and activity of the motor system. Journal of Morphology 171:321–353.

Gregory, W.K., and L.A. Adams. 1915. The temporal fossae of vertebrates in relation to the jaw muscles. Science 41:763–765.

Grosse, I., E.R. Dumont, C. Coletta., and A. Tolleson. 2007. Techniques for modeling muscle-induced forces in finite element models of skeletal structure. Anatomical Record 290:1069–1088.

Fukunaga, T.M., M. Miyatani, M. Kouzaki, Y. Kawakami, and H. Kanehisa. 2001. Muscle volume is a major determinant of joint torque in humans. Acta Physiologica Scandinavica 172:249–255.

Haas, G. 1973. Muscles of the jaws and associated structures in the Rhynchocephalia and Squamata. pp. 285–490 in C. Gans, and T.S. Parsons (eds.), Biology of the Reptilia Volume 4. Academic Press, New York and London.

Hall, B.K. 1983. Epigenetic control in development and evolution. pp. 353–370 in B.C. Goodwin, N. Holder, and C.C. Wylie (eds.), Development and Evolution. Cambridge University Press, Cambridge.

Hall, B.K. 1988. The embryonic development of bone. American Scientist 76:174–181.

Hall, B.K. 1990. Genetic and epigenetic control of vertebrate embryonic development. Netherlands Journal of Zoology 40:352–361.

Halliday, D., R. Resnick, and J. Walker. 2001. Fundamentals of Physics. John Wiley & Sons Inc., New York, 272 pp.

Hecht, M.K. 1992. A new choristodere (Reptilia, Diapsida) from the Oligocene of France: an example of the Lazarus effect. Geobios 25:115–131.

Henderson, D.M. 2002. The eyes have it: the sizes, shapes, and orientations of theropod orbits as indicators of cranium strength and bite force. Journal of Vertebrate Paleontology 22:766–778.

Henderson, D.M. 2003. Effects of stomach stones on the buoyancy and equilibrium of a floating crocodilian: a computational analysis. Canadian Journal of Zoology 81:1346–1357.

Herrel, A., J.C. O'Reilly, and A.M. Richmond. 2002. Evolution of bite performance in turtles. Journal of Evolutionary Biology 15:1083–1094.

Herrel, A., J. Podos, S.K. Huber, and A.P. Henry. 2005. Bite performance and morphology in a population of Darwin's finches: implications for the evolution of beak shape. Functional Ecology 19:43–48.

Holliday, C.M., and L.M. Witmer. 2007. Archosaur adductor chamber evolution: integrations of musculoskeletal and topological criteria in jaw muscle homology. Journal of Morphology 268:457–484.

Huiskes, R. 2000. If bone is the answer, then what is the question? Journal of Anatomy 197:145–146.

Huiskes, R., and E.Y.S. Chao. 1983. A survey of finite-element analysis in orthopedic biomechanics—the first decade. Journal of Biomechanics 16:385–409.

Huiskes, R., and S.J. Hollister. 1993. From structure to process, from organ to cell: recent developments of FE-analysis in orthopaedic biomechanics. Journal of Biomechanical Engineering 115:520–527.

Iordansky, N.N. 1973. The skull of the Crocodilia. pp. 201–262 in C. Gans, and T. Parsons (eds.), Biology of the Reptilia. Academic Press, London.

Iordansky, N.N. 2000. Jaw muscle of the crocodiles: structure, synonymy, and some implications on homology and functions. Russian Journal of Herpetology 7:41–50.

Jalil, N.E. 1997. A new prolacertiform diapsid from the Triassic of North Africa and the interrelationships of the Prolacertiformes. Journal of Vertebrate Paleontology 7:506–525.

Jaslow, C.R. 1990. Mechanical-properties of cranial sutures. Journal of Biomechanics 23 313–321.

Johnston, I.A. 1985. Sustained force development: specializations and variation among the vertebrates. Journal of Experimental Biology 115:219–251.

Jones, M.E.H., N. Curtis, P. O'Higgins, M. Fagan, and S.E. Evans. 2009. The head and neck muscles associated with feeding in *Sphenodon* (Reptilia: Lepidosauria: Rhynchocephalia). Palaeontologia Electronica 12:56 pp.

Juul-Kristensen, B., F. Bojsen-Møller, L. Finsen, J. Eriksson, G. Johansson, F. Ståhlberg, and C. Ekdahl. 2000. Muscle sizes and moment arms determined by magnetic resonance imaging. Cells, Tissues, Organs 167:214–222.

Katsura, Y. 2004. Sexual dimorphism in *Champsosaurus* (Diapsida, Choristodera). Lethaia 37:245–253.

Kawakami, Y. T. Abe, S.Y. Kun, and T. Fukunaga. 1995. Training-induced changes in muscle architecture and specific tension. European Journal of Applied Physiology 72:37–43.

Keshner, E.A., K.D. Statler, and S.L. Delp. 1997. Kinematics of the freely moving head and neck of the cat. Experimental Brain Research 115:257–266.

Ksepka, T.D., K. Gao., and M.A. Norrell. 2005. A new Choristodera from the Cretaceous of Mongolia. American Museum Novitates 3648:1–22.

Lakjer, T. 1926. Studien über die trigeminus-versorgte kaumuskulatur der sauropsiden. Bianco Lunos Buchdruckerei, Kopenhagen.

Langston, W. 1973. The crocodilian skull in historical perspective. pp. 263–284 in C. Gans, and T. Parsons (eds.), Biology of the Reptilia. Academic Press, London.

Lydekker, R. 1888. Catalogue of the fossil Reptilia and Amphibia in the British Museum (Natural History), Part 1. British Musuem (Natural History).

Lü, J., Q. Zhu, X. Cheng, and X. Du. 1999. Computed tomography (CT) of nasal cavity of *Ikechosaurus sunailinae* (Reptilia: Choristodera). Chinese Science Bulletin 44:2277–2281.

Mallison, H., A. Hohloch, and H.-U. Pfretzschner. 2009. Mechanical digitizing for paleontology – new and improved techniques. Palaeotologica Electronica 12: 41pp.

Matsumoto, R., S.E. Evans, and M. Manabe. 2007. The choristoderan reptile *Monjurosuchus* from the Early Cretaceous of Japan. Acta Palaeontologica Polonica 52:329–350.

Matsumoto, R., S. Suzuki, K. Tsogbaatar, and S.E. Evans. 2009. New material of the enigmatic reptile *Khurendukhosaurus* (Diapsida: Choristodera) from Mongolia. Naturwissenschaften 96:233–242.

McHenry, C.R. 2009. Devourer of gods: the palaeoecology of the Cretaceous pliosaur *Kronosaurus queenslandicus*. Ph.D. dissertation, University of Newcastle, Newcastle, Australia.

McHenry, C.R., P.D. Clausen, W.J.T. Daniel, M.B. Meers, and A. Pendharkar. 2006. Biomechanics of the rostrum in crocodilians: a comparative analysis using finite element analysis. Anatomical Record Part A 288:827–849.

Moazen, M., N. Curtis, S.E. Evans, P. O'Higgins, and M. Fagan. 2008. Rigid-body analysis of a lizard skull: modelling the skull of *Uromastyx hardwickii*. Journal of Biomechanics 41:1274–1280.

Moreno, K., S. Wroe, P. Clausen, C. McHenry, D.C. D'Amore, E.J. Rayfield, and E. Cunningham. 2008. Cranial performance in the Komodo dragon (*Varanus komodoensis*) as revealed by high-resolution 3-D element analysis. Journal of Anatomy 212:736–746.

Müller, J. 2004. The relationships among diapsid reptiles and the influence of taxon selection; pp. 379–408 in G. Arratia, R. Cloutier, V.H. Wilson (eds.), Recent advances in the origin and early radiation of vertebrates. Pfeil, München.

Olsen, E.C. 1961. Jaw mechanisms in rhipidistians, amphibians, reptiles. American Zoologist 1:205–215.

Osi, A., and D.B. Weishampel. 2009. Jaw mechanism and dental function in the Late Cretaceous basal eusuchians *Iharkutosuchus*. Journal of Morphology 270:903–920.

Ostrom, J. 1962. On the constrictor dorsalis muscles of *Sphenodon*. Copeia 1962:732–735.

Oxnard, C.E., F. Lannigan, and P. O'Higgins. 1995. The mechanism of bone adaptations: tension and resorption in the human incus. pp. 105–125 in A. Odegaard, and H. Weinans (eds.), Bone Structure and Remodelling, Recent Advances in Human Biology 2: Series Editor Oxnard, C.E. World Scientific, Singapore.

Parks, W.A. 1927. *Champsosaurus albertensis*, a new species of rhynchocephalians from the Edmonton Formation of Alberta. University of Toronto Studies, Geological Series 23:1–48.

Parks, W.A. 1933. New species of *Champsosaurus* from the Belly River Formation of Alberta, Canada. The Transactions of the Royal Society of Canada, Third Series, Section IV 26:121–137.

Patterson, C. 1982. Morphological characters and homology. pp. 21–74 in K.A. Joysey and A.E. Friday (eds.), Problems of Phylogenetic Reconstruction. Academic Press, New York.

Pierce, S.E., K.D. Angielczyk, and E.J. Rayfield. 2008. Patterns of morphospace occupation and mechanical performance in extant crocodilian skulls: a combined geometric morphometic and finite element modeling approach. Journal of Morphology 269:840–864.

Poglayen-Neuwall, I. 1953. Untersuchungen über die trigeminusmuskulatur von *Hatteria*. Zeitschrift Wisenschaft Zoologie 157:57–76.

Prothero, D.R. 1994. The Eocene-Oligocene transition: paradise lost. Columbia University Press, New York, 291 pp.

Rayfield, E.J. 2004. Cranial mechanics and feeding in *Tyrannosaurus rex*. Proceeding os the Royal Society London B 271:1451–1459.

Rayfield, E.J. 2005. Aspects of comparative cranial mechanics in the theropod dinosaurs *Coelophysis*, *Allosaurus*, and *Tyrannosaurus*. Zoological Journal of the Linnean Society 144:309–316.

Rayfield, E.J. 2007. Finite element analysis in vertebrate morphology. Annual Review of Earth and Planetary Sciences 35:541–576.

Rayfield, E.J., D.B. Norman, C.C. Horner, J.R. Horner, P.M. Smith, J.J. Thomason, and P. Upchurch. 2001. Cranial design and function in a large theropod dinosaur. Nature 409:1033–1037.

Richardson, L.F. 1910. The approximate arithmetical solution by finite differences of physical problems. Transactions of the Royal Society of London A 210:307–357.

Rieppel, O. 1993. Eurapsid relationships: a preliminary analysis. Neus Jahrbuch für Geologie und Paläeontologie 188:241–264.

Rieppel, O. 1998. The status of the sauropterygians reptile genera *Ceresiosaurus*, *Lariosaurus*, and *Silvestrosaurus* from the Middle Triassic of Europe. Fieldiana 38:1–46.

Rieppel, O. 2000. Turtles as diapsid reptiles. Zoologica Scripta 29:199–212.

Rieppel, O., and R.W. Gronowski. 1981. The loss of the lower temporal arcade in diapsid reptiles. Zoological Journal of the Linnean Society 72:203–217.

Russell, L.S. 1956. The Cretaceous reptile *Champsosaurus natator* Parks. National Museum of Canada, Bulletin 145:1–51.

Schumacher, G.H. 1973. The head muscles of hyolaryngal skeleton of turtles and crocodilians. pp. 101–199 in C. Gans, and T.H. Parsons (eds.), Biology of the Reptilia 4 Morphology. Academic Press, London and New York.

Schwarz-Wings, D., C.A. Meyer, E. Frey, H.-R. Manz-Steiner, and R. Schumacher. 2009. Mechanical implications of pneumatic neck vertebrae in sauropod dinosaurs. Proceedings of the Royal Society B 277:11–17.

Sigogneau-Russell, D. 1981. Présence d'un Champsosauridé dans le Cretace supérieur de Chine. Comptes Rendus de l' Académie des Sciences, Paris 292:1–4.

Sigogneau-Russell, D. 1985. Definition of the type-species of *Simoedosaurus*, *S. lemoinei* Gervais, 1877 (Choristodera, Reptilia). Journal of Paleontology 59:766–767.

Sigogneau-Russell, D., and D. Baird. 1978. Présence du genre *Simoedosaurus* (Reptilia, Choristodera) en Amérique du Nord. Geobios 11:251–255.

Sigogneau-Russell, D., and D.E. Russell. 1978. Étude ostéologique du reptile *Simoedosaurus* (Choristodera). Annales de Paléontologie (Vertébrés) 64:1–84.

Skutschas, P.P. 2008. A choristoderan reptile from the Lower Cretaceous of Transbaikalia. Neus Jarhbuch für Geologie und Paläeontologie, Abhandlungen 247:63–78.

Snively, E., D.M. Henderson, and D.S. Phillips. 2006. Fused and vaulted nasals of tyrannosaurid dinosaurs: implications for cranial strength and feeding mechanics. Acta Palaeontologica Polonica 51:435–454.

Snively, E., and A.P. Russell. 2007. Craniocervical feeding dynamics of *Tyrannosaurus rex*. Paleobiology 33:610–638.

Snively, E., and A. Cox. 2008. Structural mechanics of pachycephalosaur crania permitted head-butting behaviour. Palaontologica Electronica 11:17 pp.

Stevens, 1984. Homology and phylogeny: morphology and systematics. Systematic Botany 9:395–409.

Storrs, G.W., and D.J. Gower. 1993. The earliest possible choristodere (Diapsida) and gaps in the fossil record of semi-aquatic reptiles. Journal of the Geological Society, London 150:1103–1107.

Storrs, G.W., D.J. Gower, and N.F. Large. 1996. The diapsid reptile, *Pachystropheus rhaeticus*, a probable choristodere from the Rhaetian of Europe. Palaeontology 39:323–349.

Taylor, M.A. 1987. How tetrapods feed in water; a functional analysis by paradigm. Zoological Journal of the Linnean Society 91:171–195.

Thomason, J.J., L.E. Grovum, A.G. Deswysen, and W.W. Bignell. 2001. *In vivo* surface strain and sterology of the frontal and maxillary bones of sheep: implications for the structural design of the mammalian skull. Anatomical Record 264:325–338.

Thorbjarnarson, J.B. 1990. Notes on the feeding behaviour of the Gharial (*Gavialis gangeticus*) under semi-natural conditions. Journal of Herpetology 24:99–100.

Tseng, Z.J. 2009. Cranial function in a late Miocene *Dinocrocuta gigantean* (Mammalia: Carnivora) revealed by comparative finite element analysis. Biological Journal of the Linnean Society 96:51–67.

Tsuihiji, T. 2005. Homologies of the transversospinalis muscles in the anterior presacral region of Sauria (crown Diapsida). Journal of Morphology 263:151–178.

Turner, M.J., R.W. Clough, H.C. Martin, and L.J. Topp. 1956. Stiffness and deflection analysis of complex structures. Journal of Aeronautical Sciences 23:805–823.

Vandermark, D., J.A. Tarduno, and D.B. Brinkman. 2007. A fossil champsosaur population from the high Arctic: Implications for Late Cretaceous

paleotemperatures. Palaeogeography, Palaeoclimatology, Palaeoecology 248:49–59.

Van Drongelen, W., and P. Dullemeijer. 1982. The feeding apparatus of *Caiman crocodilus*; a functional-morphological study. Anatomischer Anzeiger 151:337–366.

Verwaijen, D., R. van Damme, and A. Herrel. 2002. Relationships between head size, bite force, prey handling efficiency and diet in two sympatic lacerid lizards. Functional Ecology 16:842–850.

Von Wettstein, O. 1931. Ordung der Klasse Reptilia Rhynchocephalia. Kükenthal und Krumbach's Handbuch der Zoologie 7:1–128.

Von Zittel, K.A. 1890. Handbuch der Palaeontologie, Vol 3, Vertebrata (Pisces, Amphibia, Reptilia, Aves). Oldenbourg, Munich.

Wilhite, R. 2003. Biomechanical reconstruction of the appendicular skeleton in three North American Jurassic sauropods. Ph.D. dissertation, Louisiana State University, Baton Rouge, USA.

Wilhite, R. 2005. Variation in the appendicular skeleton of North American sauropod dinosaurs: taxonomic implicaions. pp. 268–301 in V. Tidwell, and K. Carpenter (eds.), Thunder Lizards. Indiana University Press, Bloomington, Indiana.

Witmer, L.M. 1995. The extant phylogenetic bracket and the importance of reconstructing soft tissues in fossils. pp. 19–33 in J.J. Thomason (ed.), Functional Morphology in Vertebrate Palaeontology. Cambridge University Press, Cambridge.

Witmer, L.M., and K.D. Rose. 1991. Biomechanics of the jaw apparatus of the gigantic Eocene bird *Diatryma*: implications for diet and mode of life. Paleobiology 17:95–120.

Witzel, U., and H. Preuschoft. 2005. Finite-element model construction for the virtual synthesis of the skulls in vertebrates: case study of *Diplodocus*. Anatomical Record A 283:391–401.

Wolff, J. 1892. Das gesetz der transformation der knochen. Translated in The Law of Bone Remodelling. Springer-Verlag, Berlin.

Wroe, S., C. McHenry, and J.J. Thomason. 2005. Bite club: comparative bite force in big biting mammals and the prediction of predatory behaviour in fossil taxa. Proceedings of the Royal Society of London Series B 272:619–625.

Wroe, S., P. Clausen, C. McHenry, K. Moreno, and E. Cunningham. 2007. Computer simulation of feeding behaviour in the thylacine and dingo as a novel test for convergence and niche overlap. Proceedings of the Royal Society B 274:2819–2828.

Wu, X.-C. 2003. Functional morphology of the temporal region in the Rhynchocephalia. Canadian Journal of Earth Sciences 40:589–607.

Zienkiewicz, O.C. 1971. The Finite Element Method in Engineering Science. McGraw-Hill, New York, 521 pp.

Zienkiewicz, O.C., R.L. Taylor, and J.Z. Zhu. 2005. The Finite Element Method: Its Basis and Fundamentals. Elsevier Butterworth-Heinemann, Amsterdam, 733 pp.